Geological, Mineralogical and Geostatistical Studies On Zarghat Magnesite Deposit, Saudi Arabia

by

Amin Ramadan Ghaleb

A Thesis Presented to the

FACULTY OF THE COLLEGE OF GRADUATE STUDIES

KING FAHD UNIVERSITY OF PETROLEUM & MINERALS

DHAHRAN, SAUDI ARABIA

In Partial Fulfillment of the
Requirements for the Degree of

MASTER OF SCIENCE

In

GEOLOGY

January, 1985

Order Number 1355750

Geological, mineralogical and geostatistical studies on Zarghat magnesite deposit, Saudi Arabia

Ghaleb, Amin Ramadan, M.S.

King Fahd University of Petroleum and Minerals (Saudi Arabia), 1985

U·M·I
300 N. Zeeb Rd.
Ann Arbor, MI 48106

University of Petroleum and Minerals

GEOLOGICAL, MINERALOGICAL AND GEOSTATISTICAL STUDIES ON ZARGHAT MAGNESITE DEPOSIT, SAUDI ARABIA

BY

AMIN RAMADAN GHALEB

A Thesis Presented to the
FACULTY OF THE COLLEGE OF GRADUATE STUDIES

In Partial Fulfillment of the
Requirements for the Degree of

MASTER OF SCIENCE IN

GEOLOGY

JANUARY, 1985

Printed By: UPM Printing Press

123 123

UNIVERSITY OF PETROLEUM & MINERALS
DHAHRAN, SAUDI ARABIA

This thesis, written by

Amin Ramadan Ghaleb

under the direction of his Thesis Committee, and approved by all its members, has been presented to and accepted by the Dean, College of Graduate Studies, in partial fulfilment of the requirements for the degree of

Master of Science in Earth Sciences (Geology)

Dean, College of Graduate Studies

Date: April 10, 1985

Department Chairman 25/3/1985

THESIS COMMITTEE

Chairman 4/3/85

Member 4.3.85

Member 4.3.1985

In the Name of ALLAH, the Most

Merciful and Most Gracious

THIS THESIS IS DEDICATED TO MY MOTHER

ACKNOWLEDGEMENT

Acknowledgement is due to the University of Petroleum and Minerals for financial and logistic support for this thesis.

I would like to express my deep appreciation, gratitude and indebtedness to my thesis supervisor Dr. S.I. Saif for his continuous encouragement, moral support and generosity in sharing his time and knowledge during fieldwork, research, and in the preparation of this manuscript.

Special thanks are also due to Dr. A. Sahin, thesis committee member, for providing guidance and supervision in the geostatistical part of the thesis. Also, my thanks to Dr. M.N. Cagatay, thesis committee member, for his advice in the field study as well as for fruitfull scientific discussions concerning the X-ray analysis. I, also, wish to thank Dr. A. Niazy for encouragement and material support towards the research during his tenure as the chairman of the department and Dr. A.R. Jado the present chairman of the department, for his helpful suggestions.

My deep appreciation should also go to Dr. O. Greis (Chemistry Department, UPM) to whom I am indebted for learning Differential Thermal Analysis and X-Ray diffraction camera techniques, and for fruitfull scientific discussions.

I, also, wish to thank Dr. A.M.S. Al-Shanti, chairman of the Economic Geology Department, Dr. H. Hakeem and Dr. O. El-Mahdy (Faculty of Earth Sciences, King Abdulaziz University) for their guidance and facilities offered to me during one of their field trips.

Thanks are also due to Mr. J. Schultz (Research Institute) for his help in thin section preparation, and to Dr. R.J. Engen (ARAMCO, Laboratory Department) for his help in working on Scanning Electron Microscope. Also, my thanks should go to BRGM who supplied me with the neccessary reports.

TABLE OF CONTENTS

LIST OF FIGURES

Page #

Page #

LIST OF TABLES

LIST OF APPENDICES

ABSTRACT

Zarghat magnesite deposit, located about 570 km NNE of Jeddah, occurs in the upper part of a carbonate sequence which together with an underlying andesite unit constitutes the Jibalah Group of Late Proterozoic age. The Jibalah Group represents the youngest rocks of the Precambrian sequence of the Arabian Shield. The reserves with a grade of 38-48% MgO is estimated by BRGM to be 3 million tons.

The magnesite is exposed on the surface in the form of small hills, and associated with dolomite, cherty limestone, and siltstone. Structurally, these rocks make a syncline which appears to be asymmetrical structural basin. Petrographic investigations with microscope and SEM show that the magnesite is mostly cryptocrystalline, massive but at places sheared and fragmented. XRD studies demonstrate that the magnesite is either in the form of pure magnesite with minor traces of dolomite or impure magnesite with abundant dolomite. Dolomite veins of a later phase with variable thickness have cut across the magnesite bodies. The DTA investigation has shown that the decomposition temperature of magnesite is about 620° C.

To determine the spatial distributions of variables within the magnesite orebody of the central-hill, semivariograms and cross-semivariograms functions for the several selected variables were

computed. These functions revealed continuous behaviour near the origin which is common in most sedimentary deposits.

The field and laboratory evidences all suggest that the magnesite has been deposited in a sedimentary shallow marine basin along with the other carbonate rocks followed by some post depositional (diagenetic) changes.

دراسات جيولوجية ومعدنية وجيولوجيا احصائية على خام الماجنيزيت
في منطقة زرغط بالمملكة العربية السعودية

ملخص :

يوجد خام الماجنيزيت في منطقة زرغط التي تبعد حوالي ٢٥٠ كم شمال شرق المدينة المنورة في الجزء العلوي من الترسبات الكربونية لمجموعة جبالا والتي تضم من الاحدث الى الاقدم - ماجنيزيت - دولوميت - حجر جيري .

لم تتعد الدراسات السابقة التي تمت على الخام عن دراسة التوزيع الجغرافي والتحليل الكيميائي لعينات من الخام تم الحصول عليها خلال برامج حفر مختلفة ، وقد دلت النتائج على ان كمية الخام الموجود في منطقة زرغط تقدر بحوالي ٣ مليون طن .

تتناول هذه الاطروحة دراسة مكثفة لخواص الخام المعدنية باستخدام ميكروسكوب الصخور والميكروسكوب الالكتروني وجهاز التحليل بالاشعة السينية .

وقد اظهرت الدراسة البتروجرافية المكثفة في الحقل وتحت الميكروسكوب على ان الماجنيزيت يحتوي على عروق من معدن الدولوميت منتشرة في كل الخام تقريبا ، وهذه العروق تختلف في الحجم والشكل ، كذلك دلت هذه الدراسة على ان نسبة الدولميت كشوائب بالخام تزداد بالقرب من حواف عدسات الماجنيزيت حيث يقل السمك وتتغير السحنة الى دولوميت بعد ذلك .

كذلك وجد ان طبقة الدولوميت التي توجد اسفل طبقة الماجنيزيت ذات رقائق طحلبية في بعض الاماكن ، ويدل ذلك على انحسار البحر في منطقة ضحلة الى منطقة عميقة .

كذلك تم اختيار نتائج التحليل الكيميائي المنشورة لاربع متغيرات (اكاسيد) بالخام اثنان في صورة اولية واثنان بعد المعالجة الكيميائية لاجراء دراسة جيواحصائية بتطبيق بعض الدوال الاحصائية الحديثة باستخدام الحاسب الالي ، وقد تم الحصول من هذه الدراسة على نتائج شبيهة بتلك التي تميز في معظم الاحيان خامات المترسبات .

مما سبق يمكن استنتاج ان اصل تكوين خام الماجنيزيت بمنطقة زرغط هو ذو نشأة رسوبية .

CHAPTER - 1

INTRODUCTION

1.1 Location and Accessibility

The Zarghat magnesite deposit is located 570 km NNE of Jeddah, in the northern part of the Arabian Shield (Lat. 26°30 N and Long. 40°35 E), Fig. 1.1. Three main outcrops, westnorthwest-hill, central-hill, and eastsoutheast-hills, are located between Zurayghit and Zarghat villages. Minor occurrences are scattered to the north of the main outcrops. The area is accessible from Medina by 250 km paved Medina-Hail road followed by 50 km unpaved road to Zarghat Fig. 1.1.

1.2 Previous Work

Occurrence of magnesite in Zarghat area was first reported by Kahr in 1962. Feugueur visited the deposit in December 1965 and filed a report (1966) in which he recommended sampling and assaying for MgO in the deposit. It was followed by a quick compass and clinometer survey and sampling by Berton in 1968, who made a geological map of the main magnesite outcrops at a scale of 1:5000. The assaying revealed good quality of the magnesite. Berton (1968), therefore, recommended diamond drilling to figure out the structure of the deposit. Subsequently, an area of about 170 sq km was mapped by

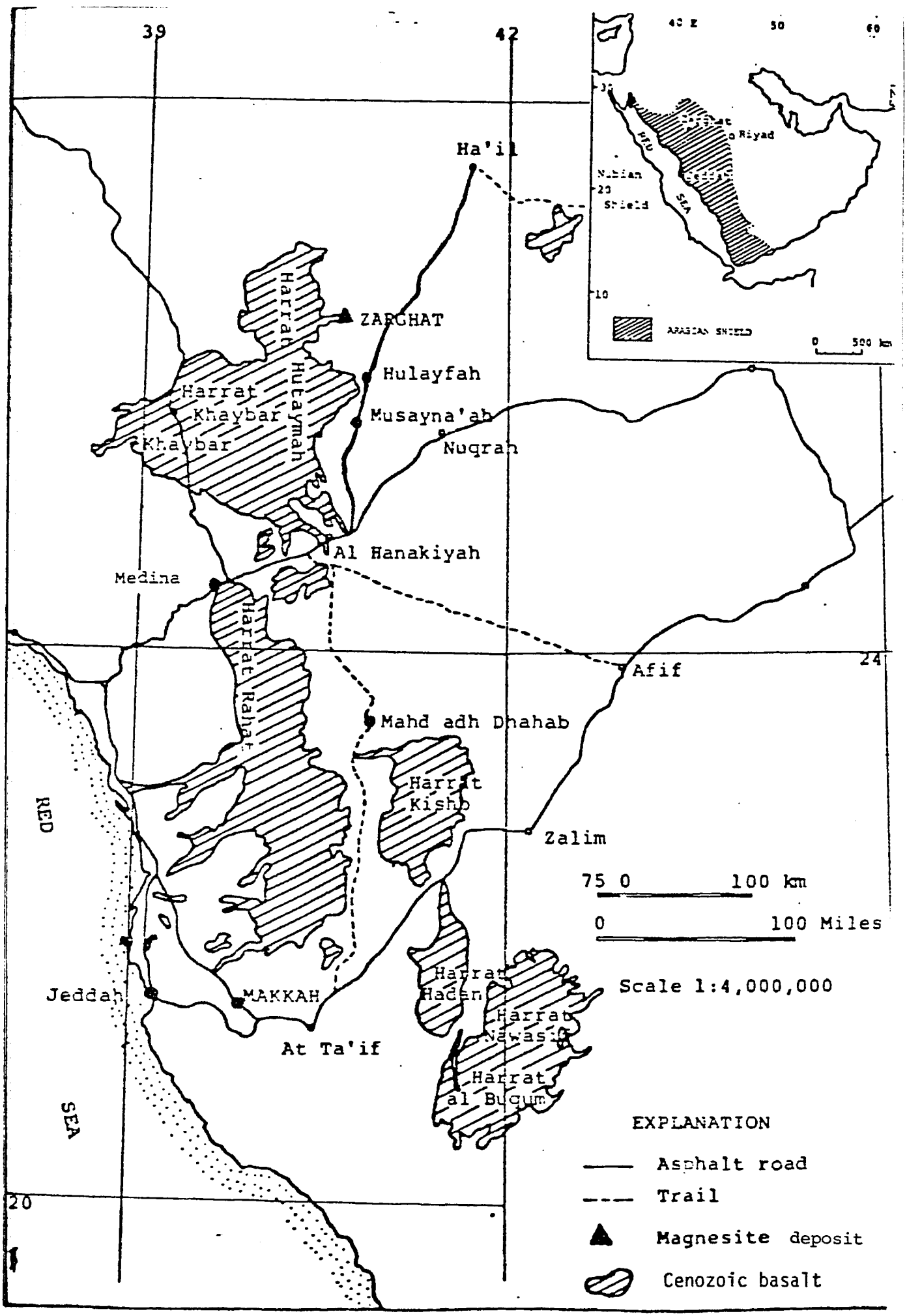

Fig.(1.1): Location map of Zarghat (Brosset, 1970)

Brosset in 1969 at a scale of 1:50000. A more detailed geological and topographic map (1:1000) of the main occurrences of magnesite was also prepared with clinometer and stadia, covering an area of about 1 sq km, and the reserve was estimated as one million metric tons (Brosset, 1970). He also recommended diamond drilling to know the thickness and quality of mineralization at depth. Delfour (1970) published his report "Preliminary data on the Zarghat Magnesite Prospect".

An exploratory drilling program was carried out by Bureau de Recherches Geologique et Minieres (BRGM) in order to delineate the extent and shape of the deposit and to ascertain its quality. The first phase of drilling was completed between 23 July and 21 September 1975, while the second phase was completed between 9 November 1975 and 10 February 1976. The core samples were assayed for MgO (Brosset, 1976). The preliminary reserve estimation, using mineralized blocks outlined by drilling, indicated the existence of 3 million tons of ore out of which 650000 were considered to be of high quality. The 3 million tons were distributed as follows:

1- East-southeast hill : 336000 tons, the magnesite tends strongly to be dolomitic.

2- Central-hill : 3 million, the magnesite is of good quality.

3- West-northwest hill : 192000 tons, the magnesite is of average quality

1.3 Purpose of the Present Investigation

The present investigation is mainly aimed to study the geological setting as well as mineralogical and textural characteristics of the magnesite deposit. Also, the spatial distributions of variables within the ore body were studied. These studies, in turn, were directed towards obtaining a clear understanding of the genesis of the deposit.

It is hoped that the present investigation will provide significant information towards some future ore benificiation, mineral processing and economic feasibility studies.

CHAPTER - 2

STUDY METHODS AND TECHNIQUES

2.1 Field Investigation Procedure

The project was initiated by fieldwork carried out in September, 1983 in collaboration with the field party of the Faculty of Earth Sciences, King Abdulaziz University. Field identification of various rock types and units occurring in the area was done. Magnesite samples for laboratory investigation were collected systematically along three traverses crossing the main outcrops of the deposit.

After obtaining and evaluating the results of the laboratory investigation and a thorough study of the literature, more detailed field investigation was carried out in May, 1984. Field characteristics and relationship of the magnesite body and the associated rocks were investigated. Pictures depicting important geological field features were taken. More samples were collected from the magnesite body as well as from the associated rocks for further laboratory investigation. A total of 97 samples were obtained from the study area. The samples locations are shown in Fig. 2.1.

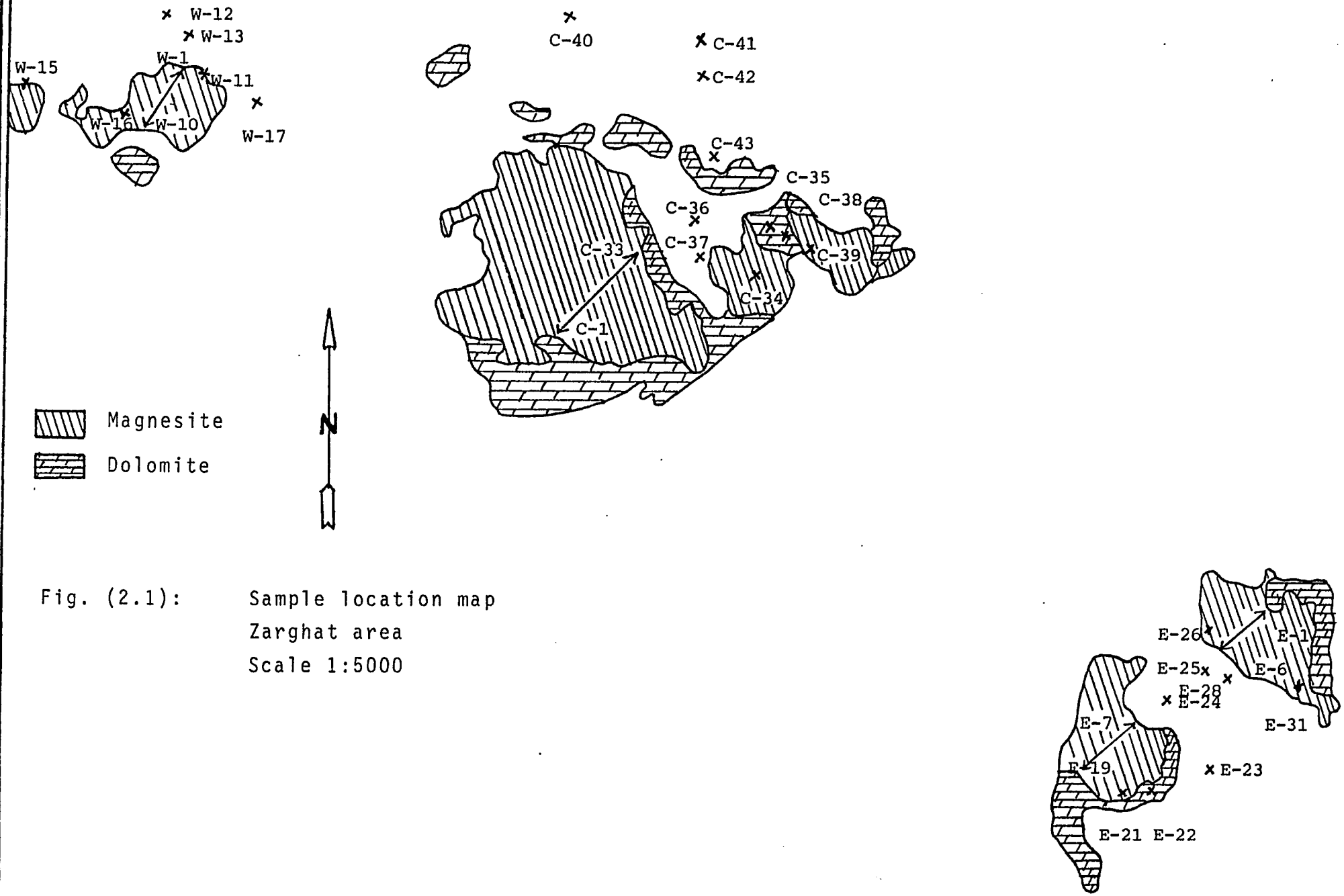

Fig. (2.1): Sample location map
Zarghat area
Scale 1:5000

2.2 Laboratory Investigation Techniques

A total of 85 thin sections from the samples were prepared and examined under petrographic microscope in order to establish the mineralogical composition and record the textural characteristics of the magnesite and the associated rocks. The microscopic study revealed the cryptocrystalline and microcrystalline nature of most magnesite samples. This necessitated further investigation by X-Ray Diffraction, Differential Thermal Analysis (DTA) and Scanning Electron Microscope (SEM) in order to identify and resolve the various mineral phases of the cryptocrystalline textural intergrowth and to study the thermal behaviour of magnesite.

Samples for the X-ray and DTA studies were ground to powder using Laboratory Vibrating Cup Mill.

Eighty samples were investigated by a Philips X-ray diffractometer PW 1349/30 Goniometer, employing Fe-filtered CoK_{α} radiation, and a goniometer speed of 1°/min. The generator was run at 20 mV and 40 kV.

Fifty-four magnesite samples in powder form were analyzed using DuPont 990 Thermal Analyzer. The DuPont high temperature differential thermal analyzer (DTA) cell (1600°C) and Pt/PtRh13 thermocouple were used. All the samples were examined at a heating

rate of 20°C/min., at atmospheric pressure under air using Aluminum Oxide (Al_2O_3) as a reference.

Two samples were investigated by SEM for which the samples were cut into discs of about 2 cm in diameter and gold-coated in vacuum. The same samples were further subjected to electron microprobe analysis for which A JEOL 35 CF-Kevex 7000 SEM with automated microprobe unit was used.

2.3 Geostatistical Computations

The drilling and assay data obtained from BRGM reports were utilized in the geostatistical evaluation of the magnesite body. The data evaluation has been carried out using the IBM 370-158 computer at the University of Petroleum and Minerals. It included semivariogram and cross-semivariogram computations in vertical as well as horizontal directions for crude MgO%, crude CaO%, calcined MgO%, and calcined CaO% contents.

CHAPTER - 3

GENERAL GEOLOGY

The western Suadi Arabia is composed of crystalline rocks of Precambrian Basement known as the Arabian Shield. To the north, east and southwest the shield is concealed and surrounded by a series of sedimentary rocks. Paleozoic, Mesozoic, and lower Tertiary sedimentary rocks are well exposed in central Saudi Arabia. They crop out in a great curved belt flanking the eastern margin of the shield. The dip of the beds is gentle and uniform towards northeast, east, and southeast, reflecting buried basement configuration. Average thickness of the sedimentary succession is about 5500 meters.

The cratonization of the Arabian Shield has been nicely described by Hadley and Schmidt, 1980 as "The Arabian Shield which occupies roughly one-third of the Arabian Peninsula (about 610000 sq km) comprises a terrain of slightly to intensively deformed Proterozoic strata and plutonic rocks which are partially remobilized. The Arabian Shield was formed by successive accretions of newly formed crust between 1000 and 600 m.y. ago. Successively younger island arcs formed to the east as west-dipping subduction zones shifted eastward. West of Bishah, the volcanic-plutonic crust had consolidated by about 780 m.y. ago when westward-directed subduction ceased.

A new marginal island arc formed subsequently east of Bishah in the southern Najd, and subduction was renewed at the Idsas suture in the eastern Najd. The volcanic arc consisted of calc-alkaline volcanic rocks (Halaban Group), dominantly andesite but ranging from basalt to dacite, and comagmatic, subvolcanic plutonic rocks, dominantly diorite but ranging from gabbro to trondhjemite. About 725 m.y. ago this primitive crust was thickened by large intermediate-depth plutons of hornblende tonalite and mafic granodiorite. Compressive tectonism produced folds and faults of northerly trends and was accompanied by greenschist facies metamorphism.

A continental collision occurred east of the Najd Province about 625 m.y. ago and initiated extensive compressional orogeny and potassic granite plutonism throughout the Shield. Large, syn-tectonic batholiths of calc-alkaline, leucocratic, biotite granodiorite-monzogranite formed the cores of large north trending gneiss domes that were asymmetric toward the west. The domes consist of tonalitic and granodioritic orthogneiss that represents the low-density, plutonic part of the earlier Halaban crust. Strong compression resulted in northerly trending structures including large west-directed thrust faults. Post-tectonic, diapiric plutons of granite and alkalic granite intruded the eroding crust at progressively shallower levels until about 600 m.y. ago. Molasse deposits of the Murdama Group transgressed westward across the eroding crust and were subsequently deformed along northerly

trends. Renewed compression of the now thick continental crust resulted in large, NW-trending Najd faults that have left-lateral displacements aggregating 300 km. The Najd faulting terminated about 560 m.y. ago. Transgressive, quartzose sandstone of early Paleozoic age subsequently covered the stabilized craton".

Several authors have proposed different lithostratigraphic sequences for the Arabian Shield which have been summarized by Hadley and Schmidt (1980) who have also prepared a new lithostratigraphic sequence Table 3.1. According to the new sequence of Hadley and Schmidt (1980), the sedimentary rocks of the Arabian Shield consist of three depositional phases. Phase I (the oldest) includes the Baish, Baha, and Jeddah Groups, which consist of an immature assemblage dominated by fine-grained meta-graywacke, graphitic schist, chert, marble, and subordinate polymictic conglomerate and meta-siltstone. The clastic rocks of Phase I are composed solely of volcanic material and do not contain plutonic or sialic detritus. Phase II (the middle) includes the Ablah, Halaban, and Murdama Groups. Meta-sandstone, polymictic conglomerate, coarse-grained meta-graywacke, and abundant marble (stromatolitic in places) characterize this phase. Plutonic and volcanic components are abundant in the clastic suite. Phase III (the youngest) consists of the Shammar and Jibalah (spelled as Jubaylah by Hadley & Schmidt and others) Groups. Sedimentary rocks of this phase are fine- to coarse-grained terrigenous clastic rocks, boulder

Hadley and Schmidt (1980		Explanation
Phase III	Jubaylah group	Also spelled as Jibalah by Delfour (1976)
	Shammar group	
Phase II	Murdama group	It also includes rocks of Fatima group
	Halaban group	
	Ablah group	
Phase I	Jeddah group	
	Bahah group	
	Baish group	

Table(3.1): General stratigraphic sequence of the Arabian Shield (after Hadley and Schmidt, 1980)
(---- surface of unconformity)

conglomerate, and stromatolitic limestone and dolomite.

All the phases include abundant volcanic rocks. Carbonate rocks are also found in all the groups of the three phases except the Shammar group Fig. 3.1. The phase I and II rocks have been metamorphosed to the greenschist and amphibolite facies whereas the rocks of phase III are unmetamorphosed.

The rocks of the three phases have been deposited in several sedimentary basins. The basins of phase I and II generally trend North, especially in the central and southern parts of the Shield. The basins of phase III are trending E-W.

Class	Rock Type	PHASE I			PHASE II			PHASE III	
		Baish	Bahah	Jiddah	Ablah	Halaban	Murdama	Shammar	Jubaylah
Carbonate rocks	Limestone and dolomite								●
	Marble	●	●	●	●	●	●		
Argillaceous rocks and chert	Mudstone		●		●				
	Chert	●	●	●		●			●
	Shale							●	●
	Slate/argillite	●	●	●	●	●	●		
Nongraywacke clastic rocks	Siltstone	●	●	●	●	●	●	●	●
	Quartzite		●						
	Sandstone			●	●	●	●	●	●
Graywacke	Graywacke	●	●	●	●	●	●		
Conglomerates	Pebble conglomerate		●		●		●	●	●
	Boulder conglomerate	●		●	●	●	●		●

Fig.(3.1): Sedimentary rock classes and types and their distribution in the eight stratigraphic groups of the Arabian Shield (Hadley and Schmidt, 1980)

CHAPTER - 4

GEOLOGY OF ZARGHAT MAGNESITE DEPOSIT

4.1 Geology of the Zarghat Area

The Precambrian rocks exposed in the Zarghat area belong to Fatima and Jibalah groups (Brown, G. F., and others, 1963). The name 'Fatima group' has not been retained in the recent classification by Hadley and Schmidt (1980). Field observations in Zarghat area suggest that rocks of what is called Fatima group may be correlated with the lower part of Jubaylah group in Mashhad area described by Hadley (1974). In fact this point needs a detailed study. The name 'Fatima group' will be used in this thesis since all the previous workers in Zarghat area used the same name. According to Al-Shanti (personal communication) the rocks of Fatima group have been included in Murdama group. As such they belong to phase II, and those of Jibalah group to phase III of the Hadley Schmidt's classification of the Arabian Shield.

The Fatima group, being older than Jibalah group, should stratigraphically underlie it, but in the Zarghat area, the two groups are juxtaposed due to a major fault as shown in Fig. 4.1 (Brown, G. F., and others, 1963).

The Fatima group comprises rhyolite, conglomerate and rhyolitic tuff and breccia. These rocks mostly strike NE, dip about 60° NW, and are intruded by stocks of red granophyre and pink granite. Near the fault the granite is jointed and sheared as well as cut by white quartz veins.

The stratigraphic succession of the Jibalah group, in the Zarghat area is given below:-

Carbonate Formation:- Constituted of the following rock units:

- Dolomite and magnesite, mainly found in the small hills at the southern edge of the basin, and in small outcrops towards its center. This unit is the main subject of the present study.

- Limestone-dolomite, reddish-brown dolomitic limestone, also interbedded with thin layers of argillaceous sandstone.

- Cherty limestone, well developed throughout the basin, interbedded with thin detrital layers of fine-grained, argillaceous sandstone, siltstone and several small lenses of dolomitic limestone.

Andesite Unit

- Brown amygdaloidal andesite and grey andesite with

small feldspar phenocrysts.

4.2 Carbonate Formation of the Jibalah Group

The carbonate formation which comprises the upper part of the Jibalah Group contains cherty limestone, dolomite, and magnesite.

4.2.1 Cherty Limestone

The lower part of the carbonate formation consists of hard brown cherty limestone which is well exposed in the central part of the Zarghat area Fig. 4.1. It is interbedded with thin layers of fine-grained brown argillaceous sandstone as well as green and yellow siltstone. At places it also contains several lenses of dark brown dolomitic limestone.

4.2.2 Bedded Dolomite

The dolomite constitutes the middle part of the carbonate formation. This dolomite will be referred to as "bedded dolomite" to distinguish it from "vein dolomite" (Section 4.2.4). The bedded dolomite is brown and hard. It is exposed at the base of the hills in which magnesite occurs. The bedded dolomite has a clear gradational contact with the magnesite. It also contains lenses of magnesite near its top in some places Fig. 4.2.

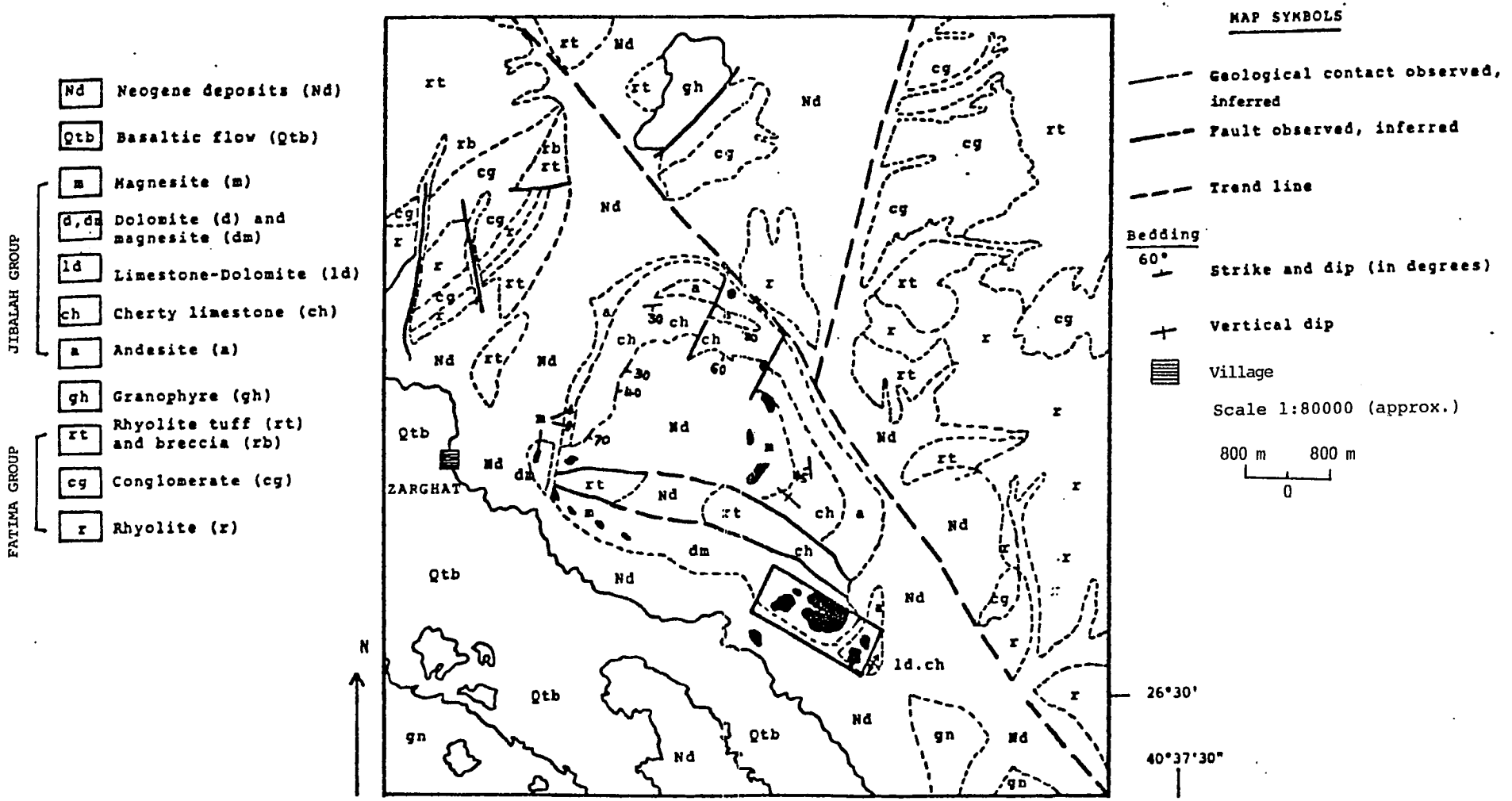

Fig.(4.1): Geology of the Zarghat area (after, Brosset, 76 JED 20)

Fig.(4.2): Lenses of magnesite within bedded dolomite
(a) WNW-hill
(b) ESE-hill

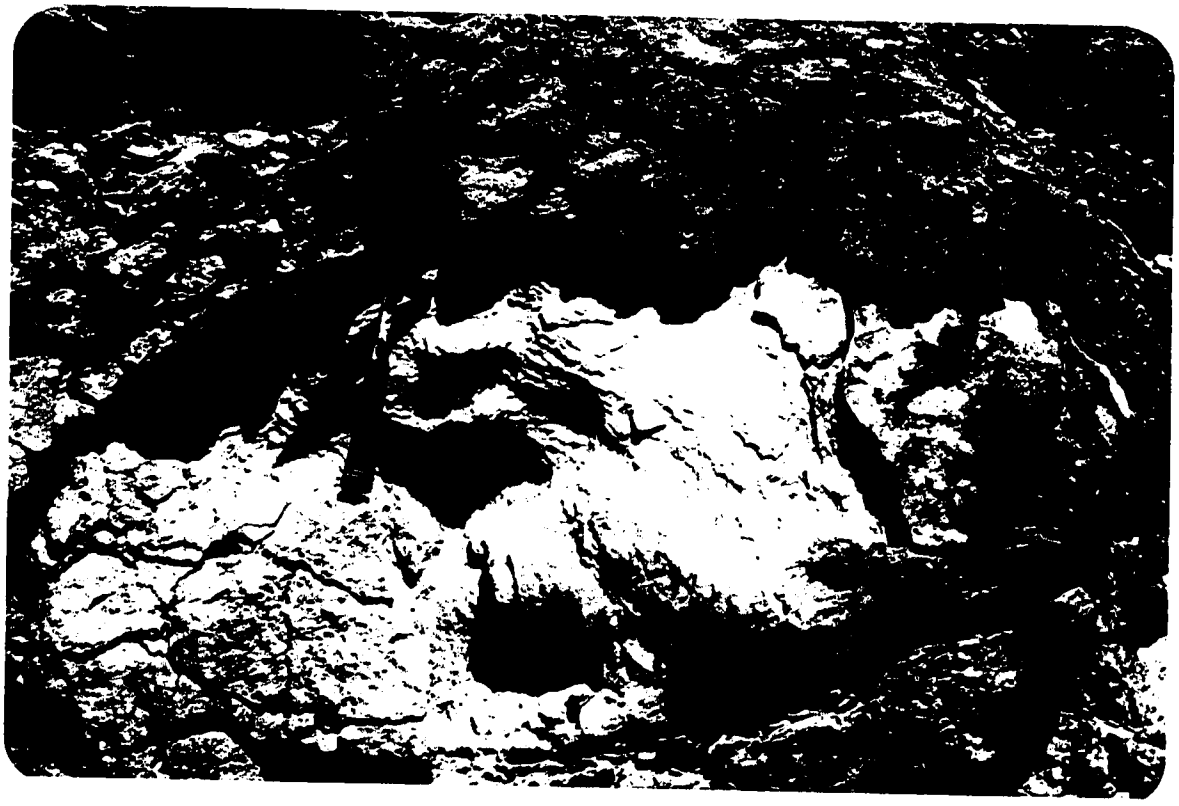

A

B

4.2.3 Magnesite

Geographically, the magnesite deposit forms small hills that run WNW-ESE over a distance of 1.5 km and are named as West-northwest (WNW), Central, and East-southeast (ESE) hills (Brosset, 1970).

The largest exposure is referred to as the Central-hill which trends E-W, and constitutes the most important part of the deposit, having maximum dimensions of 200 x 45 m. The top of the hill lies 16 m above the plain. The hill has been segmented by erosion into three smaller magnesite bodies. Between these hills the subjacent dolomite and dolomitic limestone are exposed Fig. 4.3.

The east-southeastern side of the deposit is composd of two small hillocks (100 x 200 m maximum) rising 4 or 5 m above the plain. A narrow valley separating these hillocks exposes several outcrops of the subjacent dolomite and dolomitic limestone interbedded with argillaceous sandstone and andesite. To the northeast and southeast of these magnesite hillocks, folded dolomitic rocks underlie the magnesite. The WNW hill trends E-W and is about 50 x 200 m in extent. The hill rises about 8 m above the pediment.

The holes drilled into the magnesite hills all intersected a layer of magnesite followed by dolomite with gradational contact. The thickness of the magnesite layer varies from 43.5 m to 5.5 m (Brosset, 76).

Fig.(4.3): A clear contact between magnesite and underlying bedded dolomite (buff), Central-hill.

Fig.(4.4): Highly sheared magnesite along shear zone in the Central-hill.

About five hundered meters southwest of the WNW-hill several small outcrops of magnesite are exposed along a WNW trending line over a distance of 250 m, and are surrounded by the bedded dolomite rock. The average outcrop width is about 40 m. The height of the outcrops does not exeed 1.5 m above the pediment.

The main body of the magnesite is located stratigraphically on the top of the Jibalah Group and constitutes the principal magnesite deposit. The gradational contact is marked by a change in color from buff dolomite to grey and white magnesite. The contact could easily be seen at the base of the hills made of magnesite Fig. 4.3. Other small occurrences of mostly dolomitic magnesite are also scattered in dolomite and cherty limestone. These are small lenses with lengths of a few ten of meters, and width up to few meters.

The magnesite on weathered surface appears dark grey or pale brown but the fresh surface is white. It is quite hard, dense and massive, but along shear zones it is fragmented and brecciated Fig. 4.4. Several joints have also affected the magnesite body producing blocks and fragments.

4.2.4 Dolomite Veins in Magnesite

The most interesting feature of the magnesite deposit is the

occurrence of numerous dolomite veins of various colors, sizes, and characteristics. They vary in size from about one meter in thickness to microscopic size veinlets Fig. 4.5. The large veins are brown to light brown whereas the smaller ones are grey. Some of them are branching, cross-cutting , or make a dendritic pattern. Good exposures of these veins are seen along the two sides of the trench in the Central-hill Fig. 4.6. The contact between the large dolomite veins and enclosing magnesite is gradational. The brown color of dolomite in the central part of the veins changes to pale brown and whitish near the contact with the enclosing magnesite Fig. 4.7. In many places remnant magnesite is observed along the two sides of the dolomite veins, some rare remnant magnesite is also seen in the central part of the vein enclosed by dolomite Fig. 4.8.

The trend of the veins is variable. Most of the large ones are trending NE-SW, generally vertical or inclined at high angles whereas a few are inclined at low angles or even horizontal. The smaller veins have a dominant general trend of E-W Fig. 4.5c.

This dolomite, occuring as veins will be referred to as "vein dolomite" to distinguish it from the "bedded dolomite" (Section 4.2.2).

Fig.(4.5): Various types of dolomite veinlets found within the magnesite body
(a) minute dendritic veinlets
(b) crystalline veins, 1-2 cm wide
(c) cross-cutting veinlets
(d) Large scale brown veins
(e) Large scale brown veins enclose magnesite

A

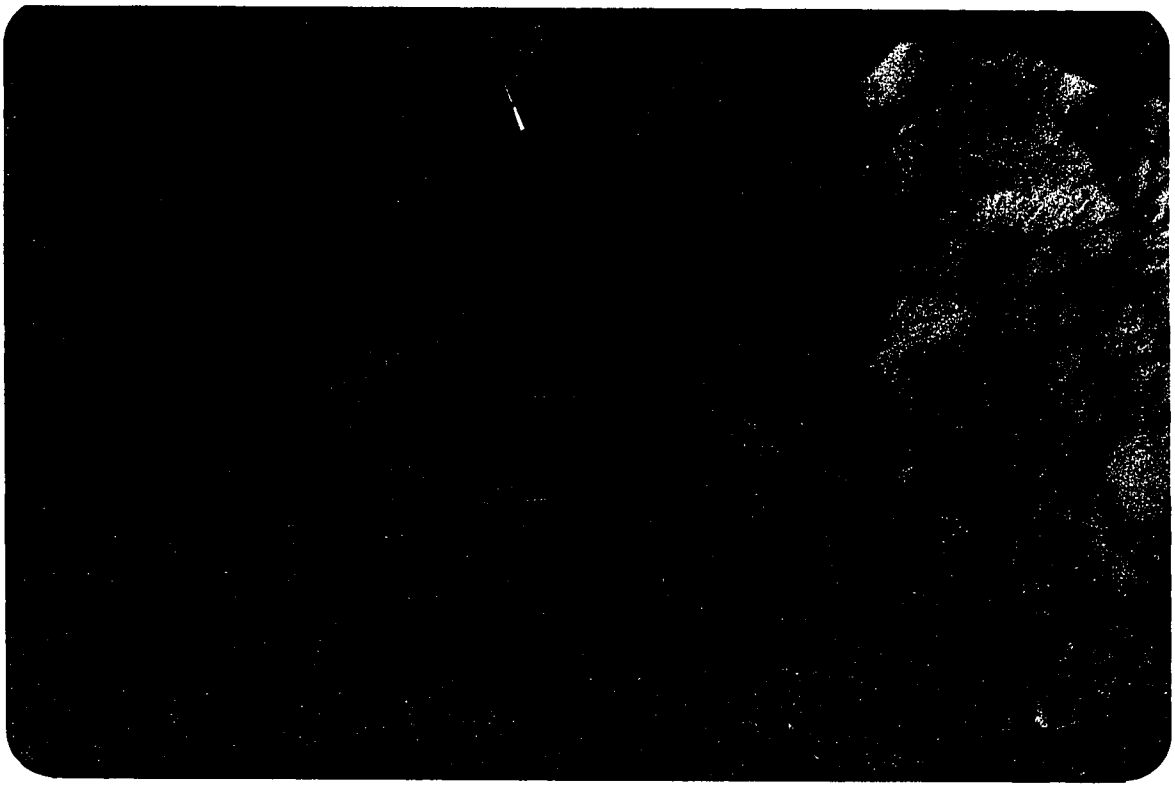

B

C

D

E

Fig.(4.6): Trench in magnesite of the Central-hill.

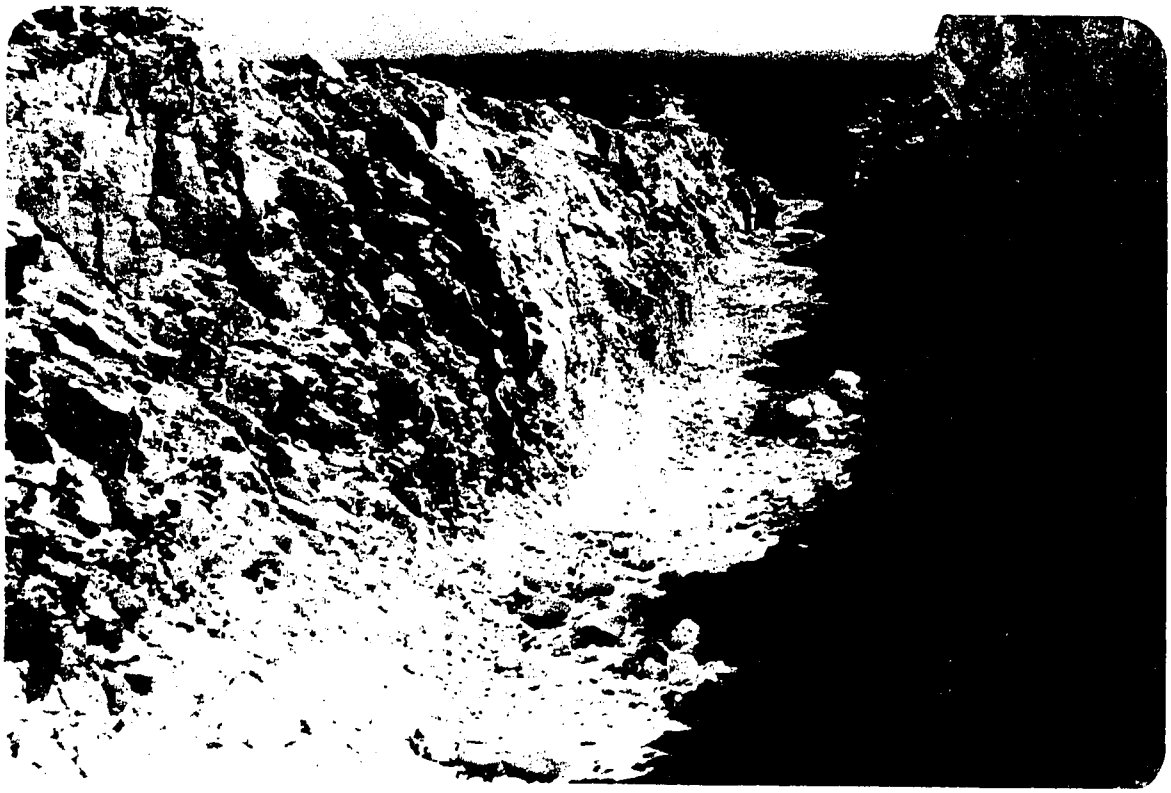

Fig.(4.7): Large dolomite veins showing a clear gradational contact with magnesite.

Fig.(4.8): Magnesite remnants encircled by brown vein dolomite in white magnesite.

4.3 Geological Structure

The strata of the Jibalah Group circumscribes a roughly triangular area which is almost surrounded by the Neogene deposits. No direct contact between the Jibalah Group and the underlying Fatima Group has been observed, but outcrops of Fatima Group are exposed in the surrounding areas Fig. 4.1.

The strike and dip of the Jibalah Group are variable. To the southeast the beds strike NW and the dip varies from 45° SW to almost vertical. In the north, the strike varies from NW to NE, whereas the dip varies from 30° to 60° towards SW and SE. It appears that the strata of the Jibalah Group make a roughly triangular synclinal structural basin.

A major fault trending NW passes through the area which is almost parallel to the northeastern boundary of the Jibalah structural basin. The fault has brought the rhyolite of the Fatima Group against the andesite of the Jibalah Group. The northwest trend of the fault is parallel to that of the general trend of Najd fault and it, therefore, may belong to the Najd fault system. One large and two small faults branch out from the major fault striking in NE direction. Both the small faults have cut across the Jibalah Group. Towards the south, two other faults trending roughly SE also cut through the Jibalah Group. They make a horst type structure as the rhyolite tuff of the

underlying Fatima Group is exposed between them. A few other small faults are also present to the NW of the Jibalah Group affecting Fatima Group.

Joints are quite common in the area, particularly in the magnesite body where smooth joint faces are seen along the trench of the Central-hill. Four sets of joints have been identified in the magnesite body with the following orientations Fig. 4.9.

N 40° W - S 40° E

N 18° E - S 18° W

N 35° E - S 35° W

S 35° E - N 35° W

These joints are closely spaced with an average interjoint space of about 2-3 cm. Apart from these major joint sets many other minor joints and irregular fractures have been observed.

The bedding, though not very commom, have been identified in magnesite Fig. 4.10, dolomite Fig. 4.11, and siltstone Fig. 4.12. The beds are generally thin, and at places folded in the form of a small antiform Fig. 4.13. Also, fine stromatolitic laminations were recorded in bedded dolomite Fig. 4.12.

Fig.(4.9): Four major directions of joints in magnesite; J_1, J_2, J_3 are shown; J_4 is parallel to the surface of the photograph.

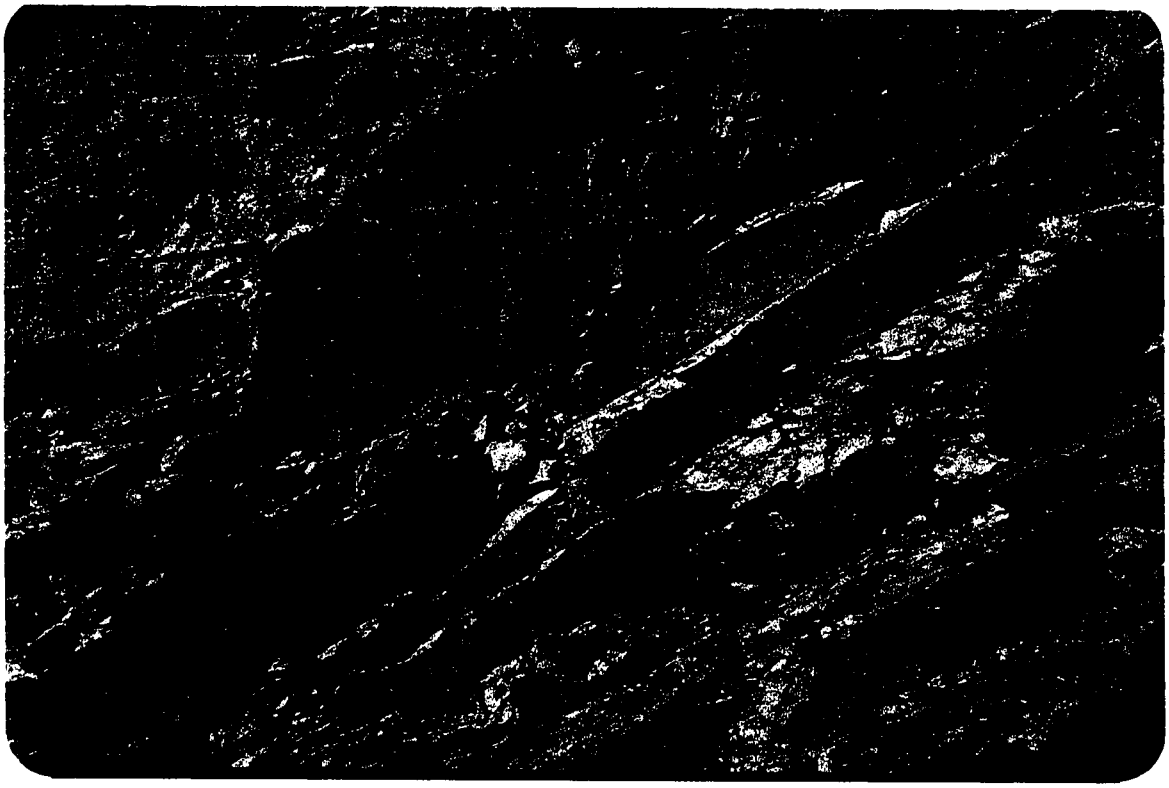

Fig.(4.10): Jointing in magnesite.

Fig.(4.11): Bedding in bedded dolomite.

Fig.(4.12): Minor folding in siltstone, overlain by bedded dolomite showing fine stromatolitic laminations.

Fig.(4.13): Outcrop showing a partly eroded plunging antiform in bedded dolomite.

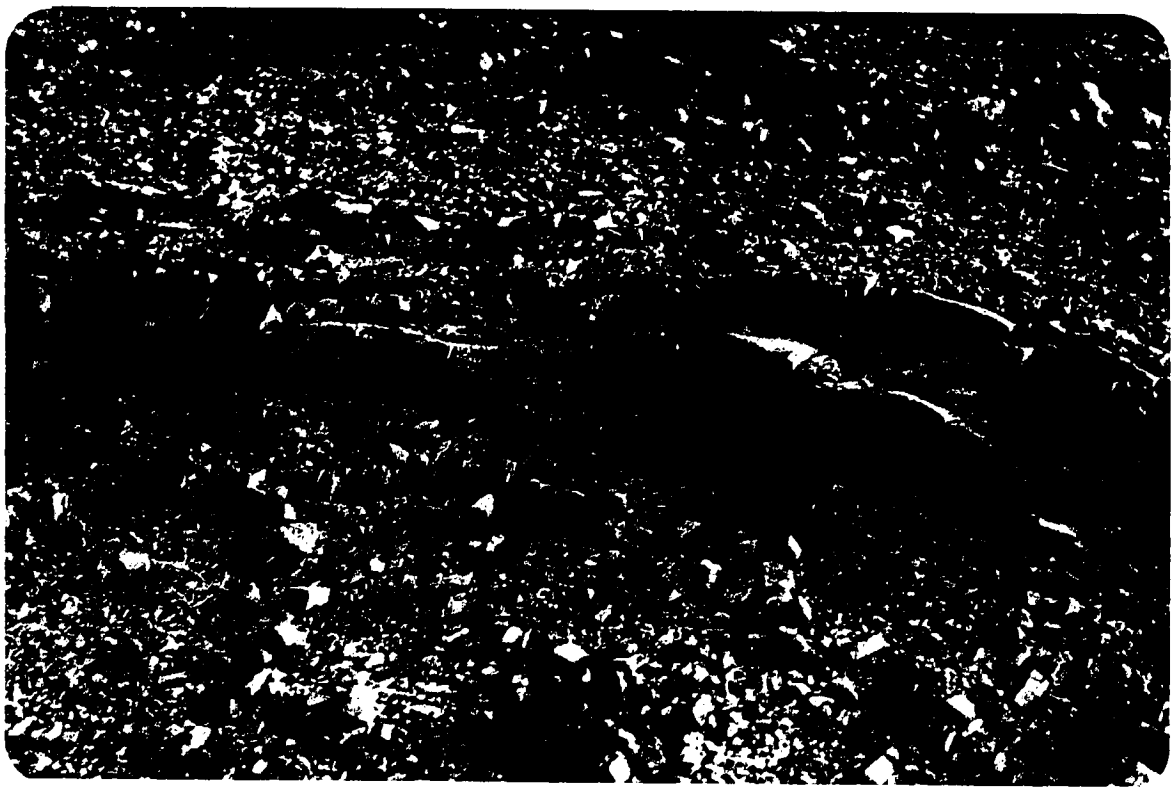

Field observations revealed that magnesite body in Zarghat area is hard, dense and massive white or grey. It is jointed and fractured, along shear zones it is highly brecciated. The contact between magnesite and the underlying bedded dolomite is clear. However, few lenses of magnesite of 1 m width and few meters length were found near the top of dolomite. These lenses are believed to have been enclosed by bedded dolomite as a result of diagenetic changes, involving the transformation of hydromagnesite to magnesite which was accompanied by shrinkage in magnesite volume and transformation of aragonite into dolomite. As a result of compaction and expelled formation water, the bedded dolomite enclosed few magnesite lenses near the top and penetrated throughout the whole magnesite body at different scales. Many sedimentary features like bedding, small scale anticlines and synclines were recorded. Stromatolitic laminations in dolomite were also observed. These stromatolites are very important in genetic interpretation of magnesite.

CHAPTER - 5

MINERALOGY AND TEXTURE OF MAGNESITE AND ASSOCIATED ROCKS

5.1 Introduction

A total of 90 samples of magnesite , closely associated bedded dolomite, and vein dolomite were studied by various laboratory techniques for the mineralogical and texural characterization. The results of these investigations are presented in this chapter.

5.2 Magnesite

Under the petrographic microscope the magnesite appears fine-grained to cryptocrystalline Fig. 5.1. Most of the samples show shearing producing micro-fragments of various sizes and shapes which are scattered in a crushed, relatively finer magnesite groundmass Fig. 5.2. Under SEM, the magnesite is observed to comprise compact clusters of anhedral crystals of magnesite Fig. 5.3 which are revealed by the high magnification of SEM. The chemical scanning done by SEM of the area shown in Fig. 5.3 gave a high Mg peak suggesting almost pure magnesite Fig. 5.4.

Fig.(5.1): Photomicrograph showing cryptocrystalline pure magnesite (Sample W-2, 800X, PP Light).

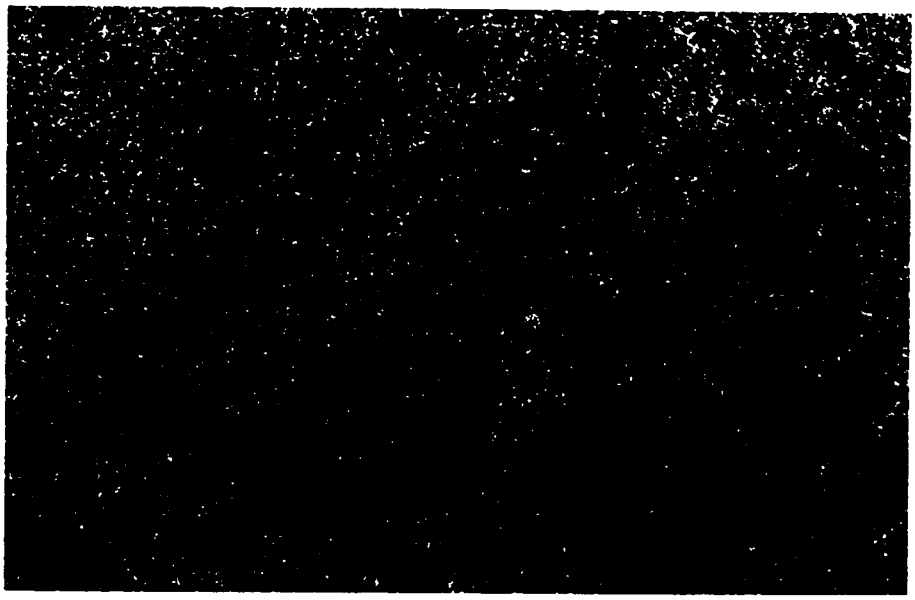

Fig.(5.2): Highly sheared magnesite (a) Sample C-8, 400X, PP Light (b) Sample C-23, 400X, PP Light.

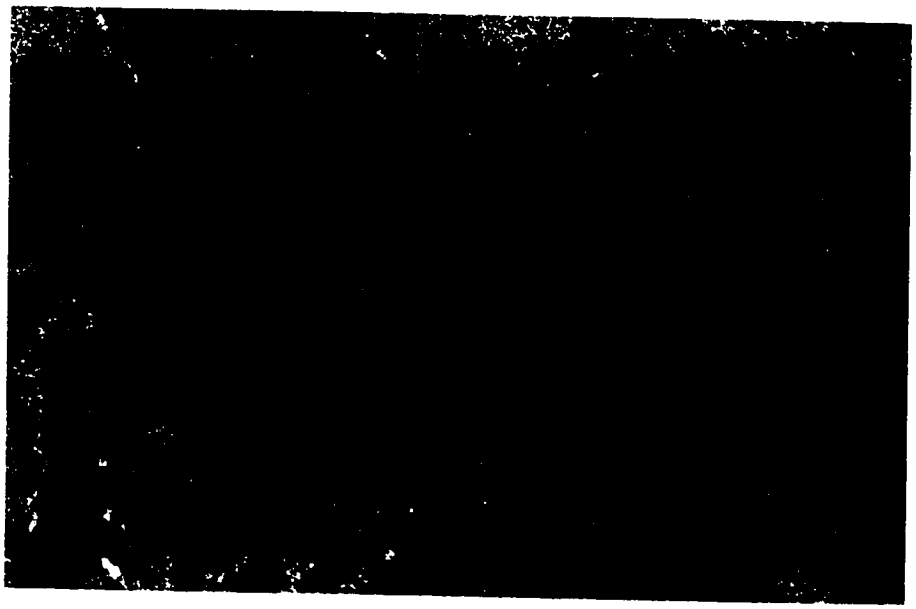

A

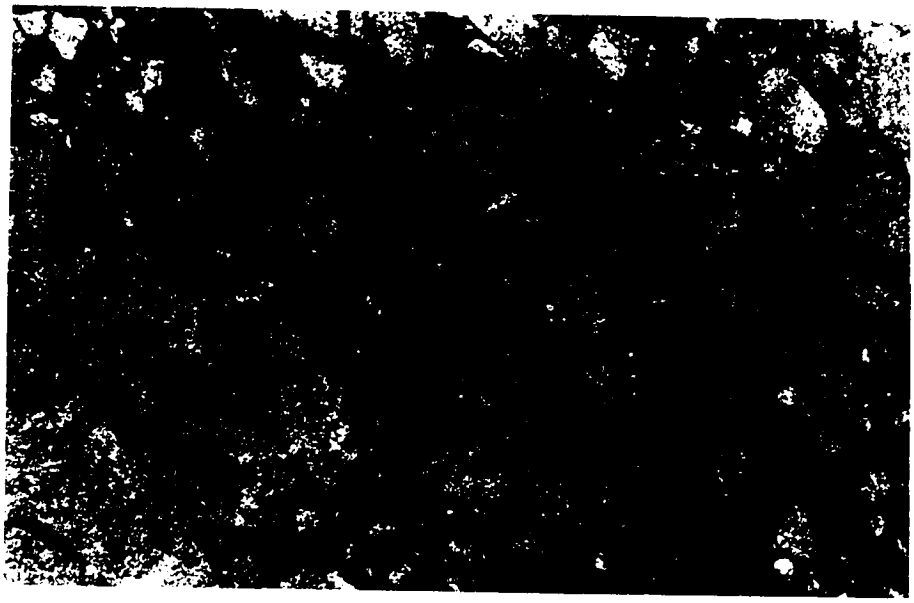

B

Fig.(5.3): SEM photomicrograph showing the cryptocrystalline nature of pure magnesite.

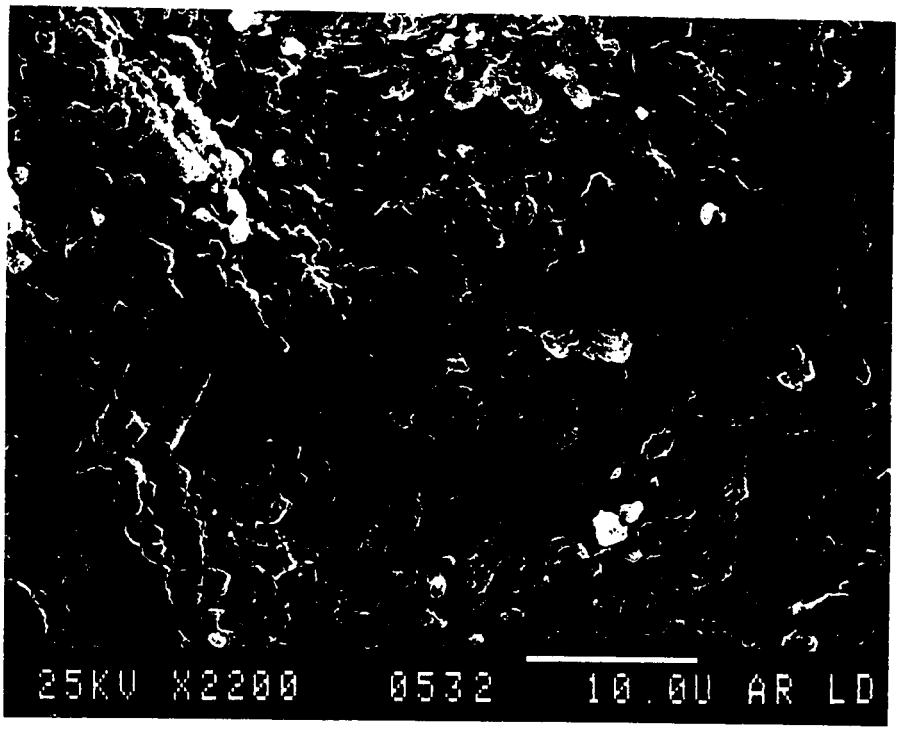
25KV X2200 0532 10.0U AR LD

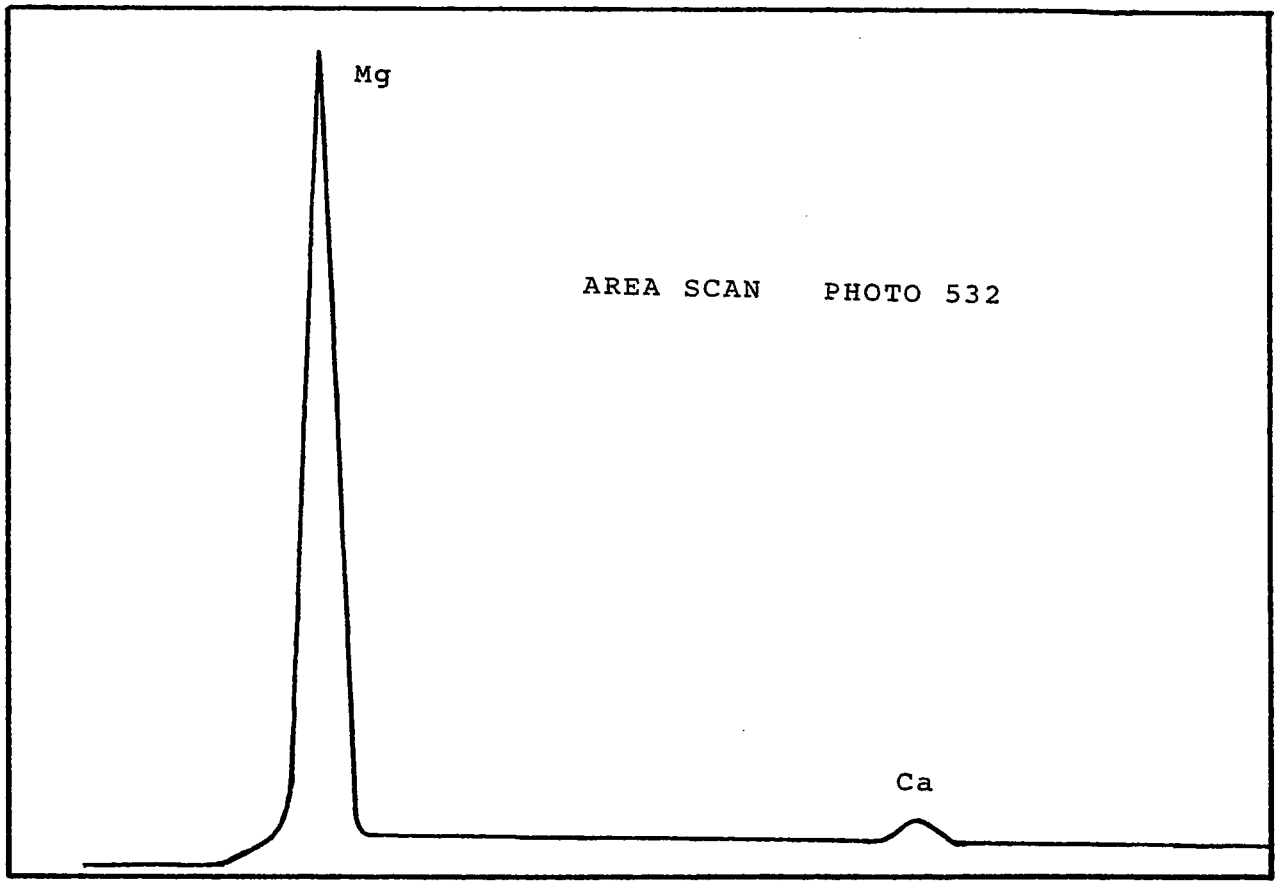

Fig.(5.4): Scanning area analysis for the magnesite area shown in Fig.(5.3).

Mineralogically, all the samples consist mostly of magnesite, containing various amounts of dolomite. The dolomite occurs in the form of minute veinlets scattered in most of the samples and represent the smallest category of the vein dolomite. In some thin sections perfect euhedral rhombic crystals of dolomite and calcite have developed in the shear zones. They were observed under both petrographic microscope Fig. 5.5 and SEM Fig. 5.6.

Fifty-two samples of magnesite were investigated by X-ray diffraction technique to study their mineralogical characteristics in more detail. The X-ray diffraction results obtained were in the form of diffractograms. A typical diffractogram for one of the magnesite sample is shown in Fig. 5.7. The horizontal axis shows the 2θ angle in degrees whereas the vertical axis shows the relative intensities of the peaks. The positions of various peaks in terms of 2θ angle can be read directly from the diffractogram, and can be calculated in terms of spacing between the atomic planes (interplanar spacing, commonly known as d-spacing, denoted as 'd') by the Bragg equation which is

$n\lambda = 2d \sin\theta$, where λ represents the wave length of the used X-ray radiation.

The positions of the peaks in terms of d-spacing are characteristic for the mineral phases and, therefore, are used in the identification of minerals. The three most characteristic peaks for the magnesite have

Fig.(5.5): Photomicrograph showing development of euhedral dolomite and calcite crystals in magnesite shear zone (Sample C-4, 1000X, PP Light).

Fig.(5.6): SEM photomicrograph showing growth of dolomite and few calcite crystals in magnesite shear zone.

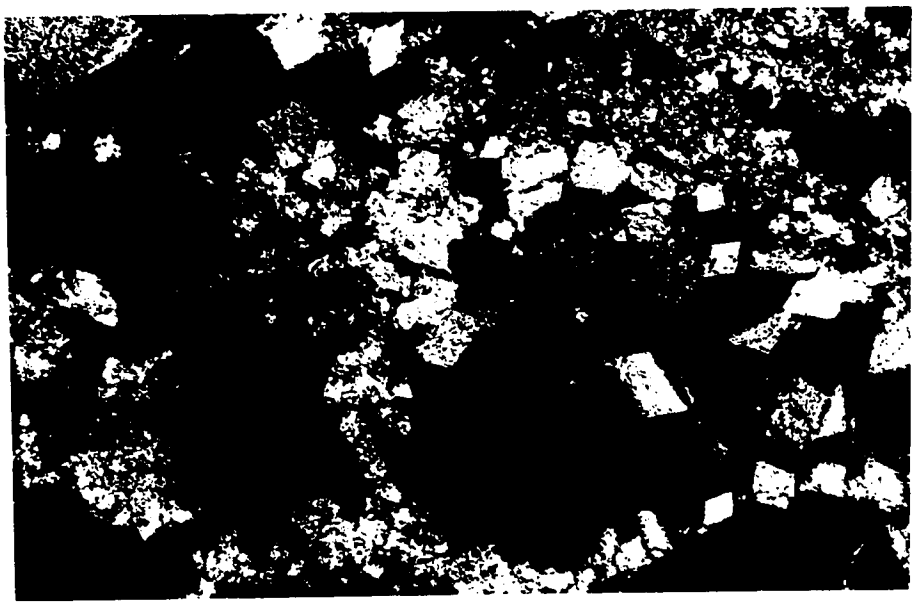

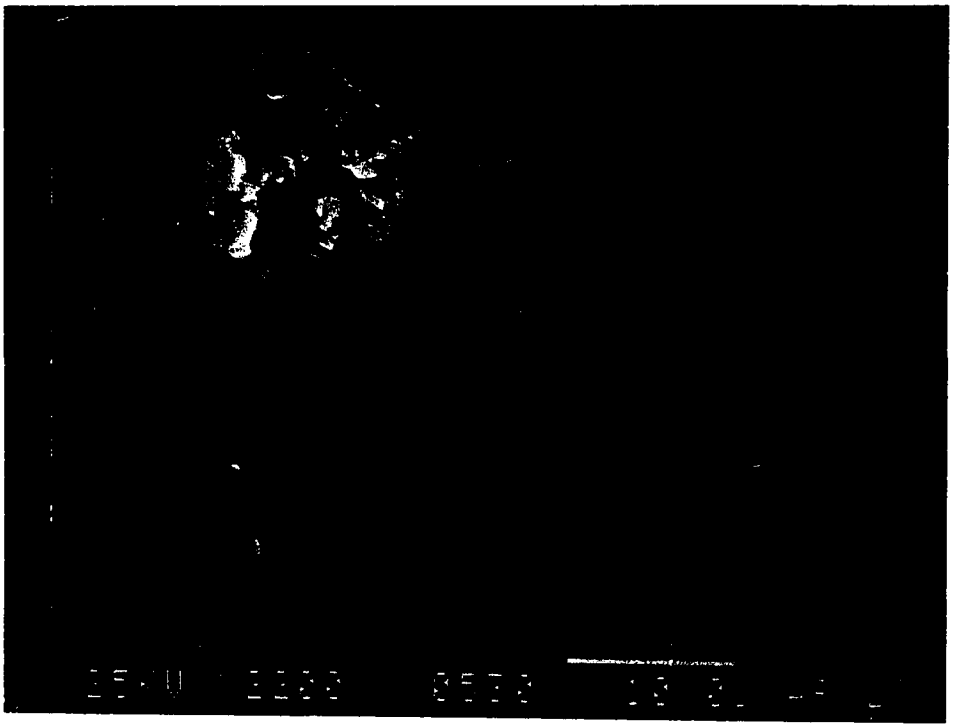

d-spacing values of 2.77 Å, 2.106 Å, and 1.70 Å (JCPDS card number 8-479).

All the magnesite samples tested by X-ray diffraction gave well developed characteristic peaks at or very close to the above mentioned d-spacing values. Out of 52 tested samples, 37 samples gave pronounced, characteristic magnesite peaks and minor dolomite peaks indicating almost pure magnesite with traces of dolomite. Fig.(5.7) shows the X-ray diffractogram of sample W-1 which is a representative of this group of samples. Complete X-ray diffraction data for these samples are shown in Appendix 1 where the most characteristic peaks are expressed in terms of d-spacing. The other 15 samples produced enhanced dolomite peaks besides the pronounced magnesite peaks, indicating an admixure of dolomite within magnesite making it impure in quality. Fig. 5.8 shows the X-ray diffractogram for sample E-4 which is a representative of this group of samples. Variation of relative amount of dolomite along a traverse in the central-hill is shown in Fig. 5.9. This variation diagram shows that near the contact with the underlying bedded dolomite there is a high dolomite content, whereas, towards the center of the hill, magnesite becomes almost pure. This may indicate the gradational contact from bedded dolomite to magnesite. Appendix 2 shows the X-ray diffraction data of the impure magnesite samples with the most characteristic peaks of magnesite and dolomite expressed in terms of d-spacing.

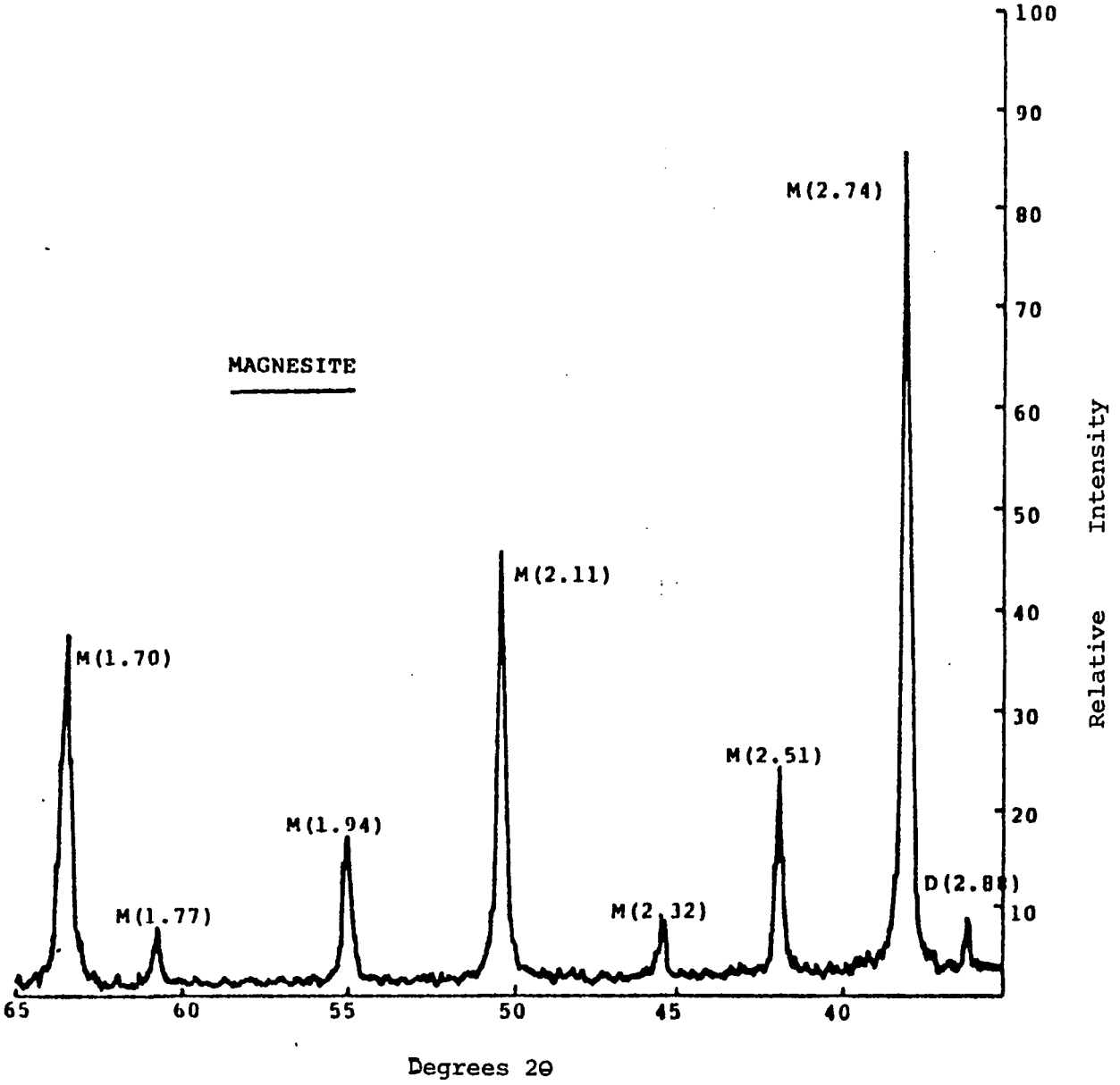

Fig.(5.7): X-ray diffractometer trace of Sample W-1
Symbols: M=Magnesite, D=Dolomite

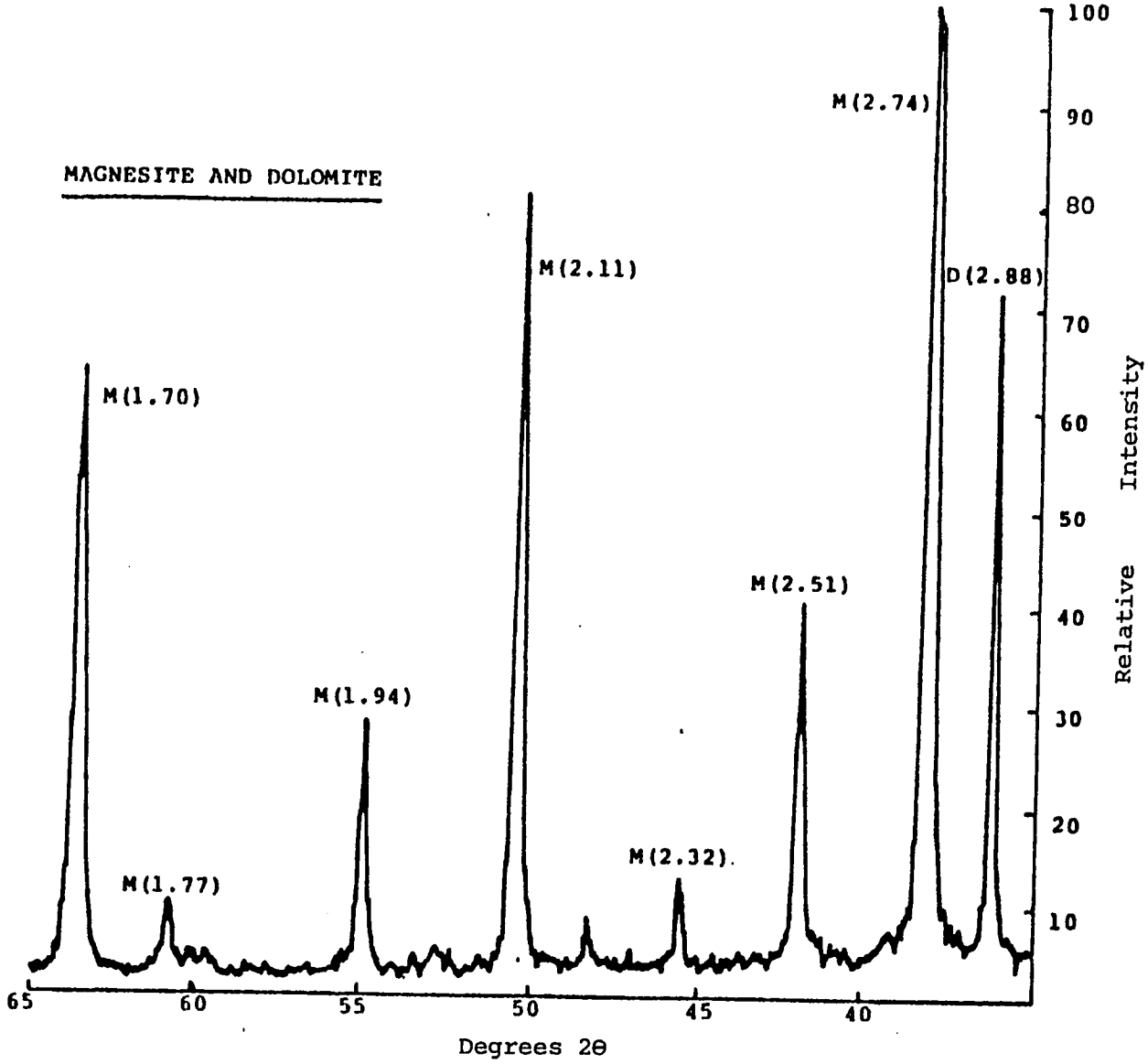

Fig.(5.8): X-ray diffractometer trace of Sample E-4
Symbols: M=Magnesite, D=Dolomite

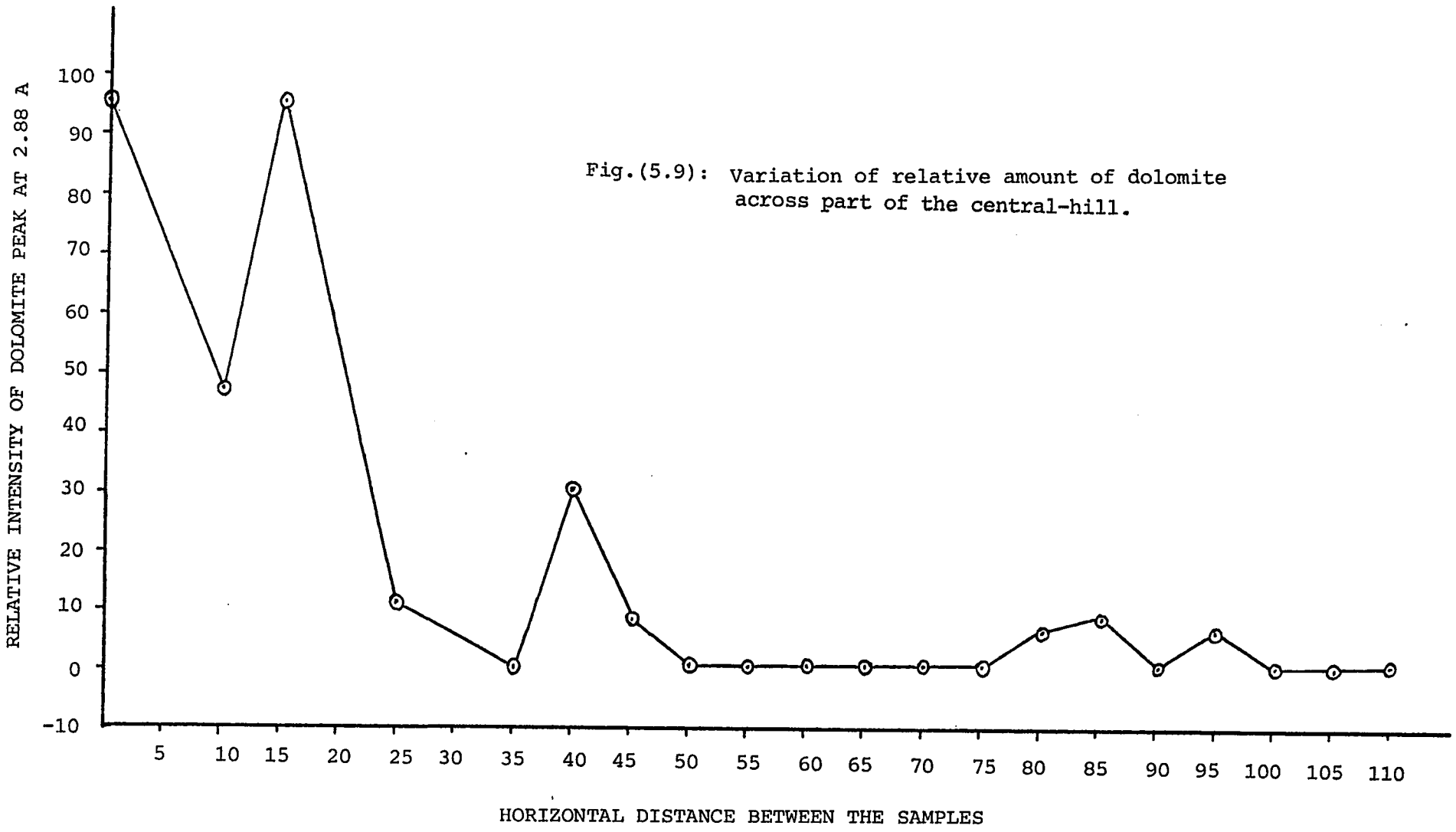

Fig.(5.9): Variation of relative amount of dolomite across part of the central-hill.

5.2.1 Thermal Behavior of Magnesite

Magnesite is an important basic refractory raw material; its thermal behaviour is, therefore, of great importance to evaluate its use for refractory purposes. A modern technique to test the thermal characteristics of minerals is the differential thermal analysis (DTA).

Differential thermal analysis (DTA) is a thermal technique in which both sample and an inert material are heated or cooled at a uniform rate. The temperature of the sample compared with the temperature of the thermally inert material, is recorded as a function of sample, inert material, or furnace temperature. Temperature changes in the sample are due to endothermic or exothermic transitions or reactions such as those caused by phase changes, fusion, crystalline structure inversions, dehydration reactions, decomposition, and other chemical reactions.

The temperature changes are detected by a differential method where the difference in temperature between the sample and reference substance is the function recorded.

The number, shape, and position of the various endothermic and exothermic peaks with reference to the temperature may be used as a mean in identification of the mineral or substance under investigation.

As most carbonate mineral decompositions are accompanied by the absorption of large amounts of energy, they generally give well-pronounced and simple DTA peaks. The simplicity of the curves for most carbonates permits their identification by means of DTA only.

Endothermic decomposition with the liberation of carbon dioxide is the most distinctive DTA property of carbonates. The rate at which carbon dioxide is evolved during heating varies considerably, not only from carbonate to carbonate but even, depending on experimental conditions for the same carbonate.

Polymorphic transitions in carbonates are usually of small magnitude and may be reversible like the transition in strontium carbonate at 900° C - or irreversible like the aragonite-calcite transformation at about 450°C (Wendlandt, 1974)

Sengupta and others (1980), studied the thermal behaviour of Salem magnesite, India. DTA analyses gave the decomposition peak range from 690°C to 700°C. To compare the thermal behaviour of Zarghat magnesite with Salem magnesite as an example, DTA analyses were carried out on 54 magnesite samples collected from the magnesite exposures.

Appendices 3, 4, and 5 show the peak temperatures and ranges for the 54 magnesite samples representing the main three hills.

Fig. 5.10 shows the DTA curve for sample W-10 which represents the pure magnesite type, where the only recorded peak is that of magnesite at 628°C. Fig. 5.11 shows the DTA curve for sample C-17 which represents the impure magnesite type, where two peaks were recorded, the first one at 622°C characterizing magnesite, and the second one at 812°C characterizing dolomite.

Decomposition temperature of Zarghat magnesite as revealed by DTA analyses is about 620°C. Although this peak temperature, as stated before, varies depending on many factors, yet, the results show relatively lower decomposition temperature than Salem magnesite.

5.3 Bedded Dolomite

Thin sections of bedded dolomite appear cryptocrystalline under petrographic microscope. The rocks are composed predominantly of dolomite with a few grains of quartz, plagioclase and iron oxides. Microcrystalline silica has been observed, occuring as minute veinlets, in which the grains are arranged in a mosaic pattern Fig. 5.12. Some of the plagiocalse grains display albite twinning Fig. 5.13.

X-ray diffraction investigation on 18 bedded dolomite samples were carried out. Six bedded dolomite samples gave only pronounced dolomite peaks of 2.886 Å, 2.192 Å, and 1.78 Å. Fig. 5.14 shows the X-ray diffractogram of a representative sample (C-43).

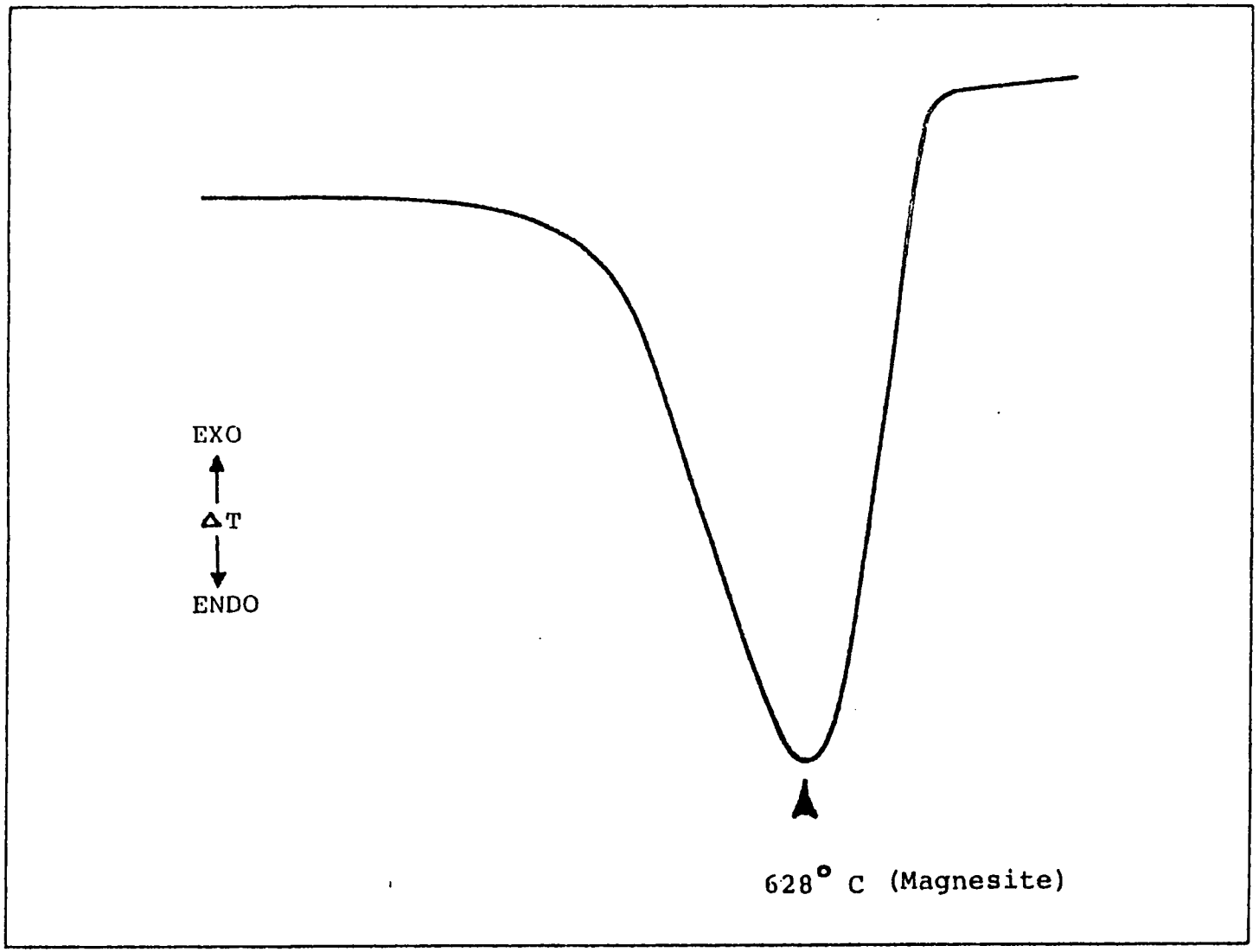

Fig.(5.10): General DTA curve for pure magnesite

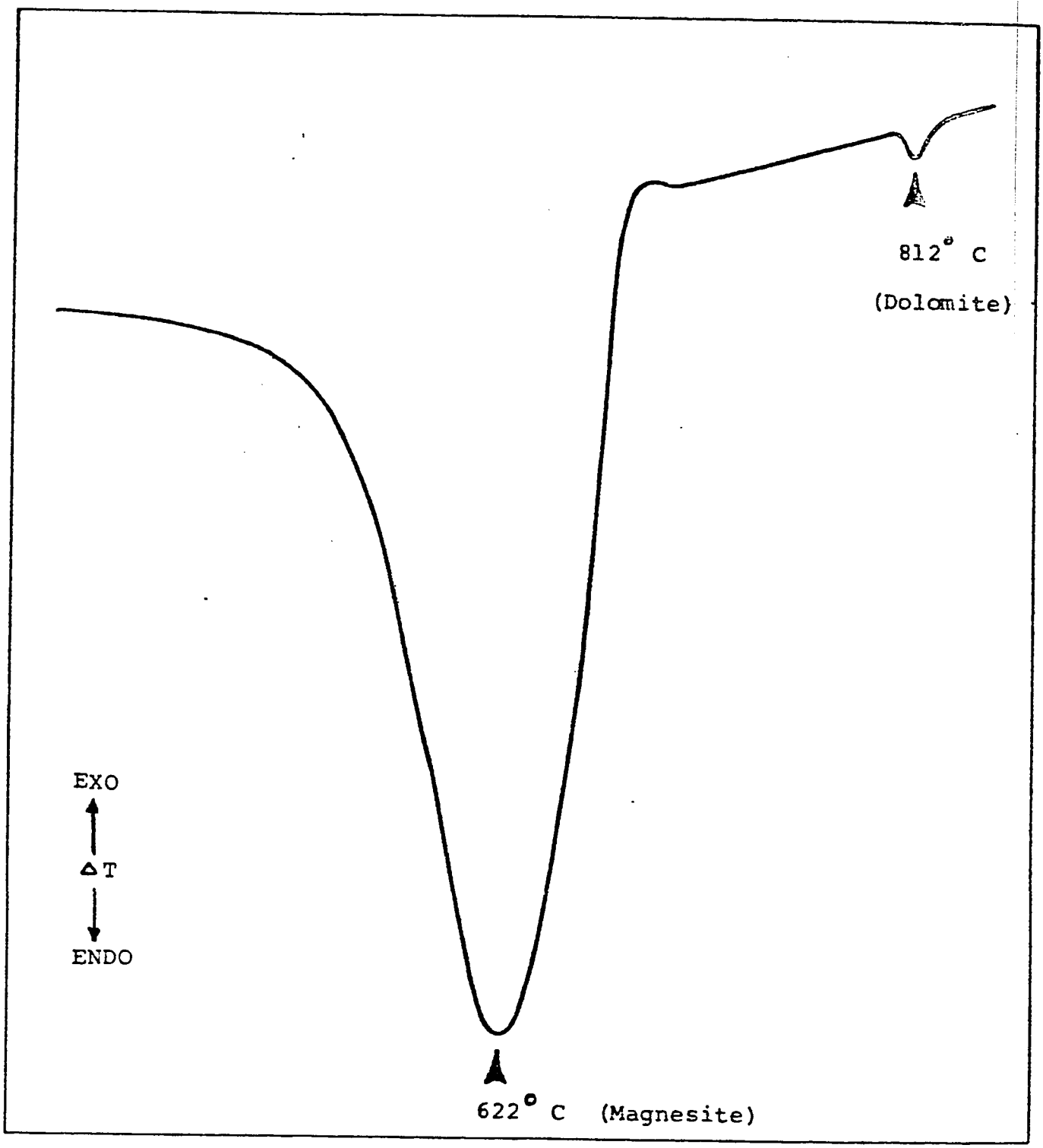

Fig.(5.11): General DTA curve for impure magnesite

Fig.(5.12): Photomicrograph showing cryptocrystalline nature of bedded dolomite and a veinlet consisting of closely interlocked quartz crystals in the form of mosaic pattern (Sample E-28, 400X, x-nicols).

Fig.(5.13): Photomicrograph showing albite twinning in plagioclase crystal in bedded dolomite (Sample C-46, 1000X, x-nicols).

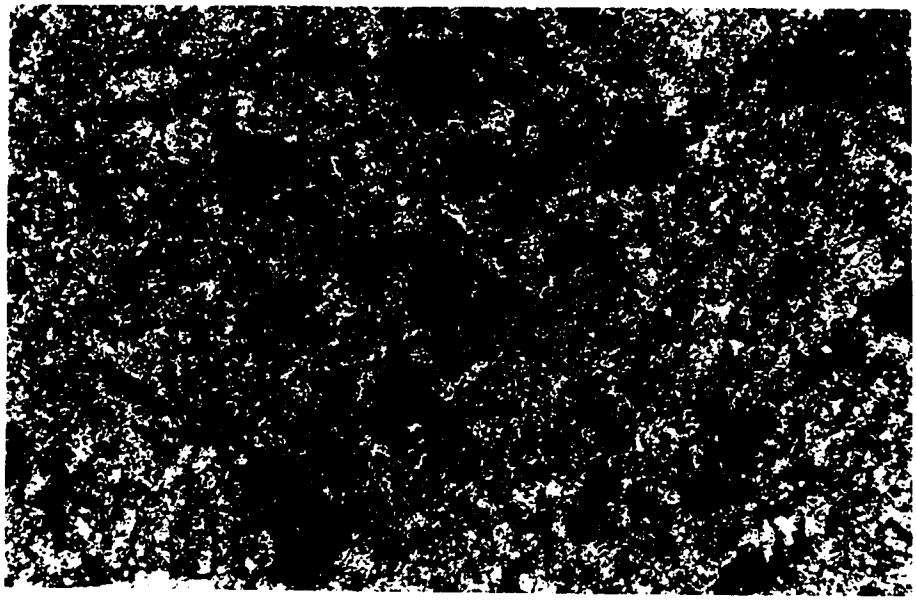

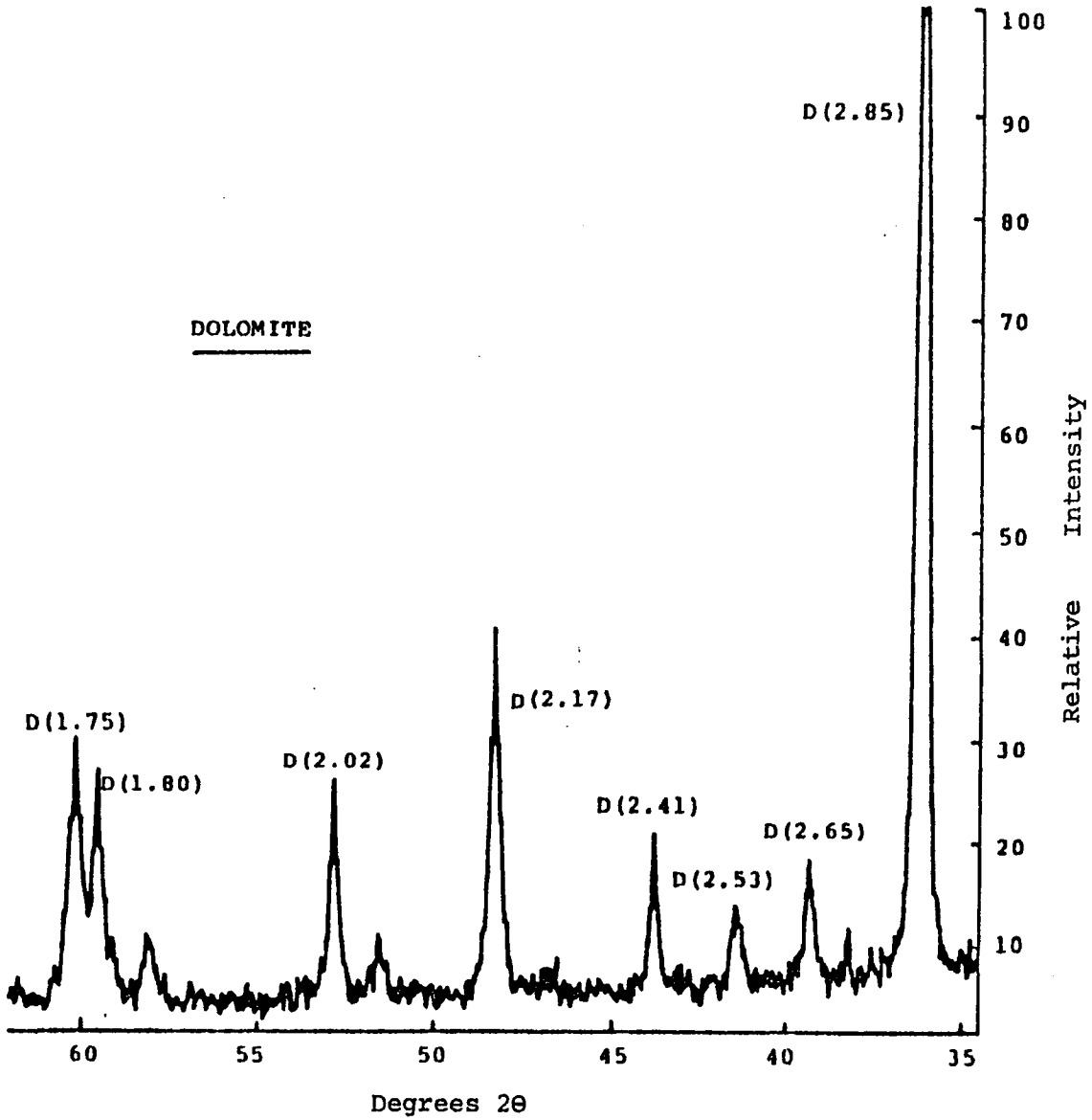

Fig.(5.14): X-ray diffractometer trace of Sample C-43
Symbols: D=Dolomite

Twelve bedded dolomite samples produced, besides dolomite peaks, also peaks characteristic of magnesite (2.744 Å, 2.106 Å, and 1.700 Å), calcite (3.035 Å, 2.282 Å, and 2.095 Å) , and quartz (3.348 Å, 2.461 Å, and 1.819 Å). Representative X-ray diffractograms for this type of samples are shown in Fig. 5.15 and Fig. 5.16.

These results indicate that some bedded dolomite samples also contain magnesite, calcite and quartz. On the basis of the microscopic observations and X-ray data the bedded dolomite can be classified into two groups, pure dolomite and impure dolomite. The X-ray diffraction data in the form of d-spacing for the pure dolomite and impure dolomite groups are shown in Appendices 6 and 7 respectively.

5.4 Vein Dolomite

Under petrographic microscope dolomite from thick veins was found to be composed mostly of fine-grained dolomite. Some of the samples are mesocrystalline with interlocking euhedral to subhedral crystals of dolomite, making a mosaic pattern Fig. 5.17. This is particularly typical of grey dolomite veins.

The small dolomite veinlets which cut through the magnesite samples are generally fine-grained but some of them are mesocrystalline or macrocrystalline. Occasionally, they also contain calcite crystals which are interlocked in a mosaic pattern with the dolomite crystals. The

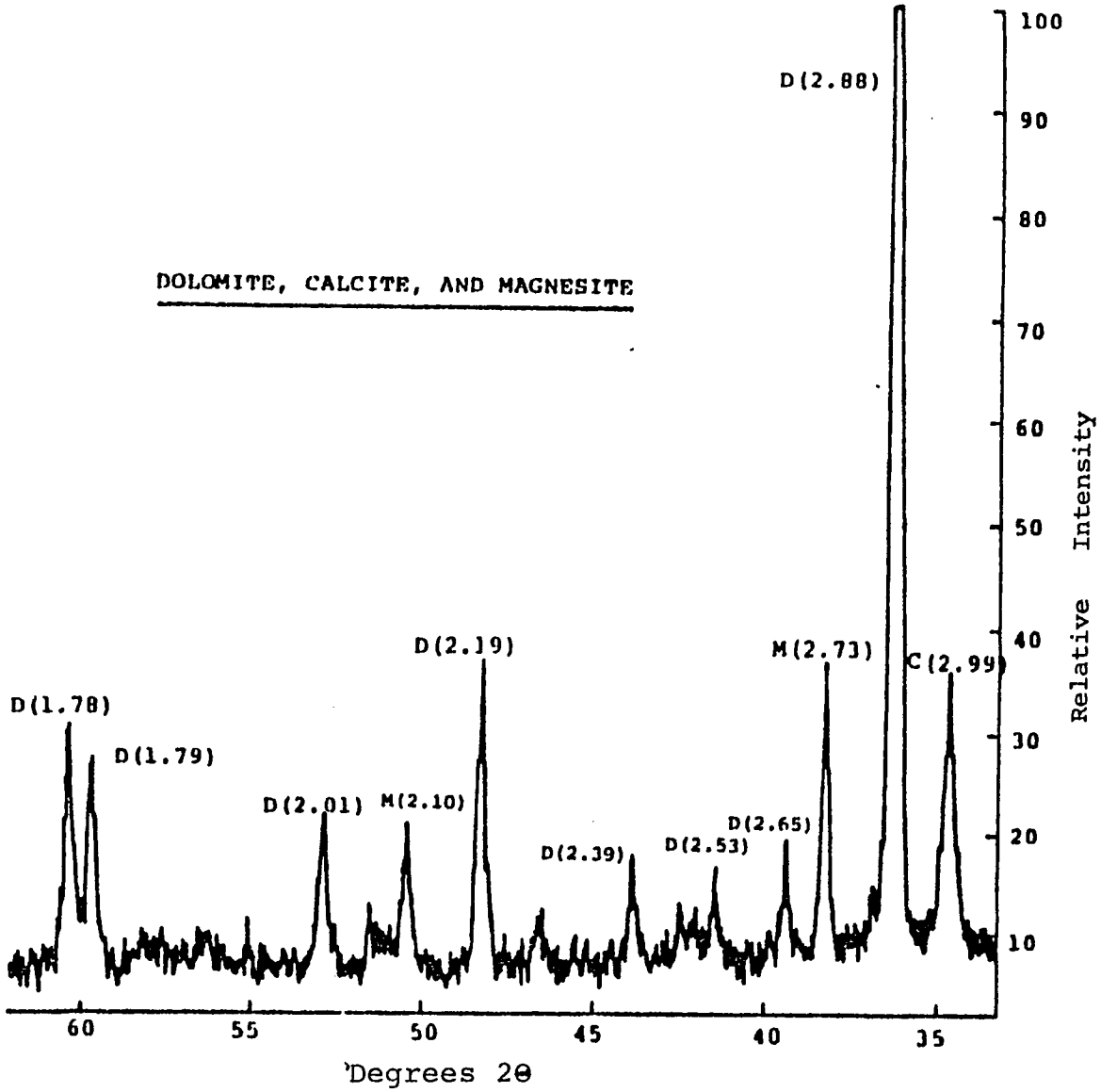

Fig.(5.15): X-ray diffractometer trace of Sample W-15A

Symbols: D=Dolomite, M=Magnesite, C=Calcite

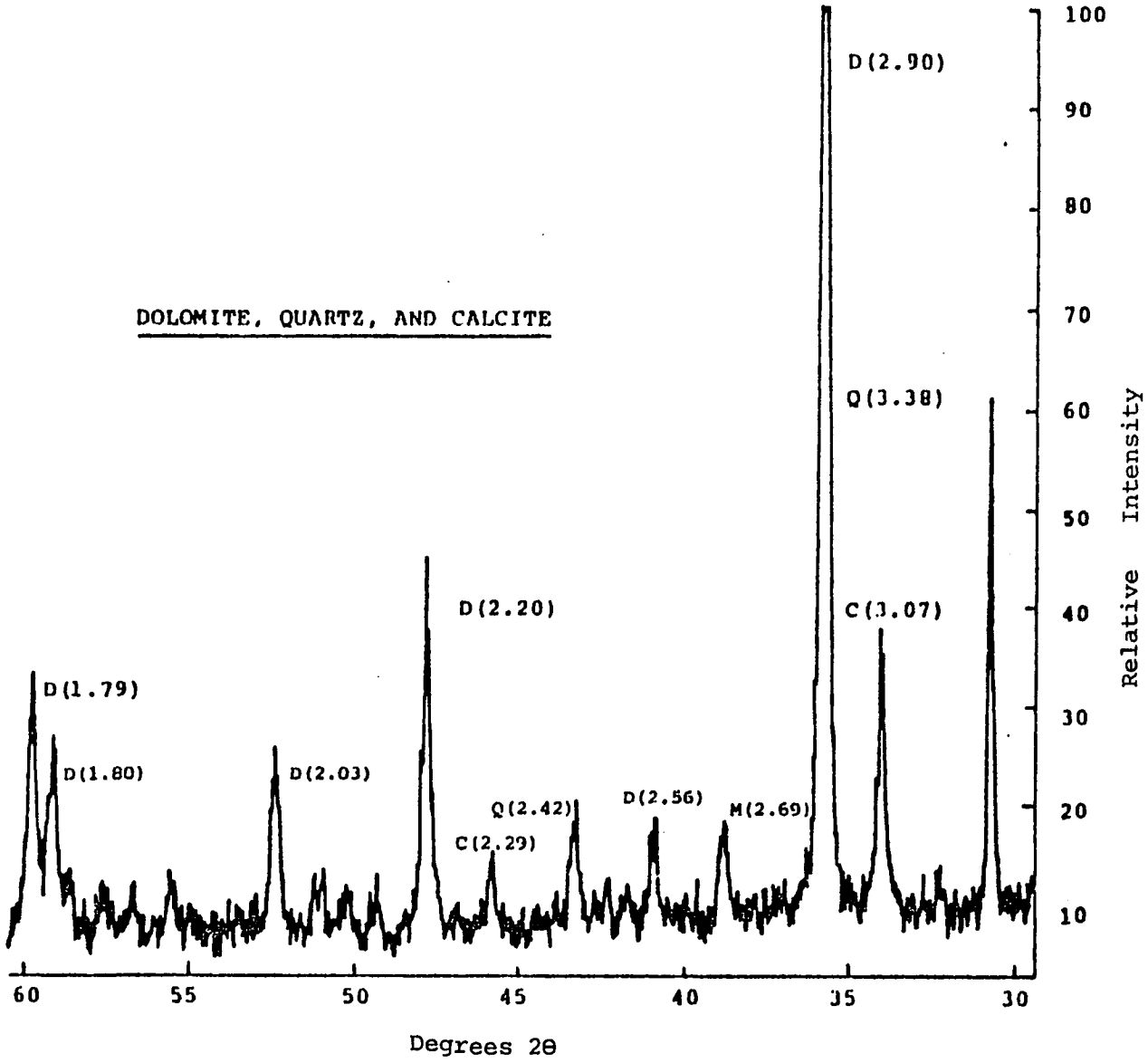

Fig.(5.16): X-ray diffractometer trace for Sample W-14
Symbols: D=Dolomite, Q=Quartz, C=Calcite

Fig.(5.17): Photomicrograph showing a mosaic of euhedral to subhedral dolomite crystals in vein dolomite (Sample E-29, 800X, x-nicols).

Fig.(5.18): Photomicrograph showing macrocrystalline dolomite veinlet and growth of calcite crystals with clear rhombohedral cleavage (Sample E-2, 400X, PP Light).

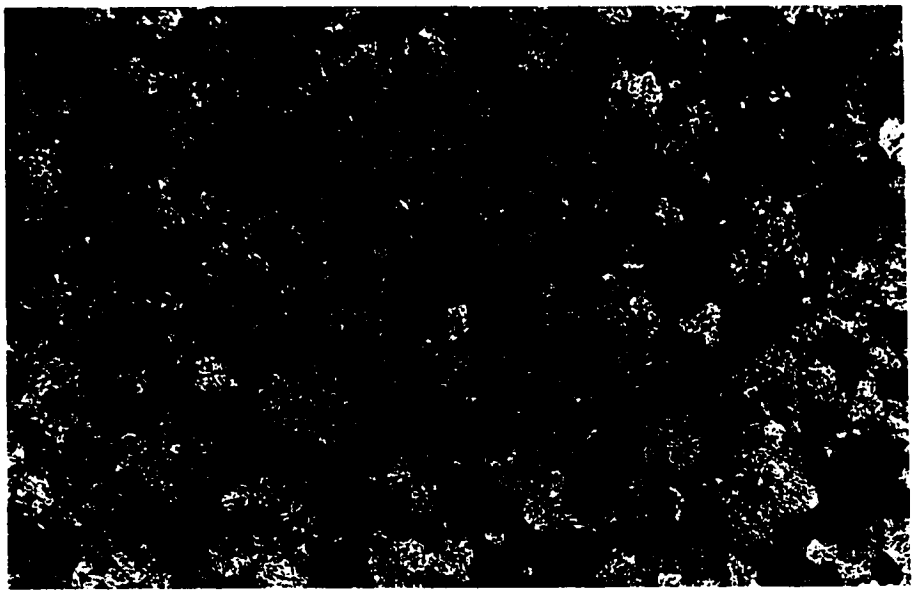

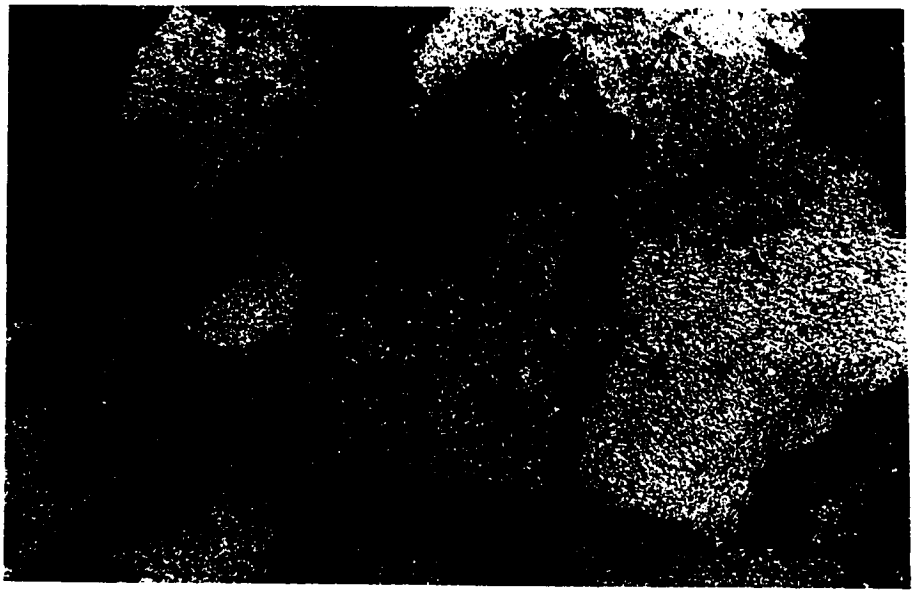

calcite crystals display rhombohedral cleavage Fig. 5.18. Under SEM, euhedral dolomite crystals with fully developed faces were found to constitute the vein Fig. 5.6), the occasional calcite crystals with rhombohedral cleavage were also identified. Some thin vein dolomite have remnants of magnesite grains within the veins Fig. 5.19. In places these fine dolomite veinlets were also seen offsetting each other Fig. 5.20. The dolomite veinlets have grown mostly along the brecciated zones in magnesite Fig. 5.21, sometimes intersecting the magnesite grains Fig. 5.22.

Other minor accessory minerals present in samples of thick dolomite veins include feldspar (microcline), quartz, and iron oxides. The microcline grains show characteristic cross-hatched twinning, and some grains have corroded boundaries Fig. 5.23.

Ten samples from vein dolomite were investigated by X-ray diffraction. The diffractogram of sample C-31 Fig. 5.24 shows pronounced peaks for both dolomite and magnesite. This sample (C-31) has been collected from the dolomite vein near its contact with magnesite. Fig. 5.25 shows the diffractogram for sample C-38 collected from the center of the same dolomite vein. In this sample, peaks for calcite and quartz, in addition to those of dolomite were recognized in the diffractogram, but no magnesite peaks were present. The X-ray diffraction results are given in Appendix 8.

Fig.(5.19): Photomicrograph showing remnants of magnesite (black color) enclosed by vein dolomite (Sample W-5, 800X, PP Light).

Fig.(5.20): Photomicrograph showing offsetting of dolomite veinlets (Sample E-4, 400X, PP Light).

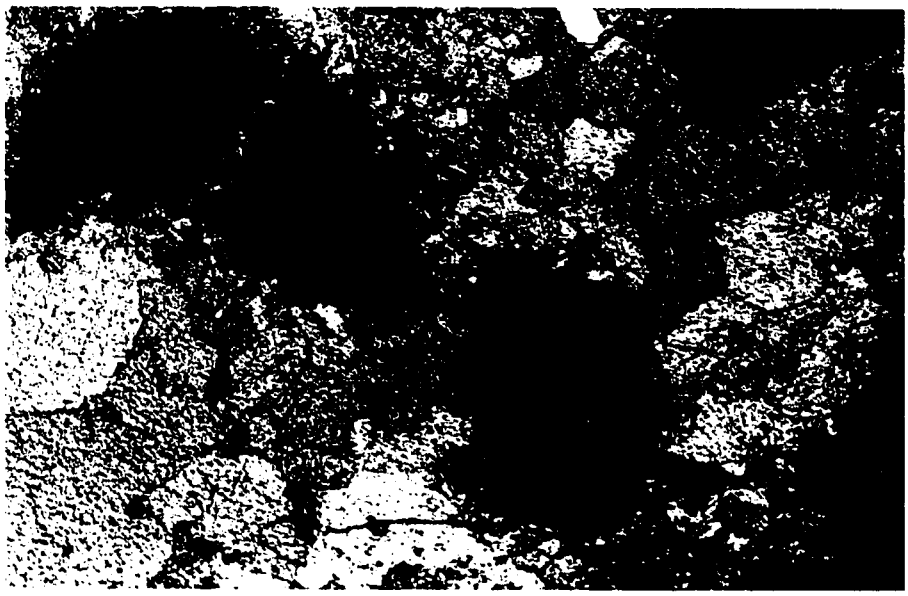

Fig.(5.21): Photomicrograph showing veinlets of fine-grained dolomite intergrowth along shear zone in magnesite (a) Sample E-2, 400X, x-nicols (b) Sample E-2, 800X, x-nicols.

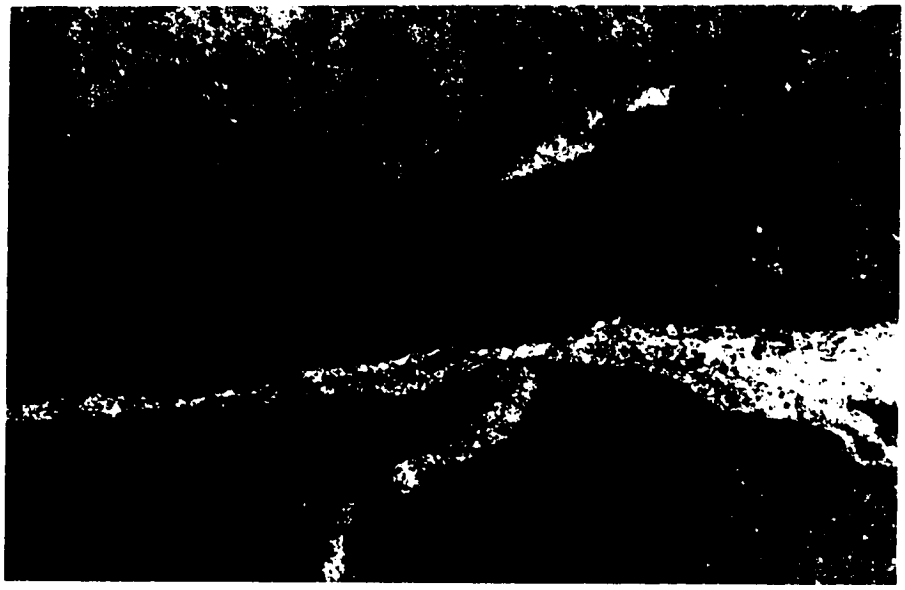

A

B

Fig.(5.22): Photomicrograph showing dolomite veinlets intersecting the magnesite grains (Sample C-8, 400X, PP Light).

Fig.(5.23): Photomicrograph showing the mineralogical composition of the vein dolomite (a) Quartz grain shows undulatory extinction (Sample W-15, 800X, x-nicols) (b) Feldspar grain with corroded boundary (Sample C-28, 800X, x-nicols) (c) Microcline (cross-hatched twinning) intersected by dolomite veinlets (Sample C-27, 500X, x-nicols) (d) Dolomite, quartz, and microcline (Sample C-28, 800X, x-nicols).

A

B

C

D

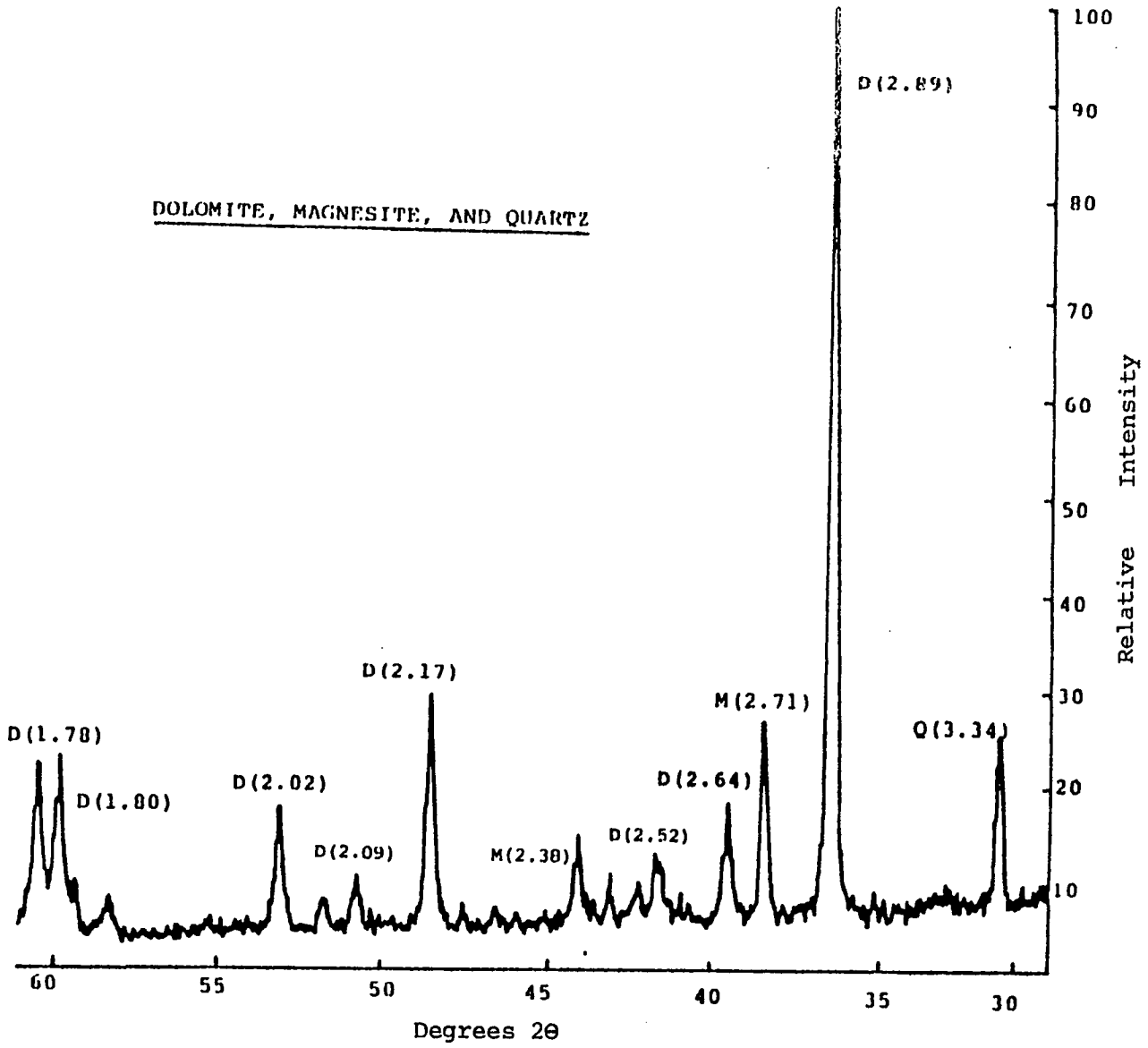

Fig.(5.24): X-ray diffractometer trace of Sample C-31
Symbols: D=Dolomite, Q=Quartz, M=Magnesite

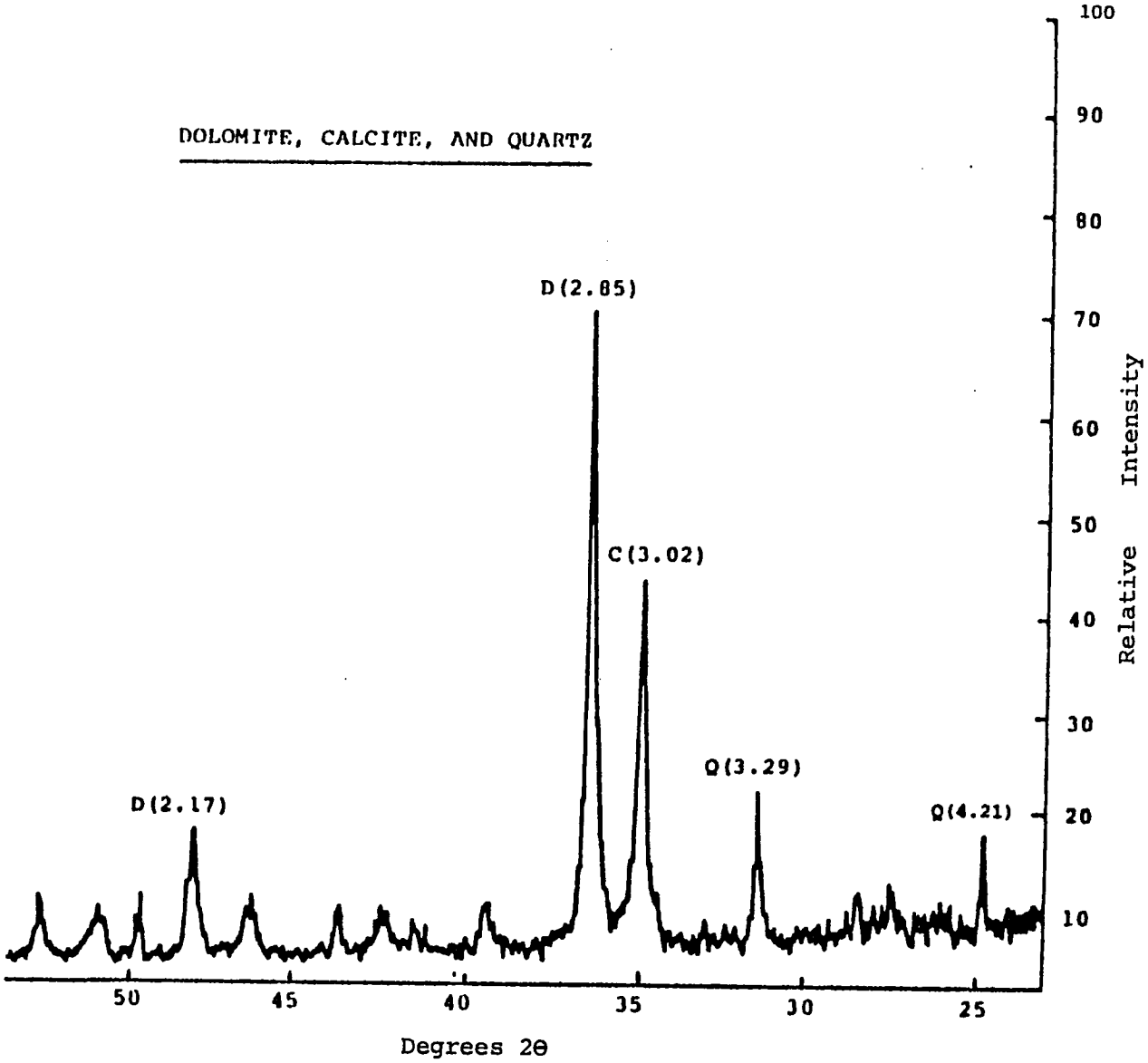

Fig.(5.25): X-ray diffractometer trace of Sample C-38
Symbols: D=Dolomite, C=Calcite, Q=Quartz

Laboratory studies revealed that the magnesite in Zarghat is of cryptocrystalline nature, consisting of anhedral fine-grained magnesite crystals (pure magnesite), or, contains dolomite as well (impure magnesite). Brecciation was also observed under the microscope and along highly brecciated zones developement of dolomite veinlets took place. More than one phase of these dolomite veins were recorded, intersecting each other or intersecting the pre-existing magnesite grains themselves. These dolomite veinlets might have been formed as the result of hydromagnesite-magnesite transformation. The excess water, which deposited these dolomite veinlets along fracture zones, originated as a result of volume shrinkage of magnesite during diagenesis.

Near the edges of the magnesite body, enrichment of dolomite was detected while towards the center magnesite becomes pure. This observation indicates the gradational change from dolomite to magnesite.

Many magnesite remnants enclosed by vein dolomite were recorded; they indicate the paragenesis of the two phases. The dolomite was formed later than magnesite as revealed also by the corroded edges of the enclosed magnesite grains.

DTA study showed that the decomposition temperature of the Zarghat magnesite is about 620°C, which is very important in considering the industrial uses of the magnesite.

Very few grains of plagioclase, quartz, and microcline were observed in bedded dolomite. Recrystallization of both silica and dolomite was observed in magnesite, this may indicate the relative high temperature nature of the solutions responsible for the diagenetic changes.

CHAPTER - 6

GEOSTATISTICS

6.1 General Introduction

Geostatistics may be defined as the application of the theory regionalized variables. The theory is very general and has found applications in many fields in the earth sciences including mineral evaluation. Regionalized variable describes the variable whose value is dependent on its position (Matheron, 1971).

Geostatistics has been used in the present study to reveal the spatial distributions of the selected variables from Zarghat magnesite deposit. Firstly, semivariogram, the basic tool in the study of spatial distribution, and the spherical model (most commonly used model), will be presented. These will be followed with the presentation of results and discussions on Zarghat magnesite deposit.

6.1.1 Semivariogram

Semivariogram is defined theoretically as the half of the mean squared difference between the values of a regionalized variables (e.g. MgO% or CaO% values within the orebody)

The mathematical expression for experimental semivariogram is:

$$\gamma(h) = \Sigma[f(x+h) - f(x)]^2 / 2N(h) \quad \text{(1)}$$

where N(h) is the total number of data pairs separated by a vector h, and f(x) is the value of the variable at point x.

6.1.2 Cross-semivariogram

The cross-semivariogram is defined as the half of the co-variance of the increments of two different regionalized variables and mathematically expressed by the following equation:

$$\gamma_{cm}(h)=\Sigma[(f_c(x+h)-f_c(x)(f_m(x+h)-f_m(x))]/2N(h) \quad \text{(2)}$$

where fg(x) and fy(x) are, the values of two regionalized variables (e.g. CaO% and MgO%) at point x in the ore body.

6.1.3 Geological Features Revealed by Semivariogram

The shape of the semivariogram depends on the spatial characteristics of the regionalized variable. This fact is the basis of the qualitative uses of the semivariogram in interpreting the geological characteristics. Semivariogram can reveal the following characteristics:

(i) Continuity

The continuity is reflected by the rate of growth of $\gamma(h)$ for small values of h. In other words, the continuity of the variable is a function of the behaviour of the semivariogram at the origin. As shown in Fig. 6.1 four types of behaviour could be distinguished.

1) Continuous type, has a parabolic behaviour at the origin representing regionalized variable with high continuity as in the case of most sedimentary deposits.
2) Linear type, is characterized by an oblique tangent at the origin, and represents a variable with average continuity.
3) Nugget type, reveals a discontinuity at the origin and corresponds to a variable representing a nugget variance.
4) Random type, represents a purely random behaviour, i.e. samples are uncorrelated at sampling interval used.

(ii) Zone of Influence

The zone of influence is the zone beyond which the influence of a sample disappears. It is the distance at which the semivariogram reaches plateau (see Fig. 6.2).

(iii) Anisotropies

It is indicated by different $\gamma(h)$ values in different directions.

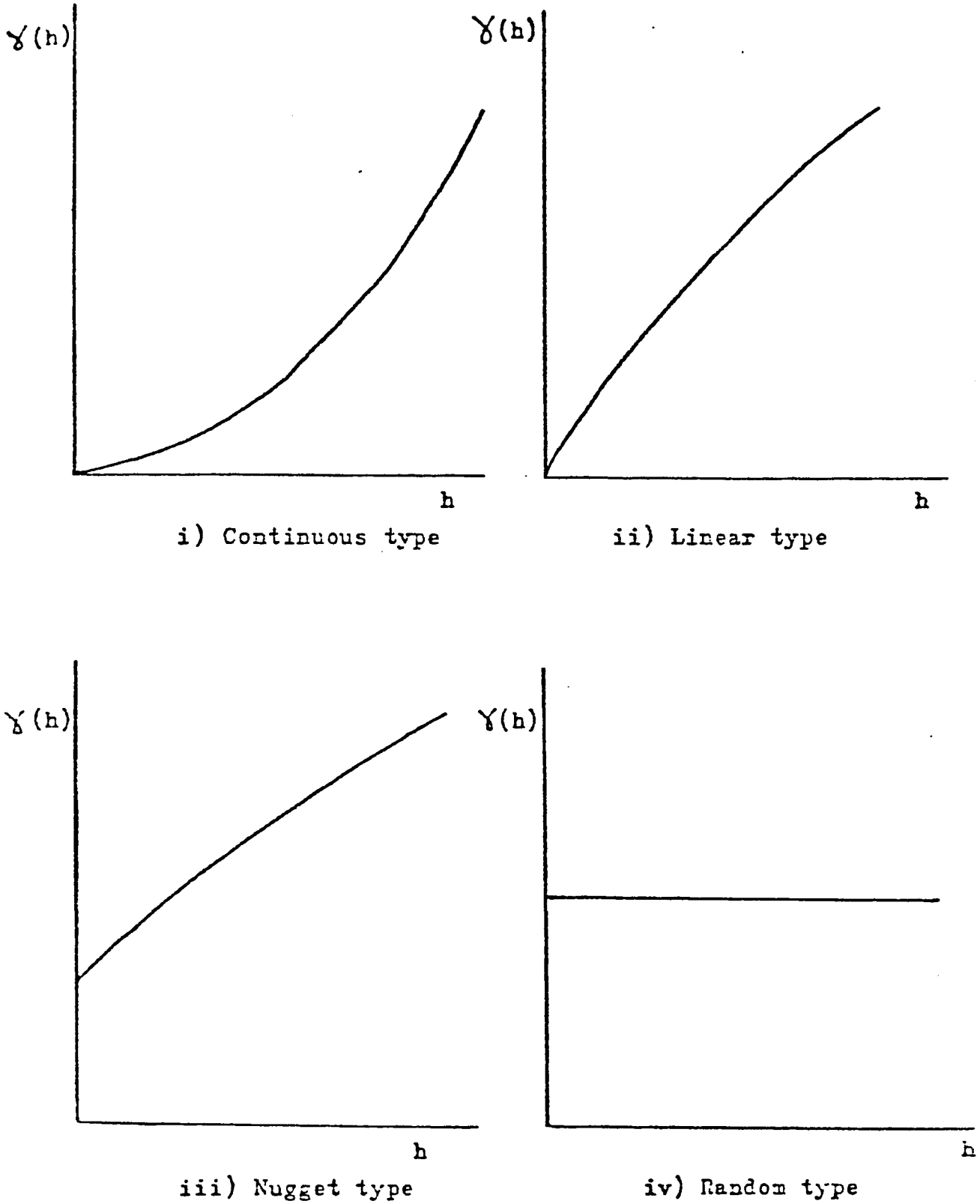

Fig.(6.1): Behaviour of variogram near origin (after, Sahin, 1977).

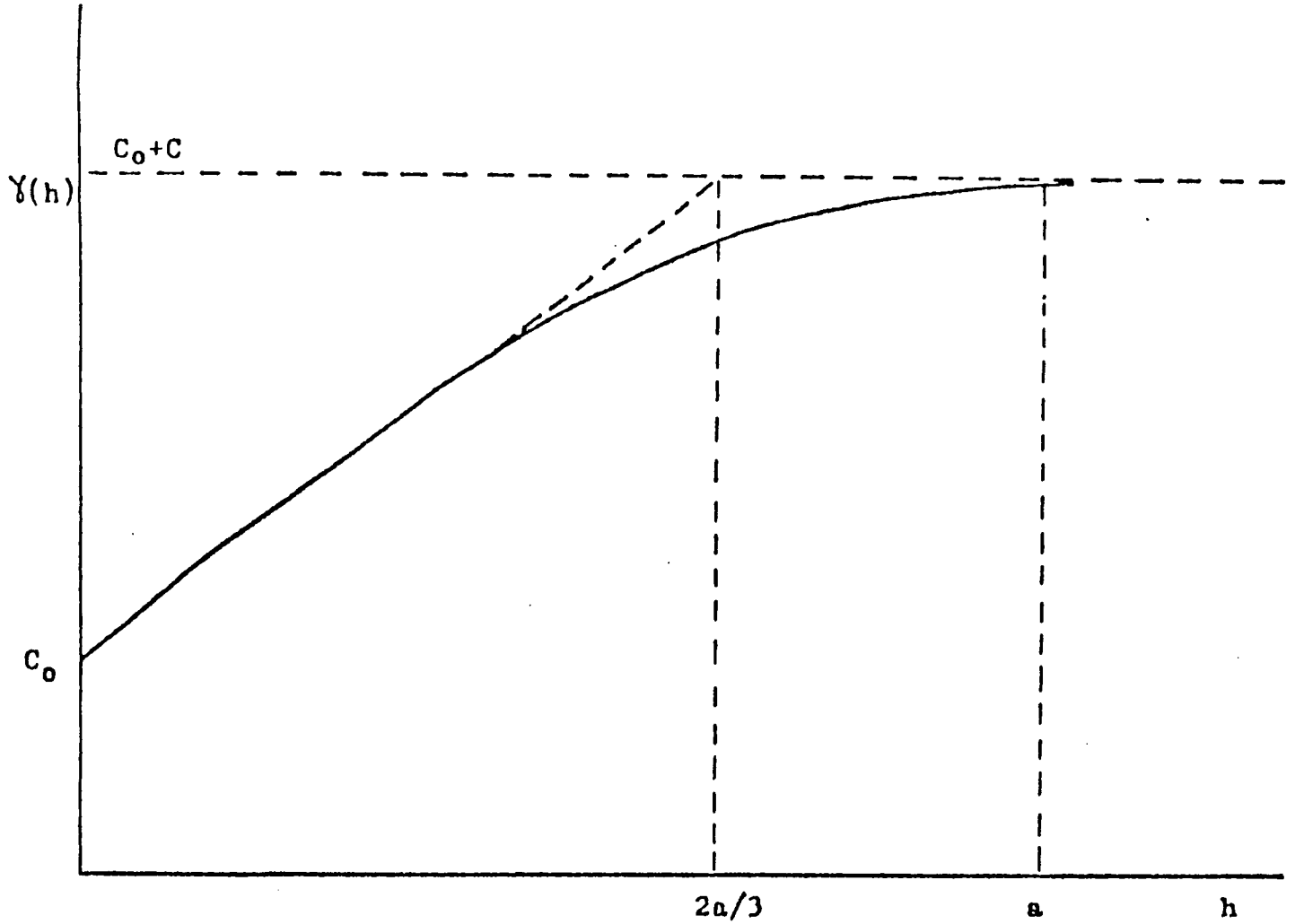

Fig.(6.2): Spherical model illustrating transition phenomenon (after, Sahin, 1977).

If $\gamma(h)$ functions in different directions are identical with each other, the regionalization is said to be isotropic.

If, on the other hand, $\gamma(h)$ functions in different directions are not identical, the regionalization is said to be anisotropic. There are two types of anisotropy: (a) geometrical anisotropy, is indicated by different ranges in different directions, which means that the zone of influence of the samples are not the same in all directions, (b) zonal anisotropy, is represented by different sill and range values in different directions. Diagrams illustrating anisotropy are given in Fig. 6.3.

6.1.4 Transition Phenomenon

This phenomenon is indicated by the semivariogram function having constant value beyond the range; and characteristic of most sedimentary deposits. The range in a particular direction, gives the approximate dimension of geological structures such as lenses or bedding in that direction.

6.1.5 The Spherical Model

The spherical model shown in Fig. 6.2. is the most commonly used model (David, 1977). This model has also been found to be applicable to the studied variables in Zarghat magnesite deposit. The details of model fitting have been discussed by several authors including David

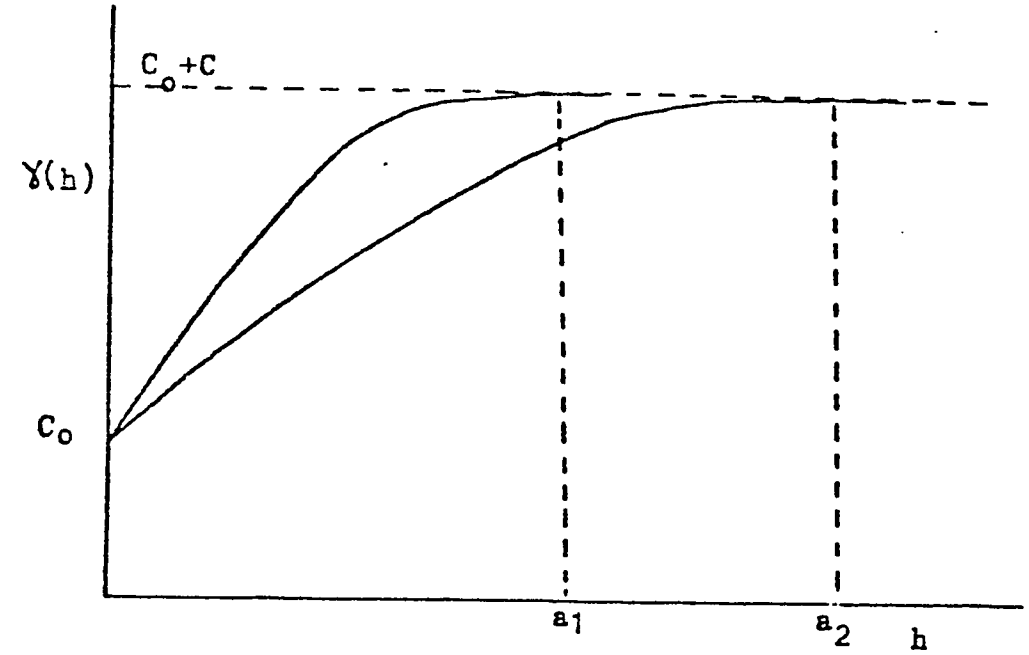

a) Geometrical

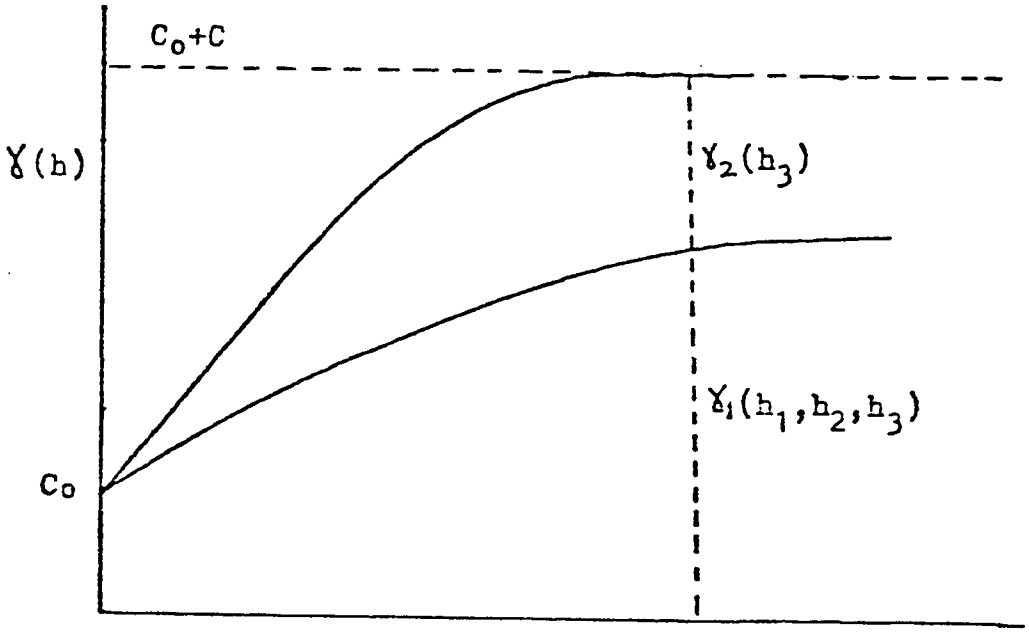

b) Zonal

Fif.(6.3): Diagrams illustrating anisotropy (after, Sahin, 1977).

(1977), Royle (19) and Clark (1980). The general expressions for the simple and compound spherical models are given in the following paragraphs.

1. Simple spherical model

$$\gamma(h)=C_0+C[3h/2a-h^3/2a^3] \quad \text{for } h\leq a$$
$$\gamma(h)=C_0+C \quad \text{for } h\geq a \qquad \text{----------(3)}$$

where a is called the range , C_0 is the nugget variance, C is the spatial variance and C_0 + C the sill.

2. Compound spherical model

$$\gamma(h)=C_0+C_1[3h/2a_1-h^3/2a_1^3] + C_2[3h/2a_2-h^3/2a_2^3] \quad \text{for } h\leq a_1$$
$$\gamma(h)=C_0+C_1+ C_2[3h/2a_2-h^3/2a_2^3] \quad \text{for } a_1\leq h\leq a_2 \qquad \text{----(4)}$$
$$\gamma(h)=C_0+C_1 + C_2 \quad \text{for } h\geq a_2$$

where a_1 and a_2 are the two ranges, C_0 is the nugget variance, C_1 and C_2 are the two spatial variances.

6.2 Zarghat Magnesite Deposit

The main objective of the present geostatistical study is to determine the spatial distribution of the selected regionalized variables (crude MgO%, crude CaO%, calcined MgO%, and calcined CaO%) within

the magnesite ore body of the central-hill where a fairly enough data are available.

The study is based on the data in BRGM open-file report, published in 1976. It comprises computations of basic statistical parameters, semivariograms, and cross-semivariograms.

6.2.1 Data Set

Nine out of 13 drill-holes of the Central-hill were used. The other 4 drill-holes did not have enough number of samples. The location map of these drill-holes is given in Fig. 6.4. The results of chemical analysis (for crude MgO%, crude CaO%, calcined MgO%, and calcined CaO%) of 199 samples in selected drill-holes (see Table 6.1) provided data for geostatistical study.

Table 6.1 samples

D.H.	No. of samples
ZA 11	5
ZA 12	25
ZA 13	44
ZA 14	15
ZA 15	11
ZA 16	10
ZA 17	43
ZA 18	40
ZA 19	8
Total	199

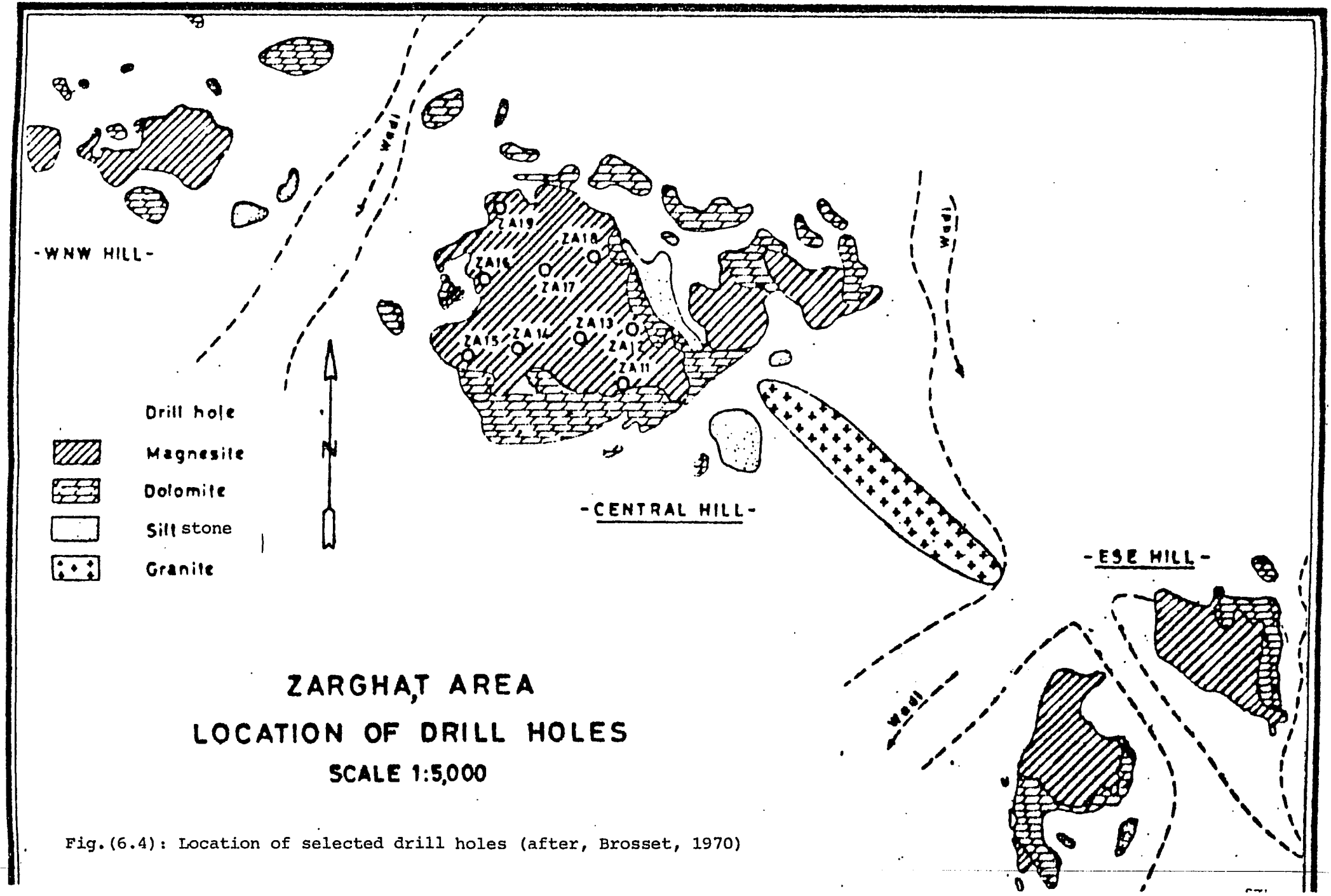

Fig.(6.4): Location of selected drill holes (after, Brosset, 1970)

6.2.2 Computations

The computations on data are made in two steps. In the first step, classical statistical parameters (e.g. mean, median, standard deviation, variance, maximum, minimum, quartiles, and correlation coefficient) were calculated and histograms were plotted for each variable.

In the second step, assuming isotropy in the horizontal direction, average semivariograms in the horizontal direction and the vertical semivariograms along drill-holes ZA 13, ZA 17, and ZA 18 were computed. The cross-semivariograms between CaO% and MgO% were also computed.

6.2.3 Results and Discussions

A- Statistics

Table 6.2 shows the results of basic statistics for the variables. In addition to these statistics, the correlation coefficient between CaO% and MgO% were also computed. The correlation coefficient between the crude CaO% and the crude MgO% was found to be -0.961 and the correlation coefficient between the calcined values of the same variables to be -0.825, i.e. high negative correlation in both cases. These correlation diagrams are given in Fig. 6.5 and Fig. 6.6. Histograms are shown in Figs. 6.7 to 6.10. Both crude and calcined MgO% show negatively skewed distribution, while, crude and calcined CaO% show

Statistical Parameters	Crude MgO%	Crude CaO%	Calcined MgO%	Calcined CaO%
No. of Samples	199	199	199	199
Mean	46.18	1.53	95.84	3.34
Standard Deviation	1.73	1.83	4.19	4.81
Variance	3.00	3.34	17.55	23.18
Maximum	48.30	11.48	99.72	46.40
Minimum	38.00	0.13	76.50	0.20

Table (6.2): Statistical parameters for the 4 selected variables (crude MgO%, crude CaO%, calcined MgO%, and calcined CaO%).

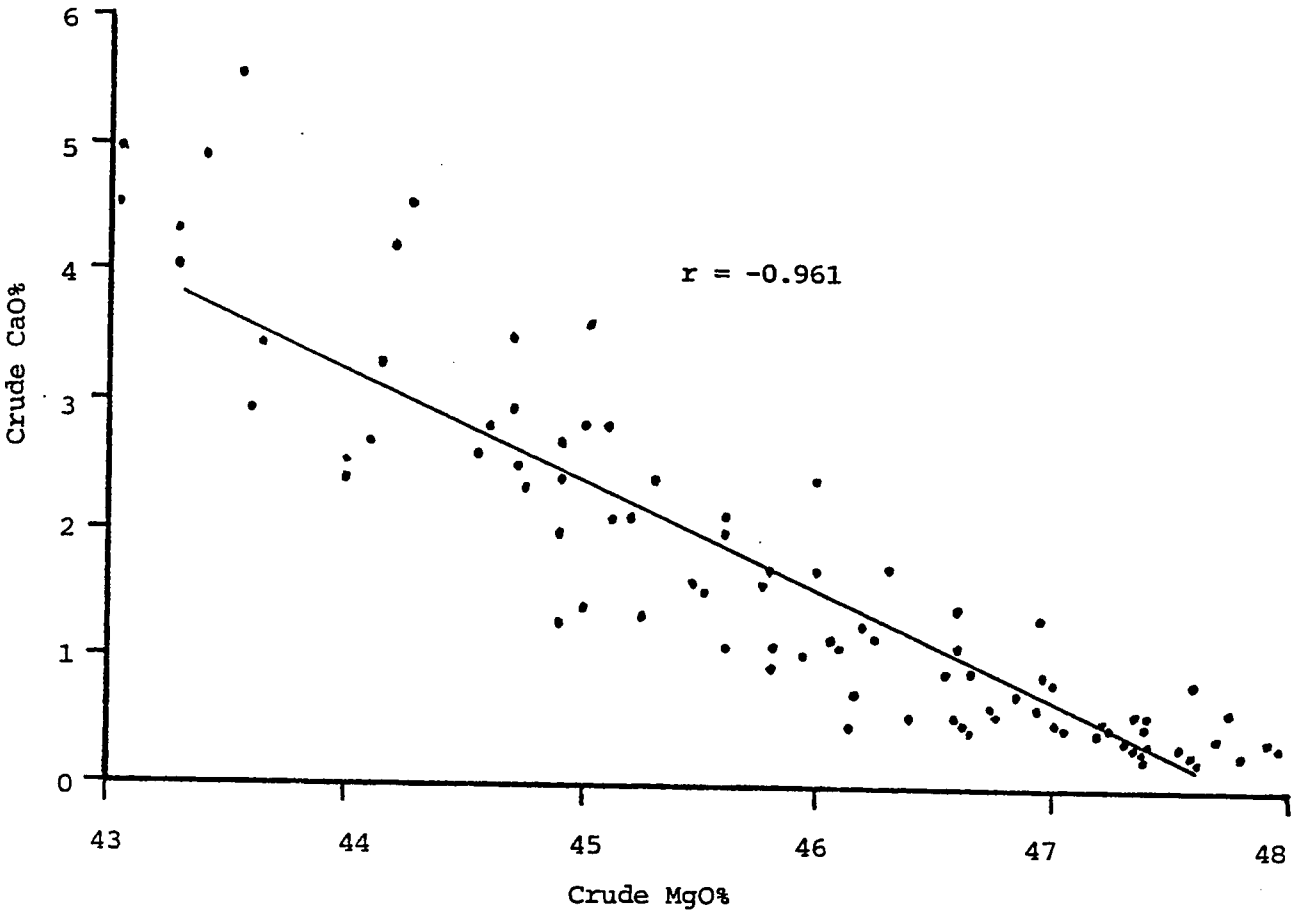

Fig.(6.5): Correlation between crude MgO% and crude CaO%.

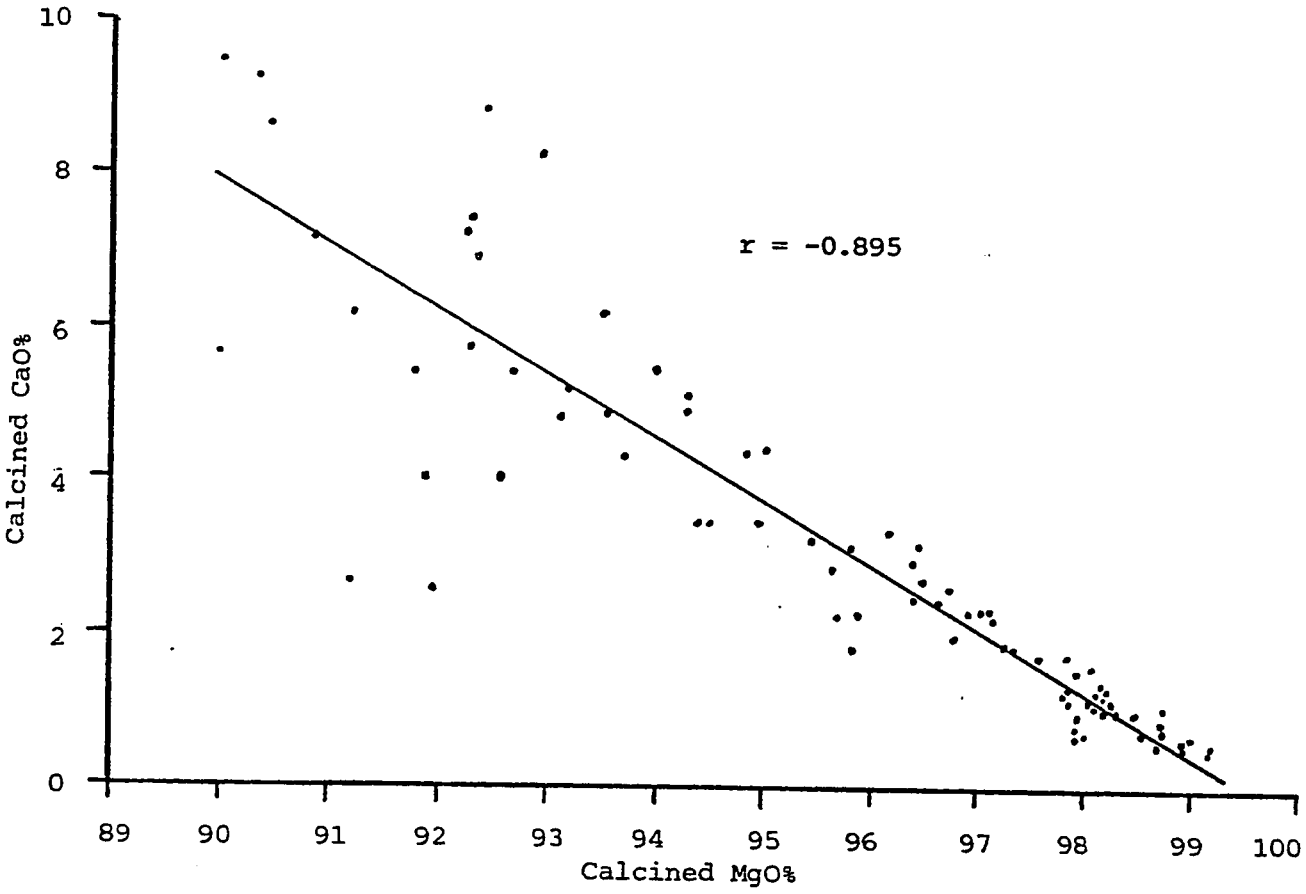

Fig.(6.6): Correlation between calcined MgO% and calcined CaO%.

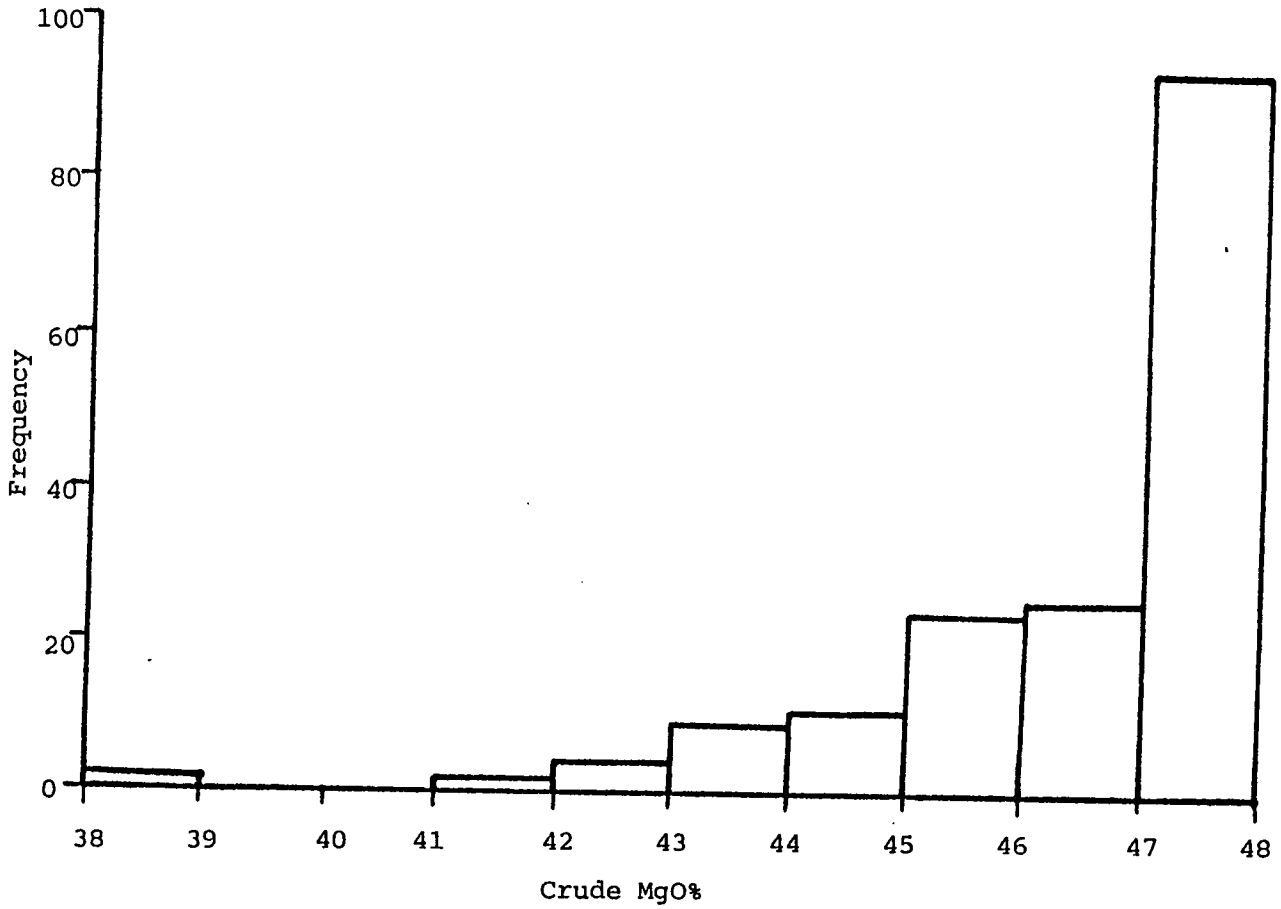

Fig.(6.7) : Histogram of crude MgO - Zarghat Magnesite Deposit

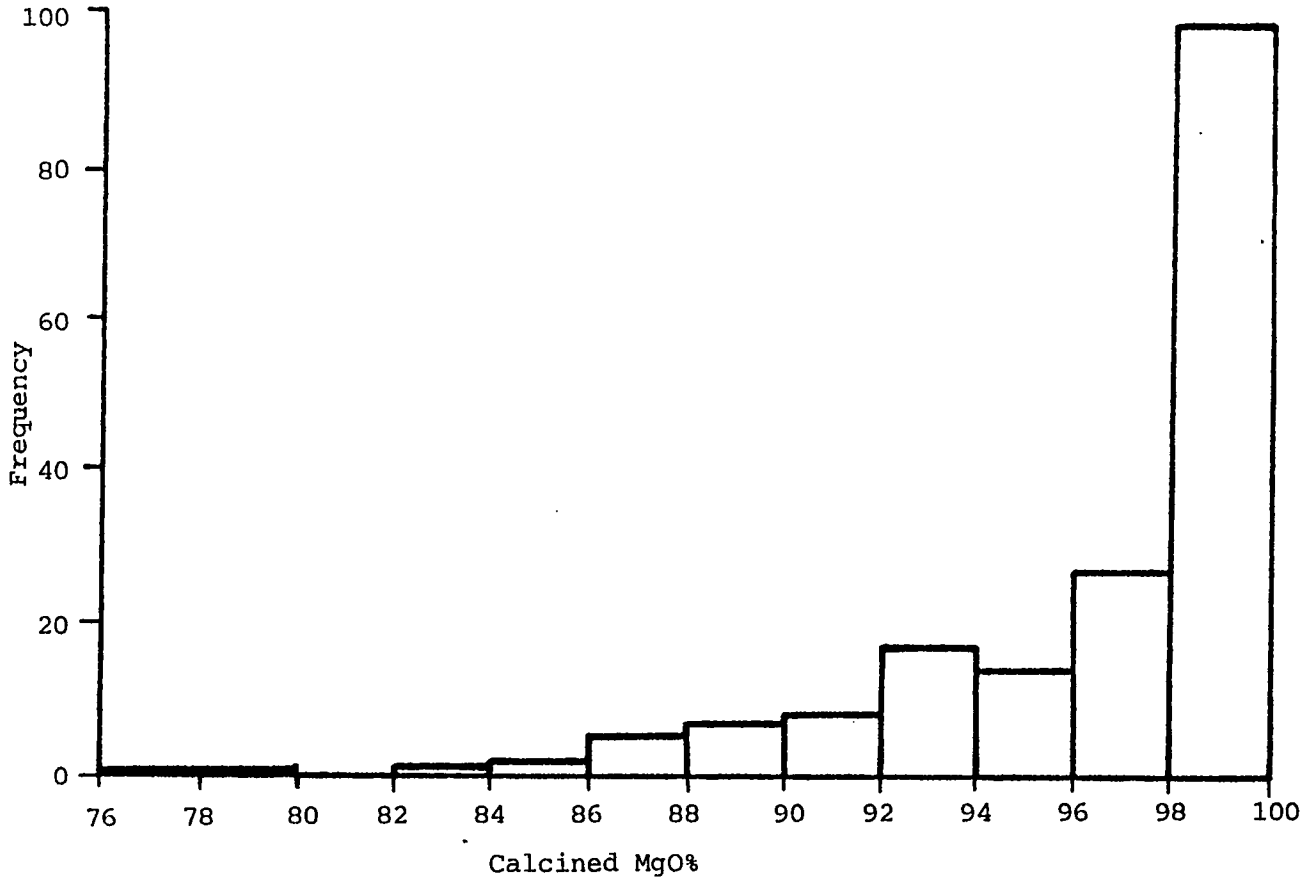

Fig.(6.8): Histogram of calcined MgO - Zarghat Magnesite Deposit

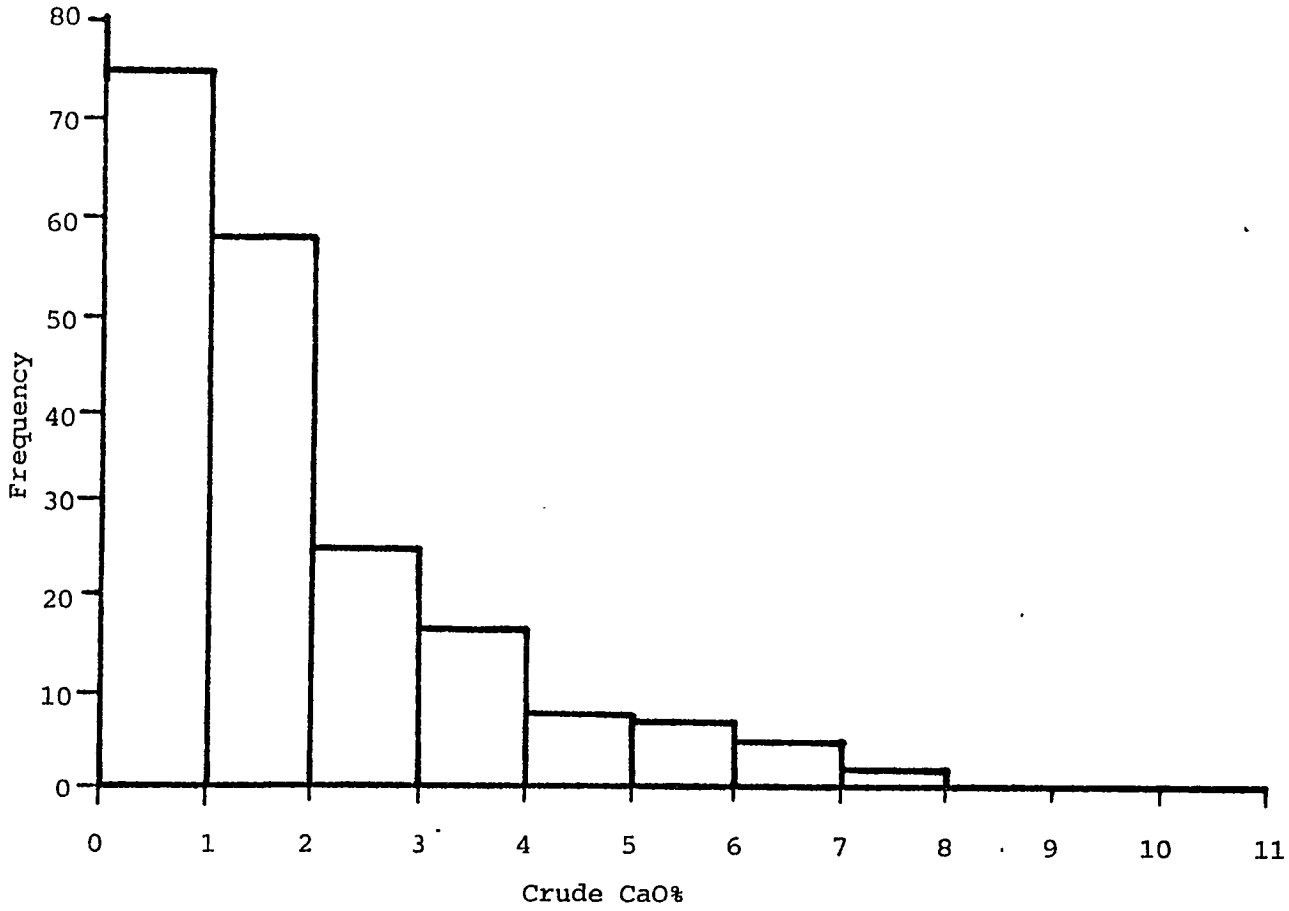

Fig.(6.9): Histogram of crude CaO - Zarghat Magnesite Deposit

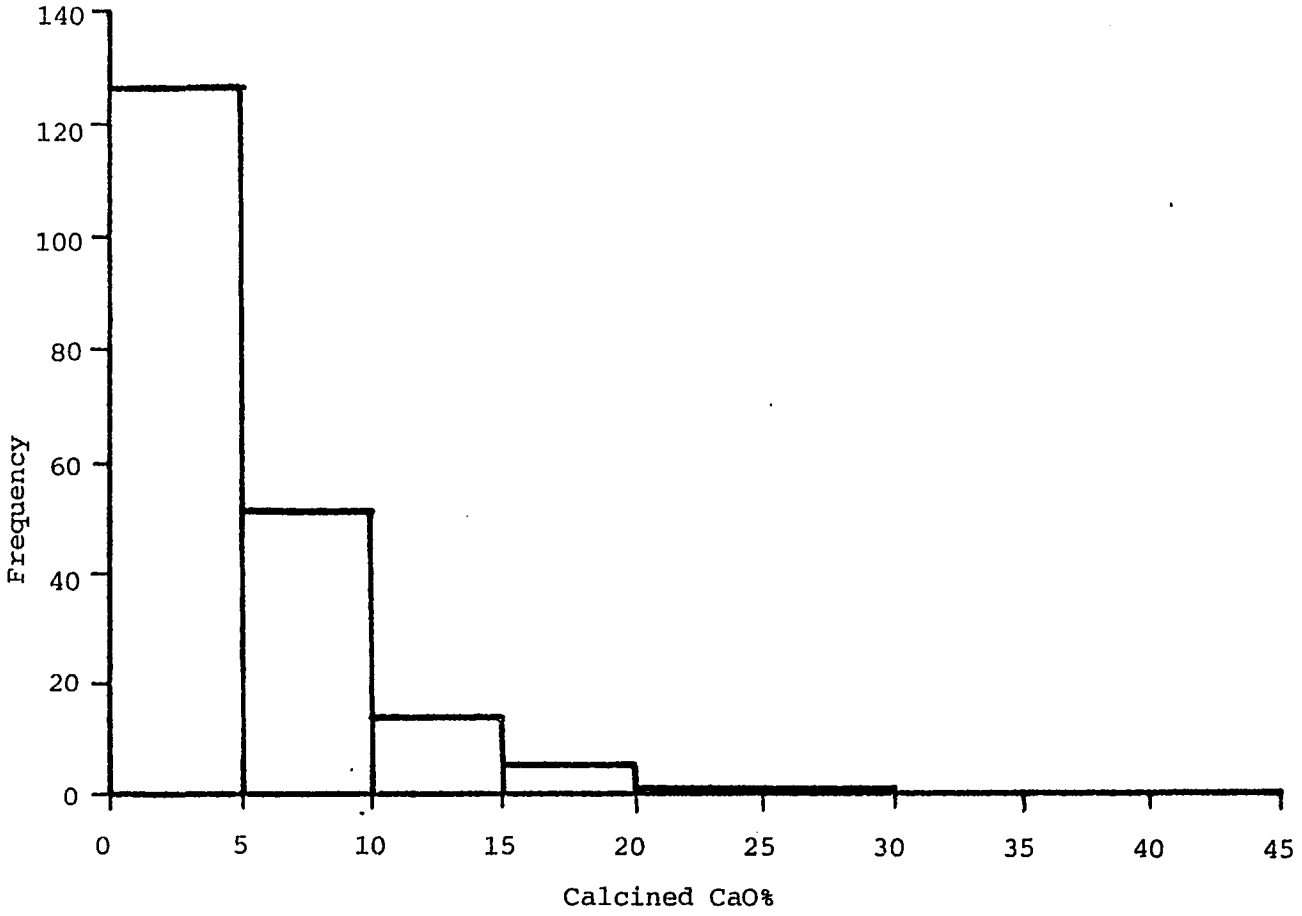

Fig.(6.10): Histogram of calcined CaO - Zarghat Magnesite Deposit

positively skewed distribution. The high negative correlation between MgO% & CaO% could be explained by the process which led to an increase in Mg-content at the expense of Ca-content. As outlined in detail in chapter 7, the process may involve the dissolution of early deposited Ca-minerals and deposition of dolomite as a result of magnesium enrichment.

B- Geostatistics

B.1. Vertical Semivariograms

The vertical semivariogram indicates the structure of the deposit in vertical direction. Vertical semivariograms were computed along three drill-holes, ZA 13 , ZA 17, and ZA 18. Because of the smaller sampling interval, study of the behaviour near the origin in the vertical direction was possible. These three drill-holes were selected as they had considerable number of samples to reveal the structure. Due to the similarities of semivariograms of studied variables along the same drill-hole, only one example from each, will be discussed.

1. Drill-hole ZA 13

Experimental vertical semivariograms for the 4 variables along this drill-hole (lacated at the central part of the orebody as shown in Fig. 6.15) are given in Figs. 6.11 to 6.14. Fig. 6.14 shows the experimental vertical semivariogram and the fitted model for crude MgO%. As the distance increases between pairs of points, fewer pairs go into the calculations. This implies that points on graph closer to the origin (small distances) will be more reliable than those for greater distances. If a line is projected through the first two calculated points, it will pass through the origin. This shows that the nugget variance is zero. As the distance increases, semivariogram rises rapidly then becomes steady about a line parallel to h. A simple spherical model with a general expression given in equation (3) was fitted. The model parameters are listed in Table 6.3.

2. Drill-hole ZA 17

Experimental vertical semivariograms for the 4 variables along this drill-hole (located at the center of the orebody as shown in Fig. 6.20) are given in Figs. 6.16 to 6.19. Fig. 6.19 shows the experimental vertical semivariogram and the fitted model for crude MgO%. The behaviour near origin is similar to the semivariogram in fig. 6.14 implying that the nugget variance equals to zero, i.e. there is no random component.

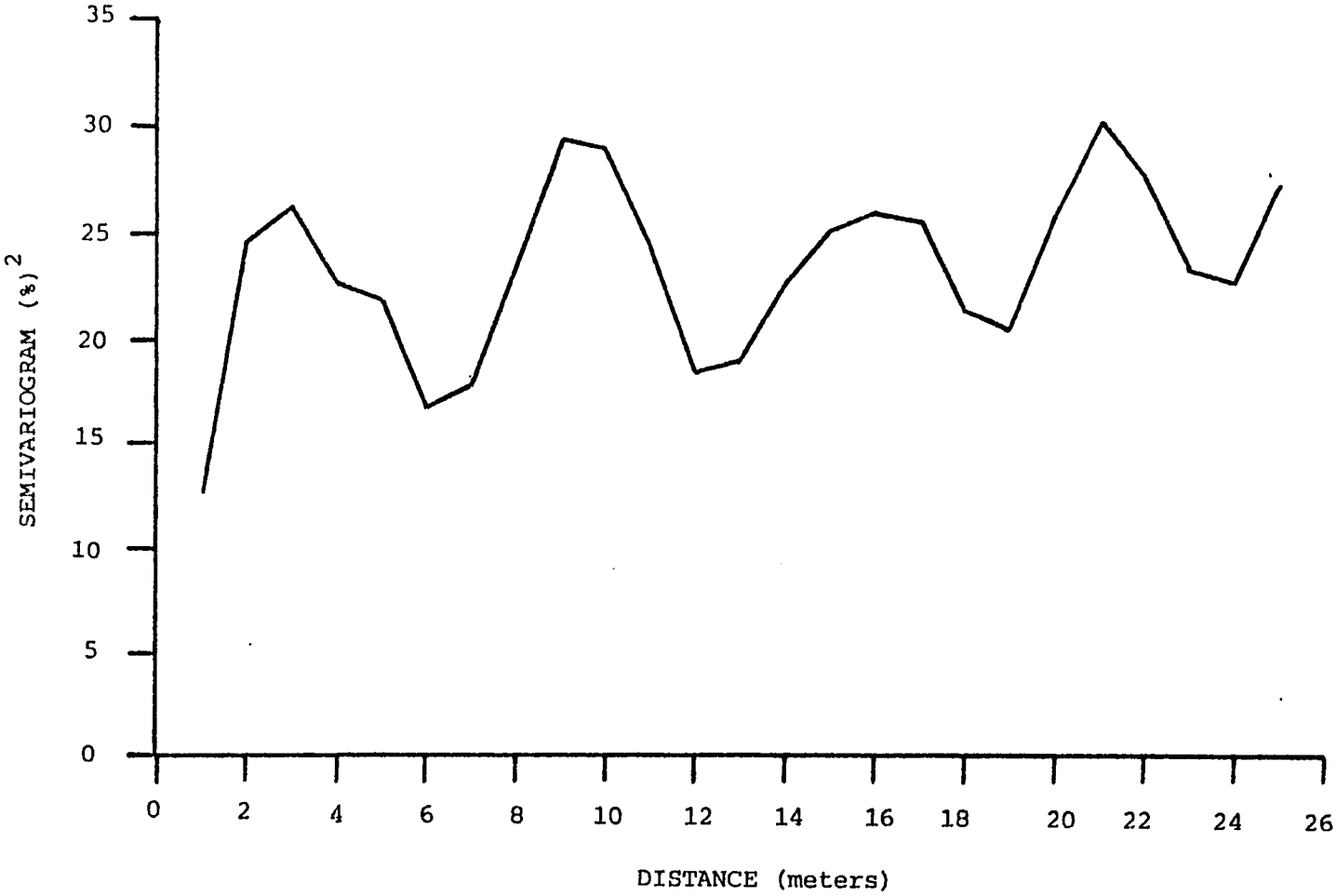

Fig.(6.11): Experimental vertical semivariogram for (calcined MgO%) D.H. 13 Zarghat Magnesite Deposit

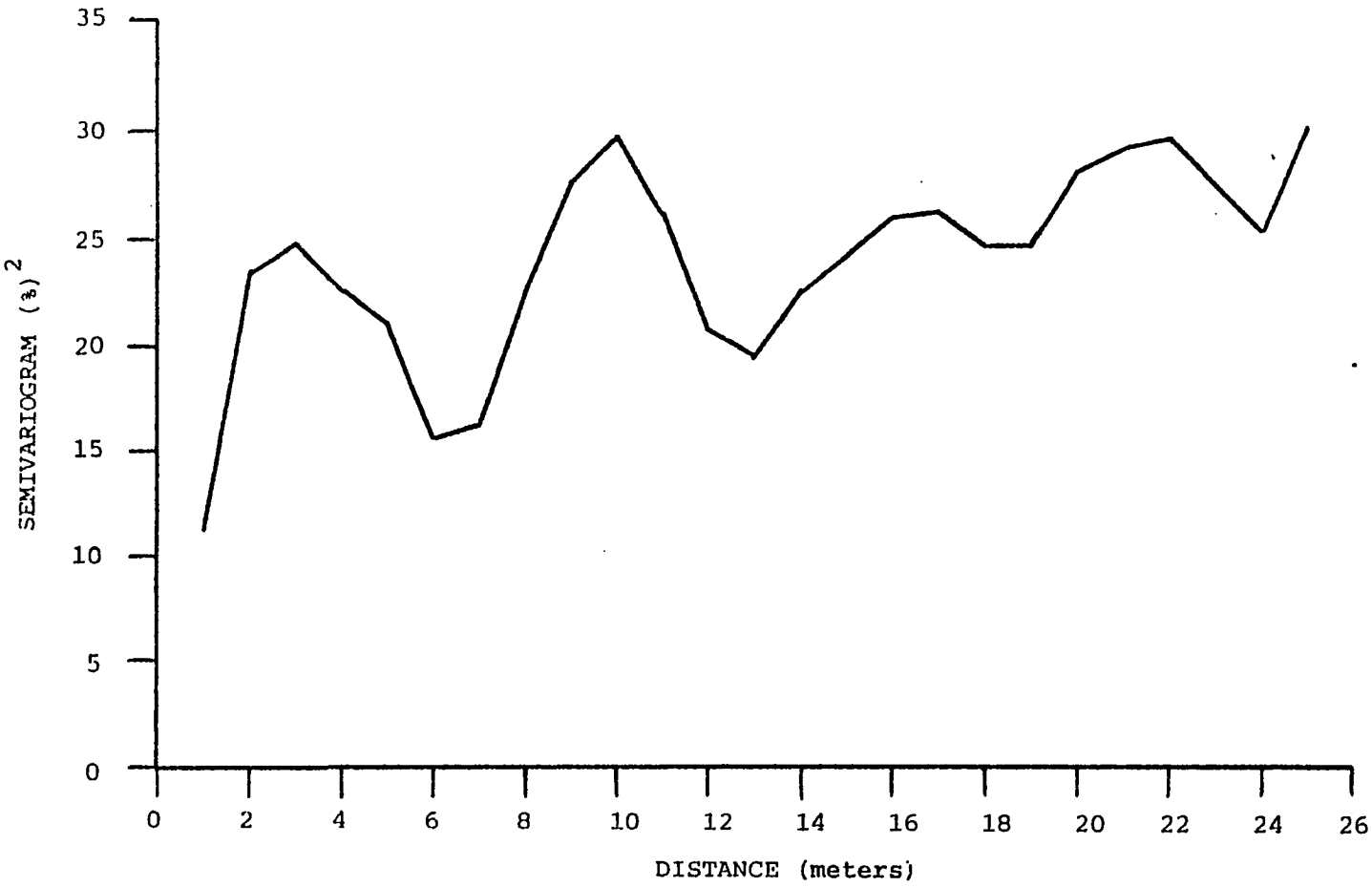

Fig (6.12): Experimental vertical semivariogram for (calcined CaO%) D.H. 13 Zarghat Magnesite Deposit

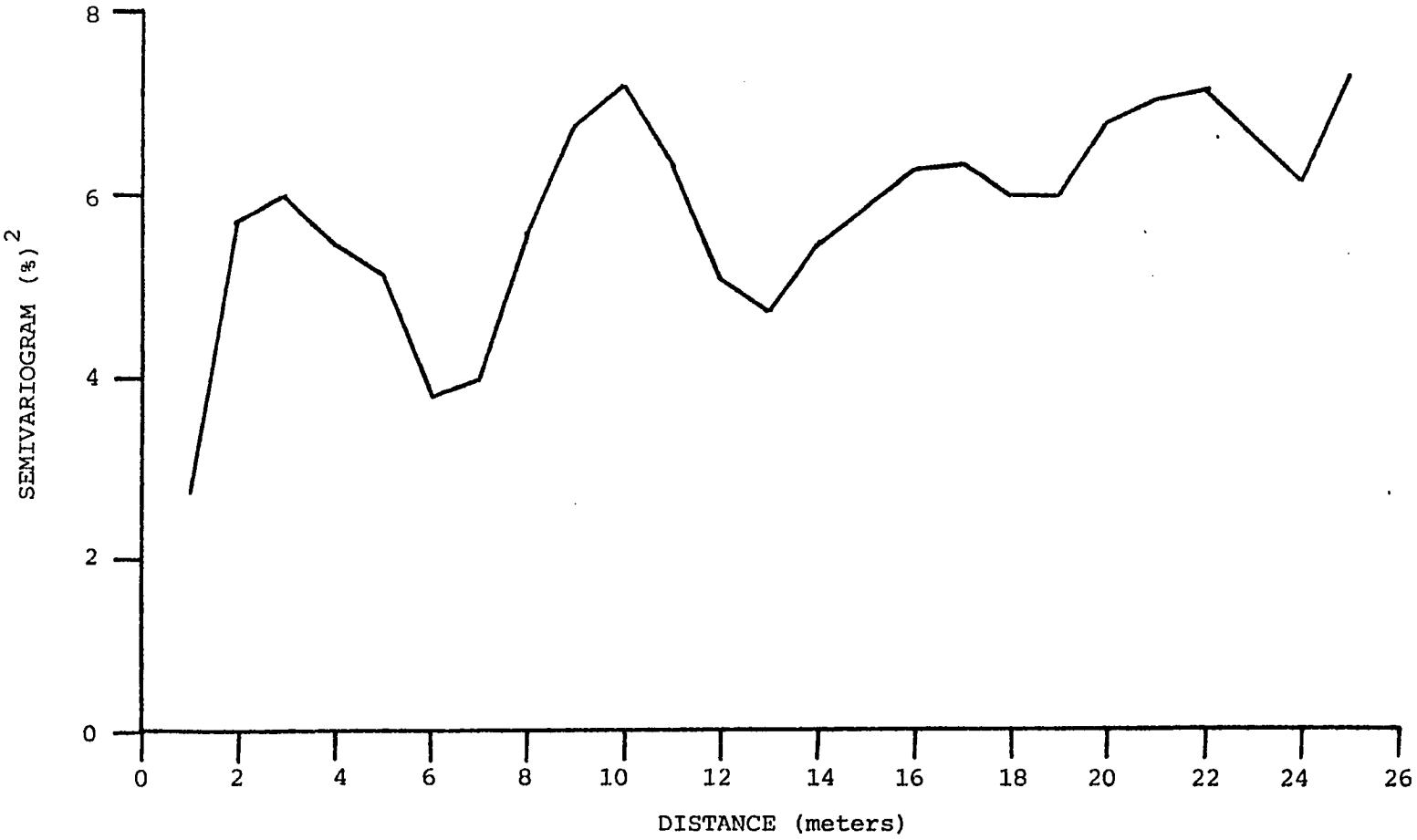

Fig.(6.13): Experimental vertical semivariogram for (crude CaO%) D.H. 13 Zarghat Magnesite Deposit

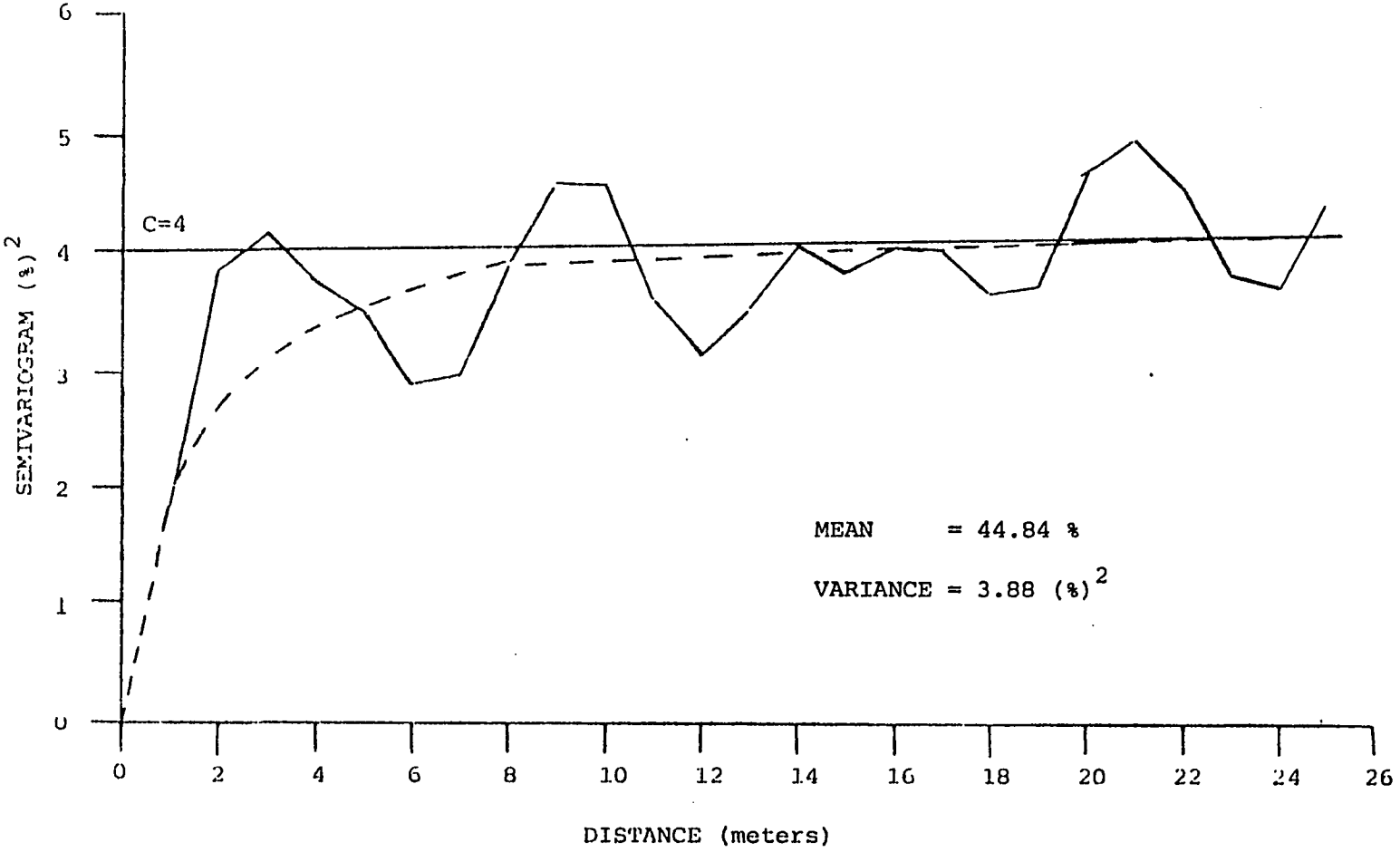

Fig.(6.14): Experimental vertical semivariogram and fitted model for (crude MgO%)

D.H. 13 Zarghat Magnesite Deposit

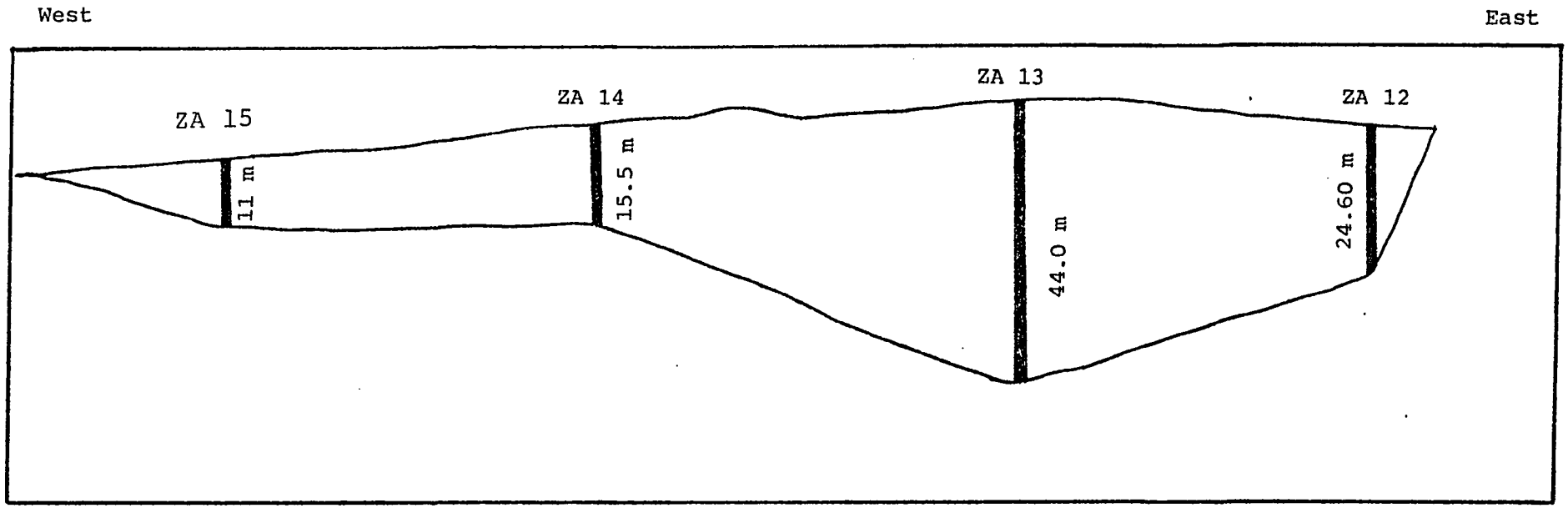

Fig.(6.15): West-East cross section in the central hill.

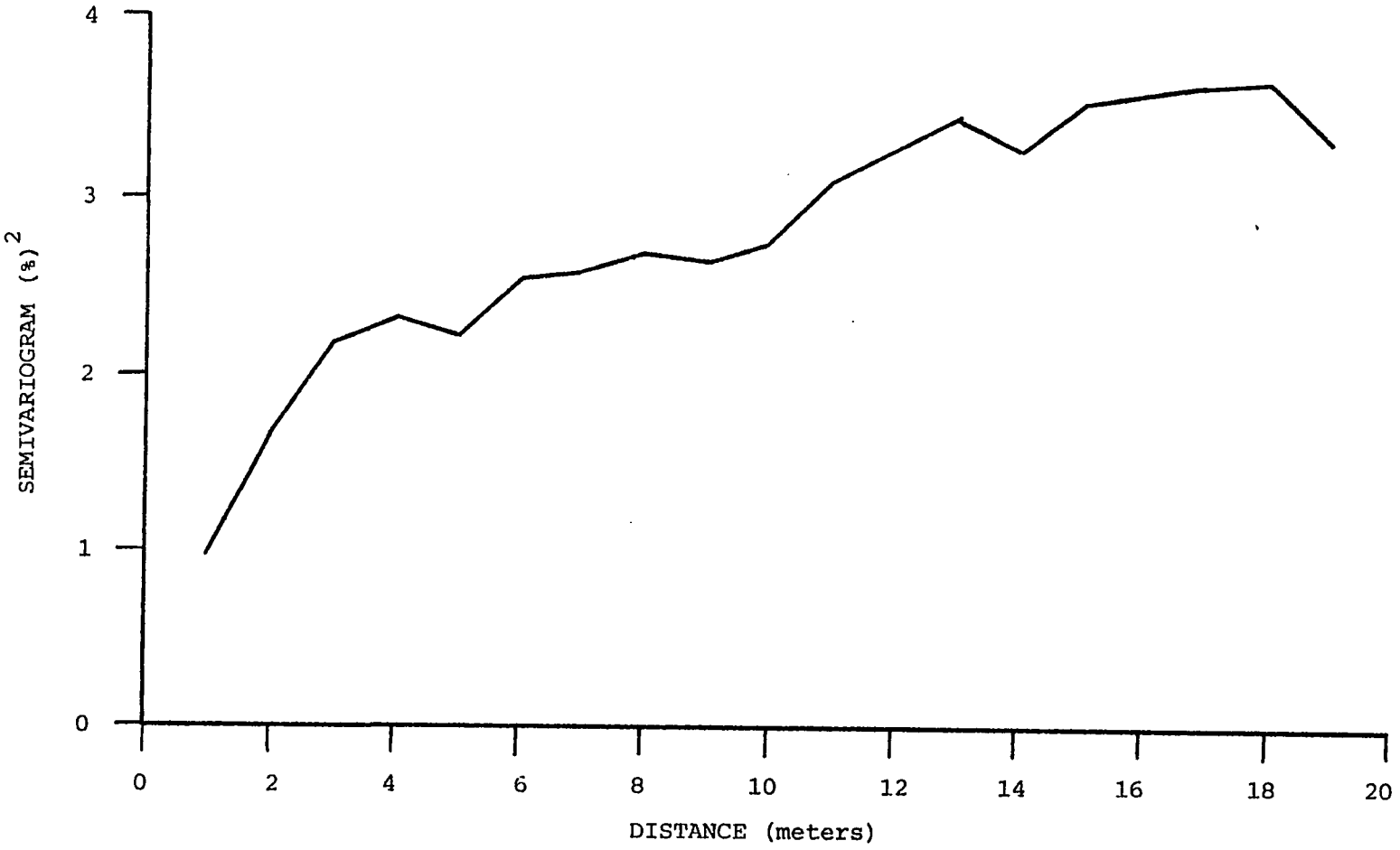

Fig.(6.16): Experimental vertical semivariogram for (calcined MgO%) D.H. 17 Zarghat Magnesite Deposit

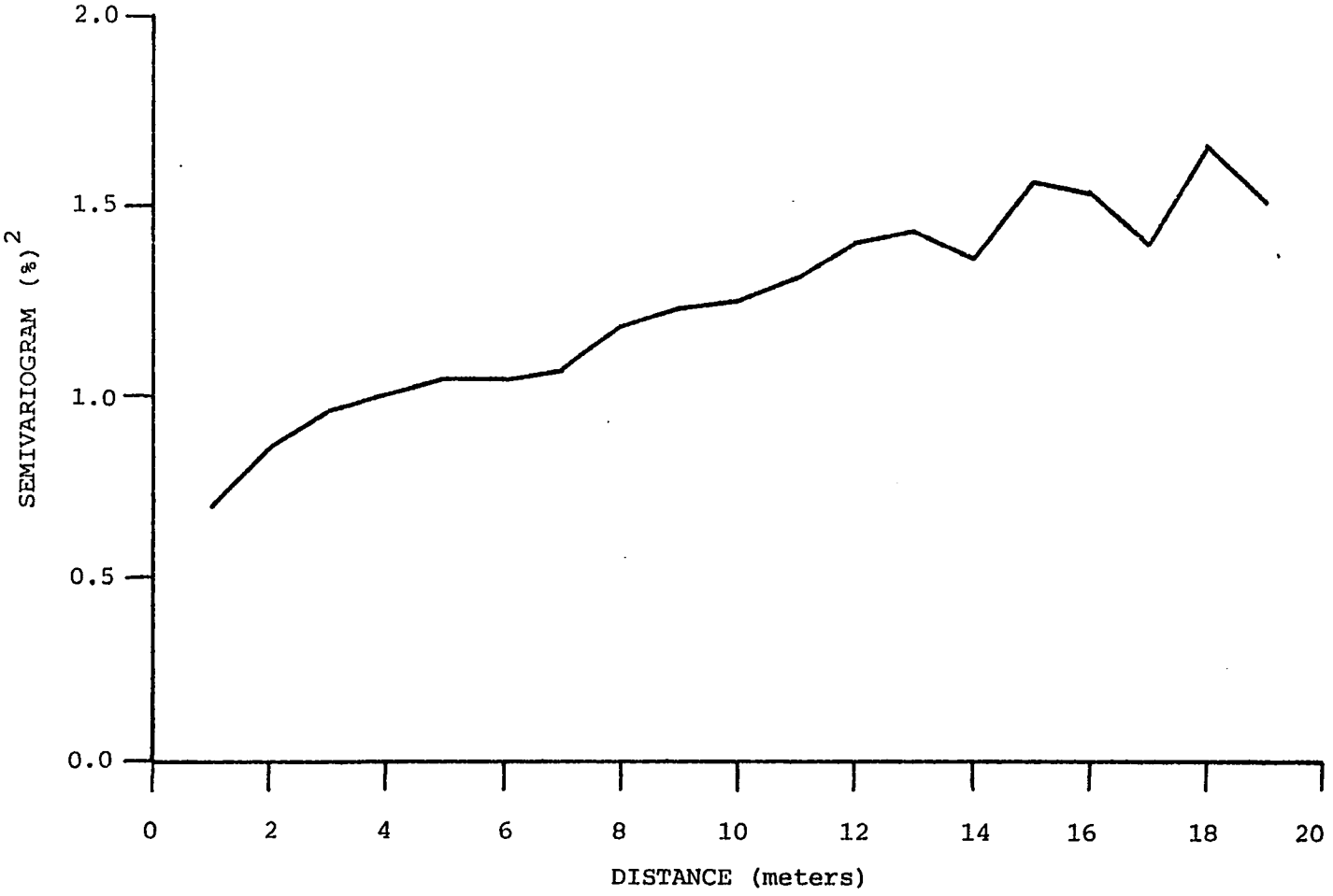

Fig.(6.17): Experimental vertical semivariogram for (calcined CaO%) D.H. 17 Zarghat Magnesite Deposit

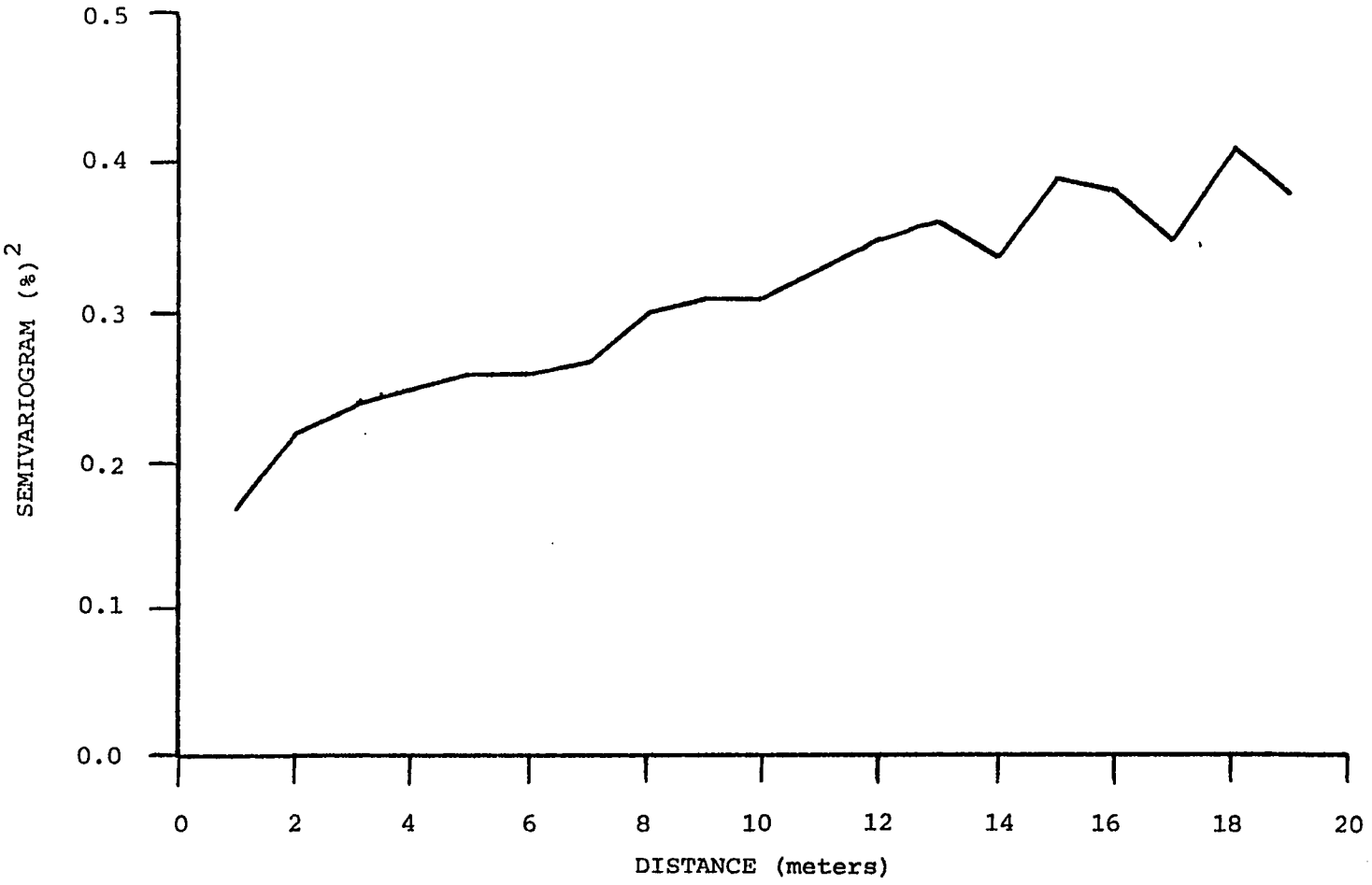

Fig.(6.18): Experimental vertical semivariogram for (crude CaO%) D.H. 17 Zarghat Magnesite Deposit

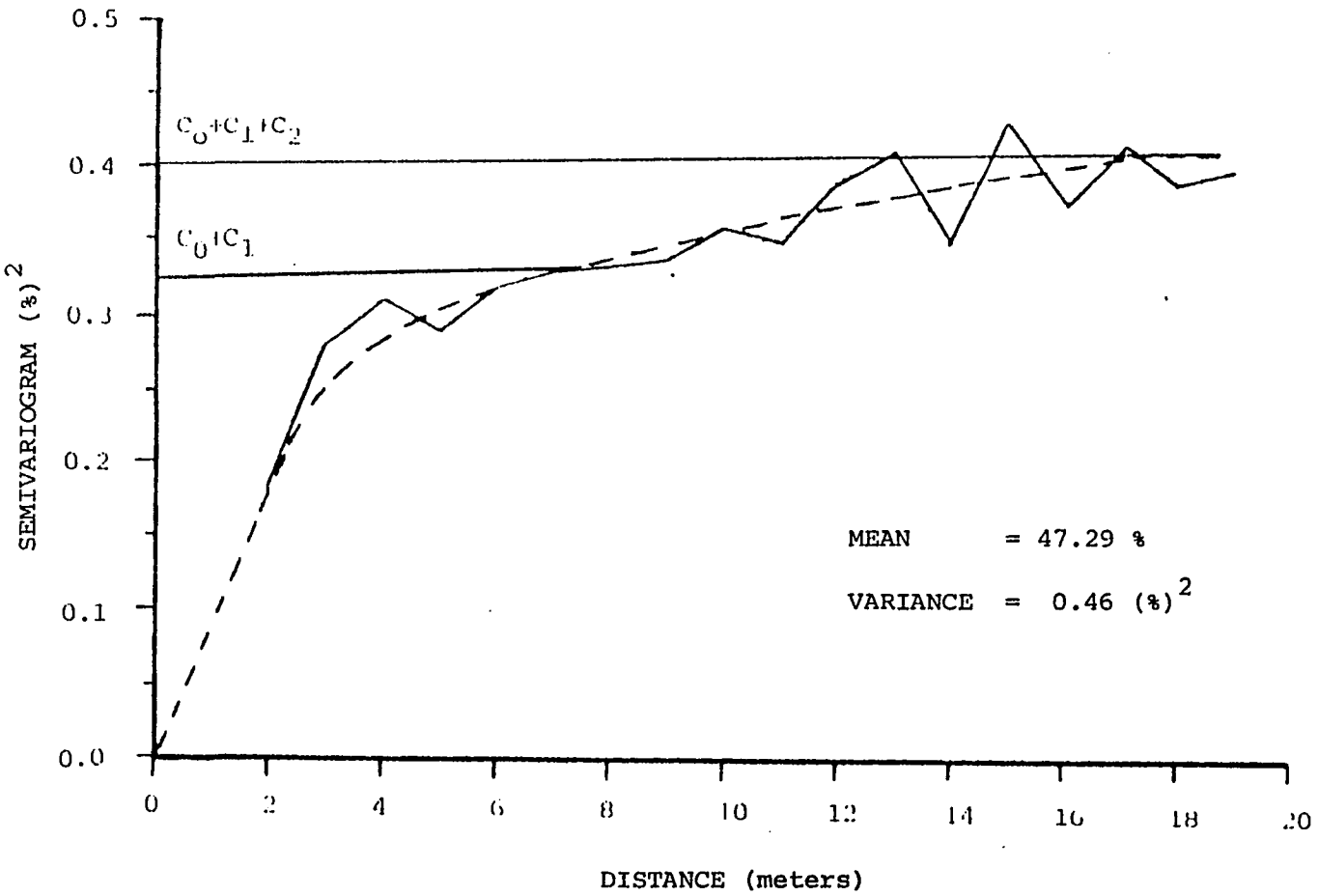

Fig.(6.19): Experimental vertical semivariogram and fitted model for (crude MgO%)

D.H. 17 Zarghat Magnesite Deposit

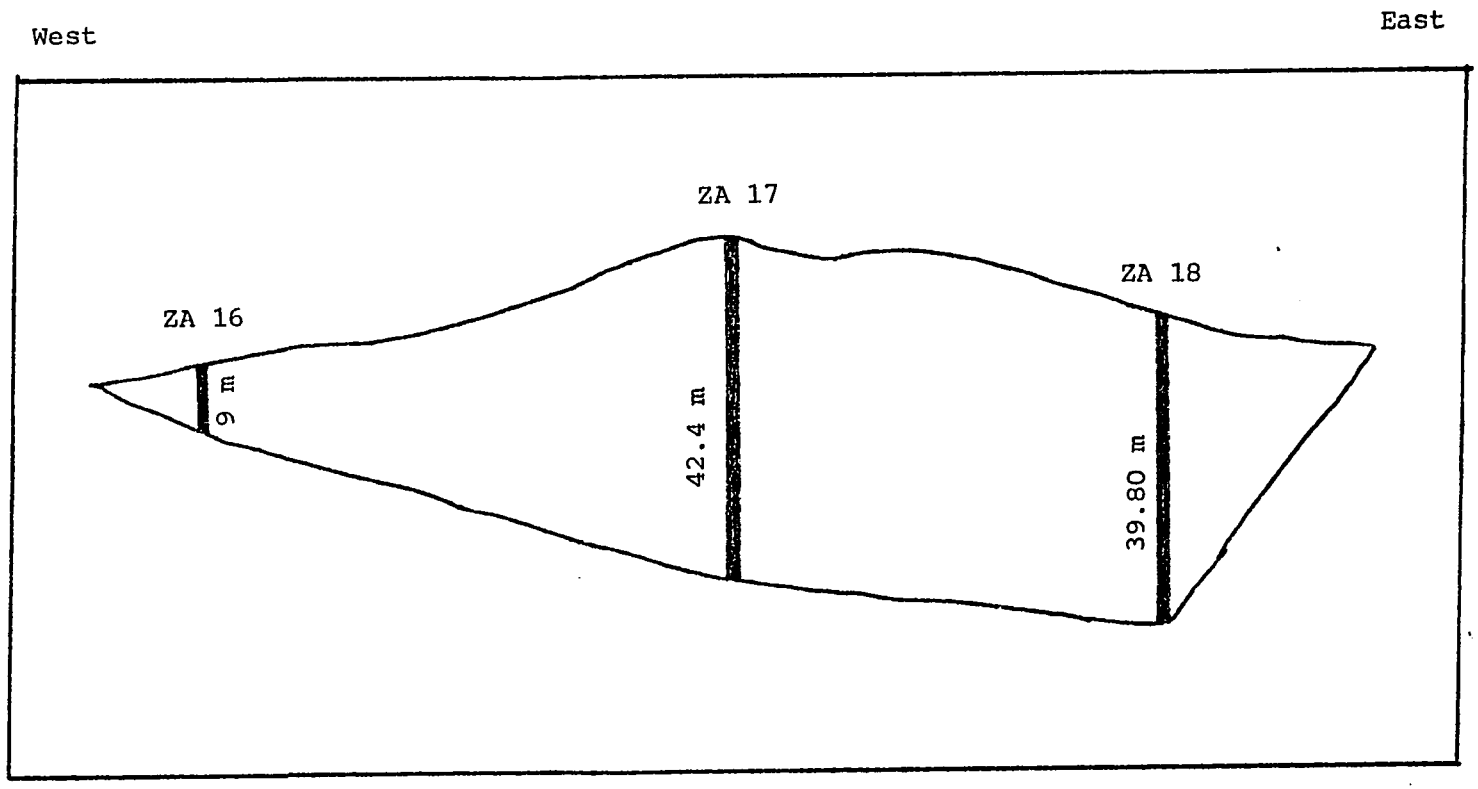

Fig.(6.20): West-East cross section in the central-hill.

The semivariogram rises rapidly from the origin up to approximately 4 meters and then rises slowly between 4 and 13 meters and finally becomes steady about a line parallel to h. The model fitted in this case is a compound spherical one (see general expression (4)) which is a combination of two spherical models. The model parameters are listed in Table 6.3, a_1 and a_2 represents the vertical dimensions of bedding.

3. Drill-hole ZA 18

Experimental vertical semivariograms for the 4 variables along this drill-hole are given in Figs. 6.21 to 6.24. Fig. 6.24 shows the experimental vertical semivariogram and the fitted model for crude MgO%. A simple spherical model with zero nugget variance was fitted to the first part of the graph (up to h=14 m). The model parameters are given in Table 6.3. At greater distances $\gamma(h)$ shows a tendency to increase as h increases (i.e. an indication of drift or trend). This trend may be due to the progressive enrichment in magnesite in vertical direction in this part of the deposit where the drill-hole is located. Similar magnesite was observed by Petrascheck et al. (1977) in carbonate sedimentary basin in Eugui-Asturreta (see chapter 7).

B.2. Vertical Cross-semivariogram

Vertical cross-semivariograms for pairs of variables were also computed along the same three drill-holes (ZA 13, ZA 17, and ZA 18).

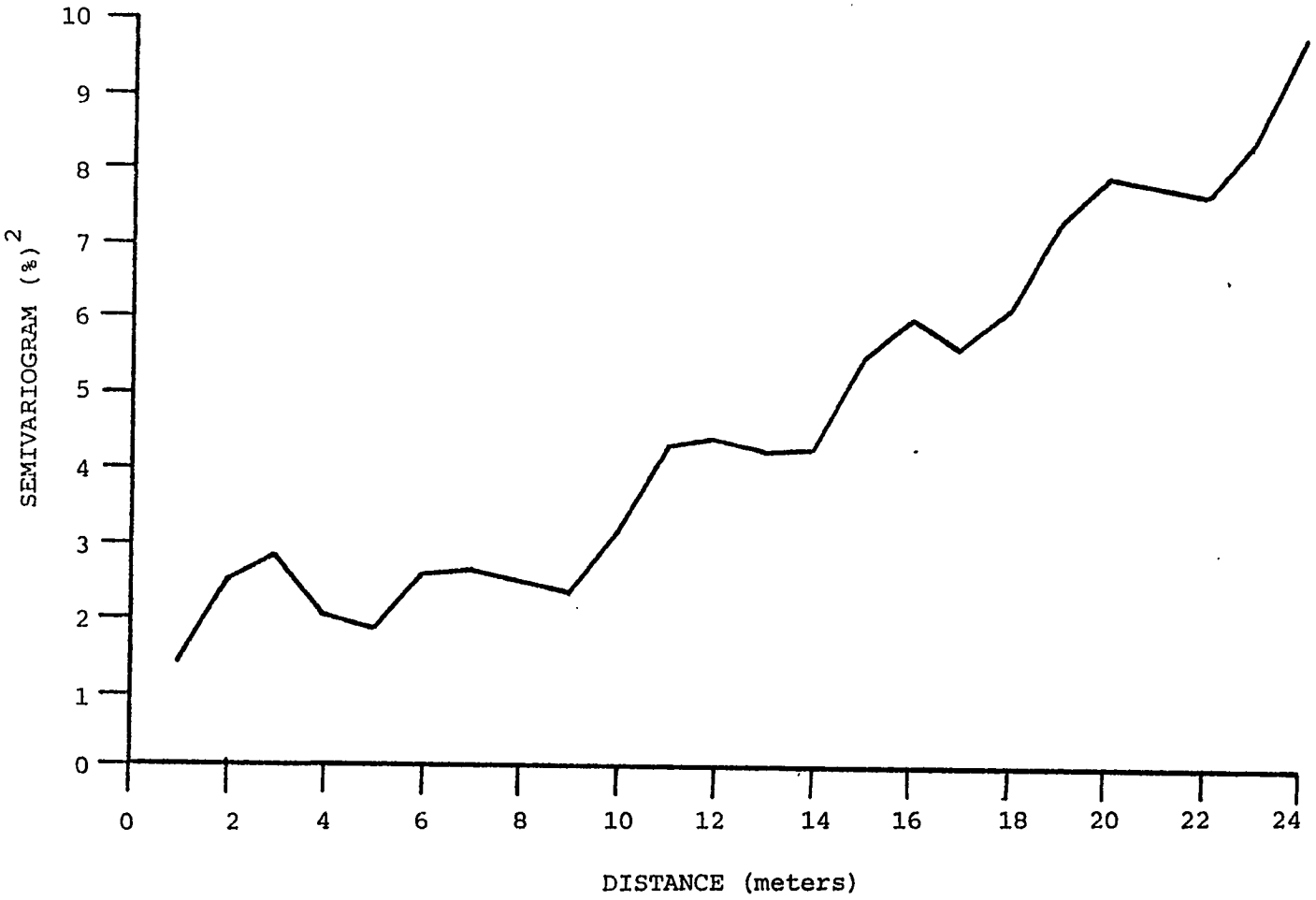

Fig.(6.21): Experimental vertical semivariogram for (calcined MgO%) D.H. 18 Zarghat Magnesite Deposit

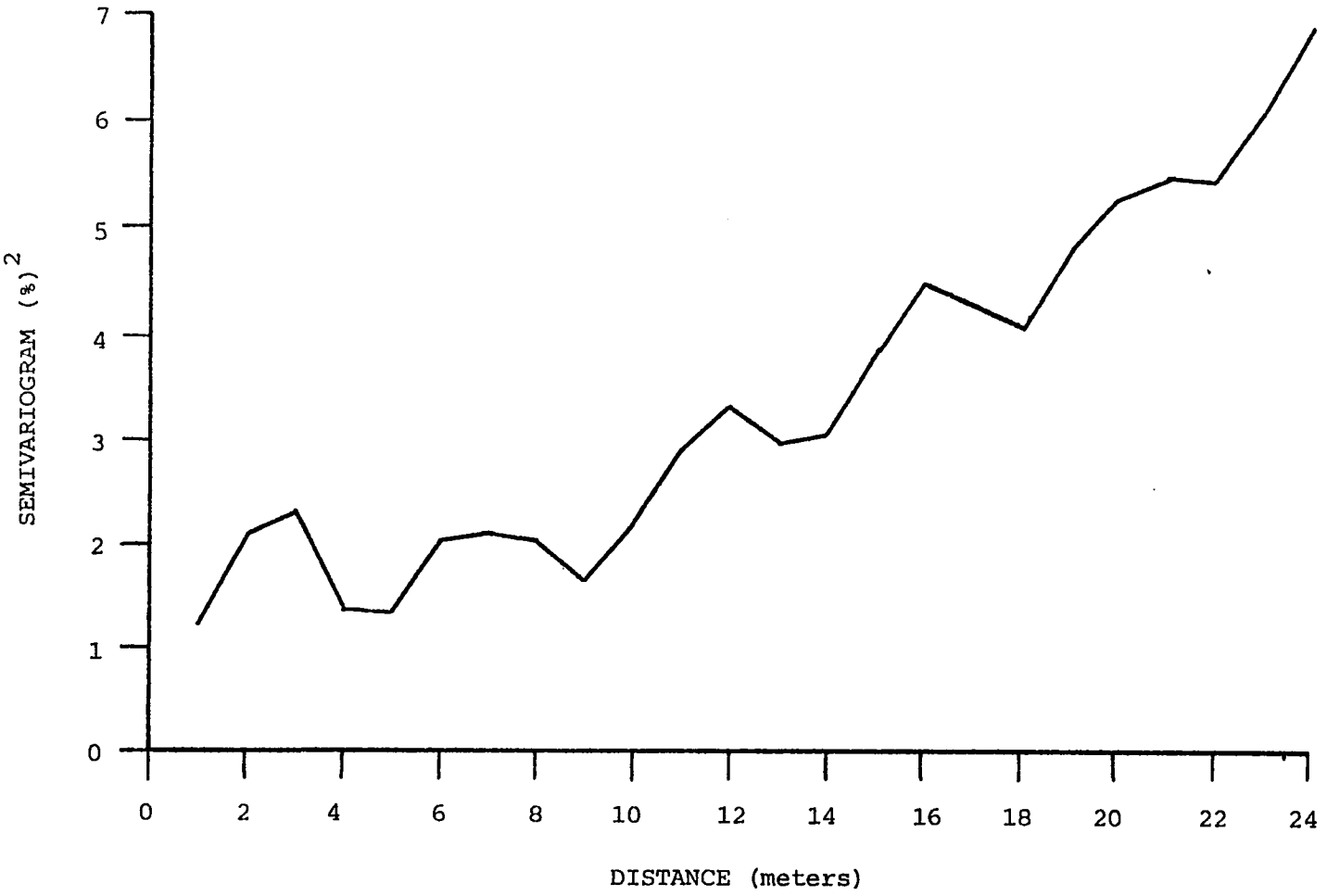

Fig.(6.22): Experimental vertical semivariogram for (calcined CaO%) D.H. 18 Zarghat Magnesite Deposit

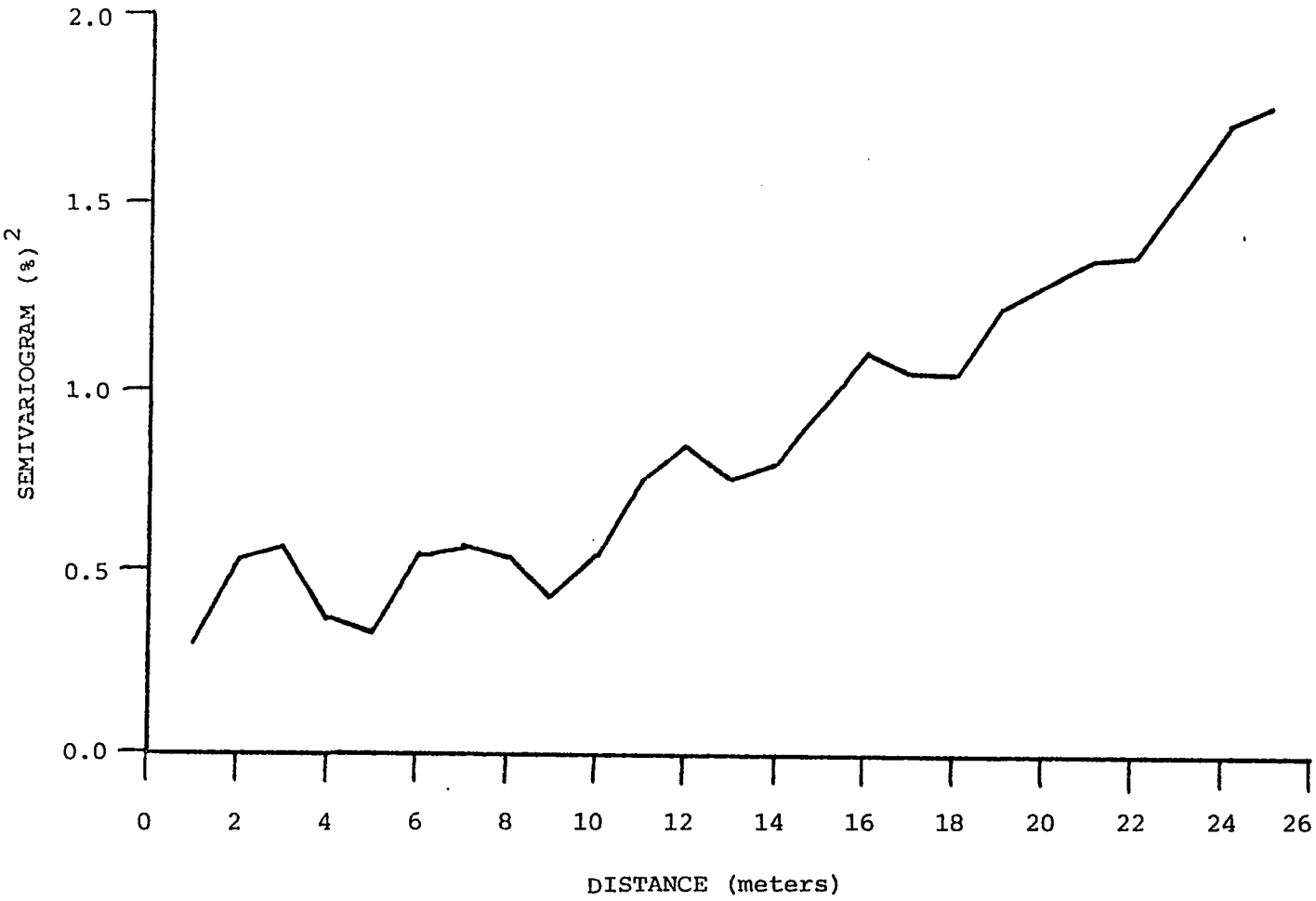

Fig.(6.23): Experimental vertical semivariogram for (crude CaO%) D.H. 18 Zarghat Magnesite Deposit

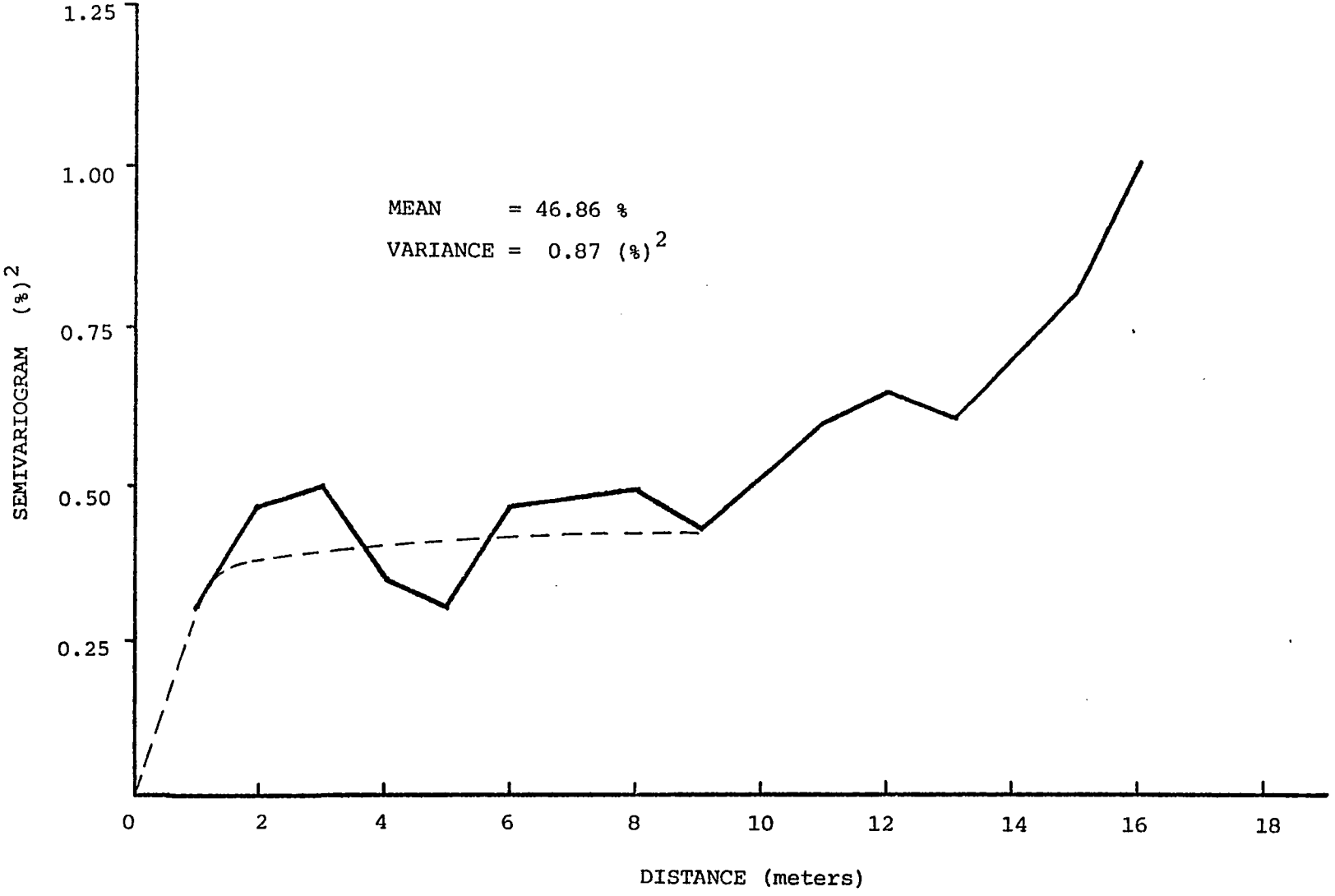

Fig.(6.24): Experimental vertical semivariogram and fitted model for (crude MgO%) D.H. 18 Zarghat Magnesite Deposit.

Along each drill hole similar cross-semivariograms were obtained. So, only one example from each will be discussed in the following paragraphs.

1. Drill-hole ZA 13

The cross-semivariograms are given in Figs. 6.25 and 6.26. Fig. 6.26 shows the experimental vertical cross-semivariogram and the fitted (spherical) model between the two variables crude MgO% and crude CaO%. The parameters are listed in Table 6.3. When the vertical cross-semivariogram with the individual vertical semivariograms of the two variables are compared, it can be seen that, the general behaviour of cross-semivariogram is similar to those of vertical semivariograms.

2. Drill-hole ZA 17

The vertical cross-semivariograms are shown in Figs. 6.27 and 6.28. Fig. 6.28 shows the experimental vertical cross-semivariogram and the fitted model for the two variables crude MgO% and crude CaO%. The behaviour of this cross-semivariogram is similar to the vertical semivariogram of crude MgO% along ZA 17. A compound spherical model was found to be suitable. The model parameters are listed in Table 6.3.

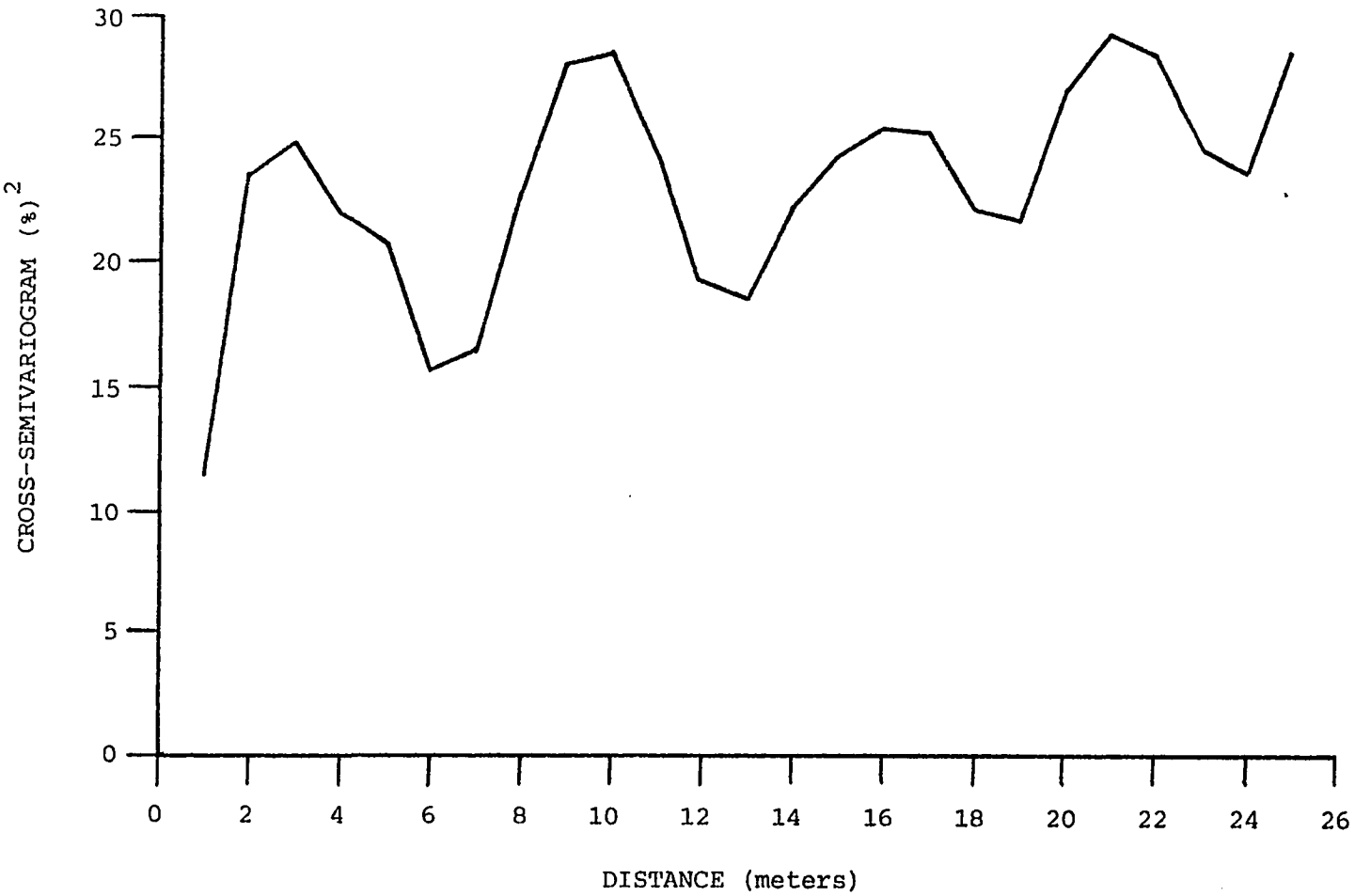

Fig.(6.25): Experimental vertical cross-semivariogram for (calcined MgO% & CaO%) D.H. 13 Zarghat Magnesite Deposit

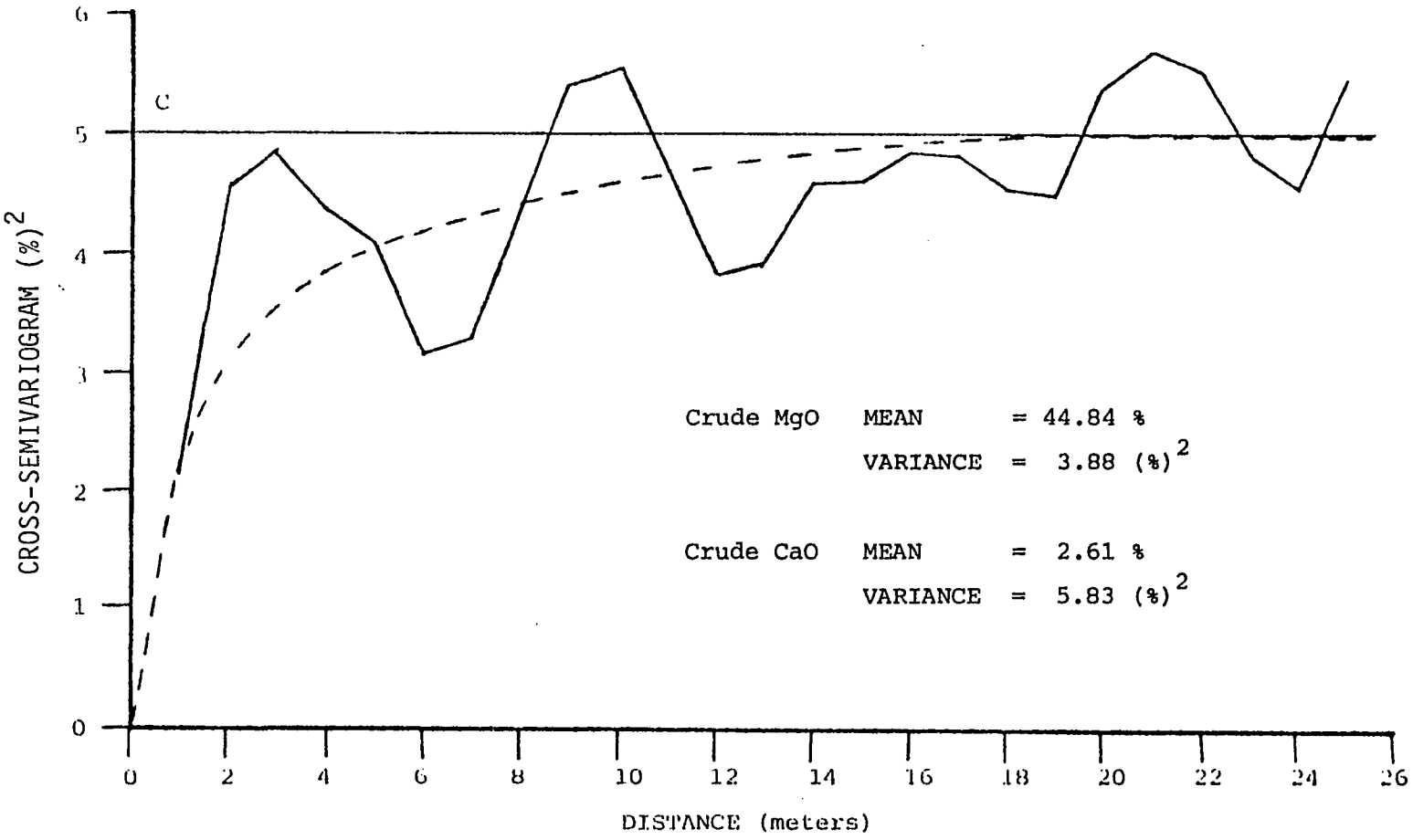

Fig.(6.26): Experimental vertical cross-semivariogram and fitted model for (crude MgO% & CaO%) D.H. 13 Zarghat Magnesite Deposit

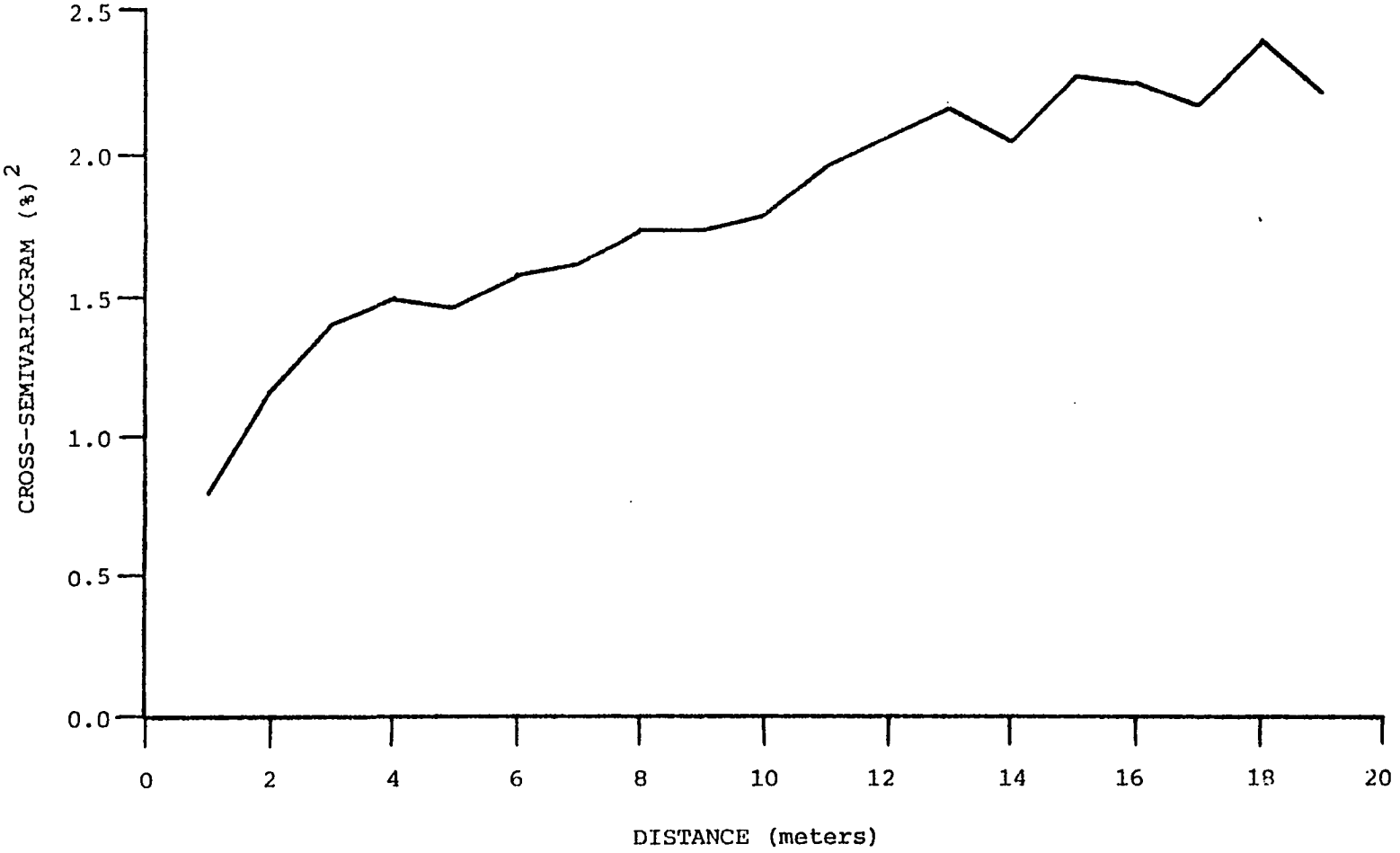

Fig.(6.27): Experiemntal vertical cross-semivariogram for (calcined MgO% & CaO%) D.H. 17 Zarghat Magnesite Deposit

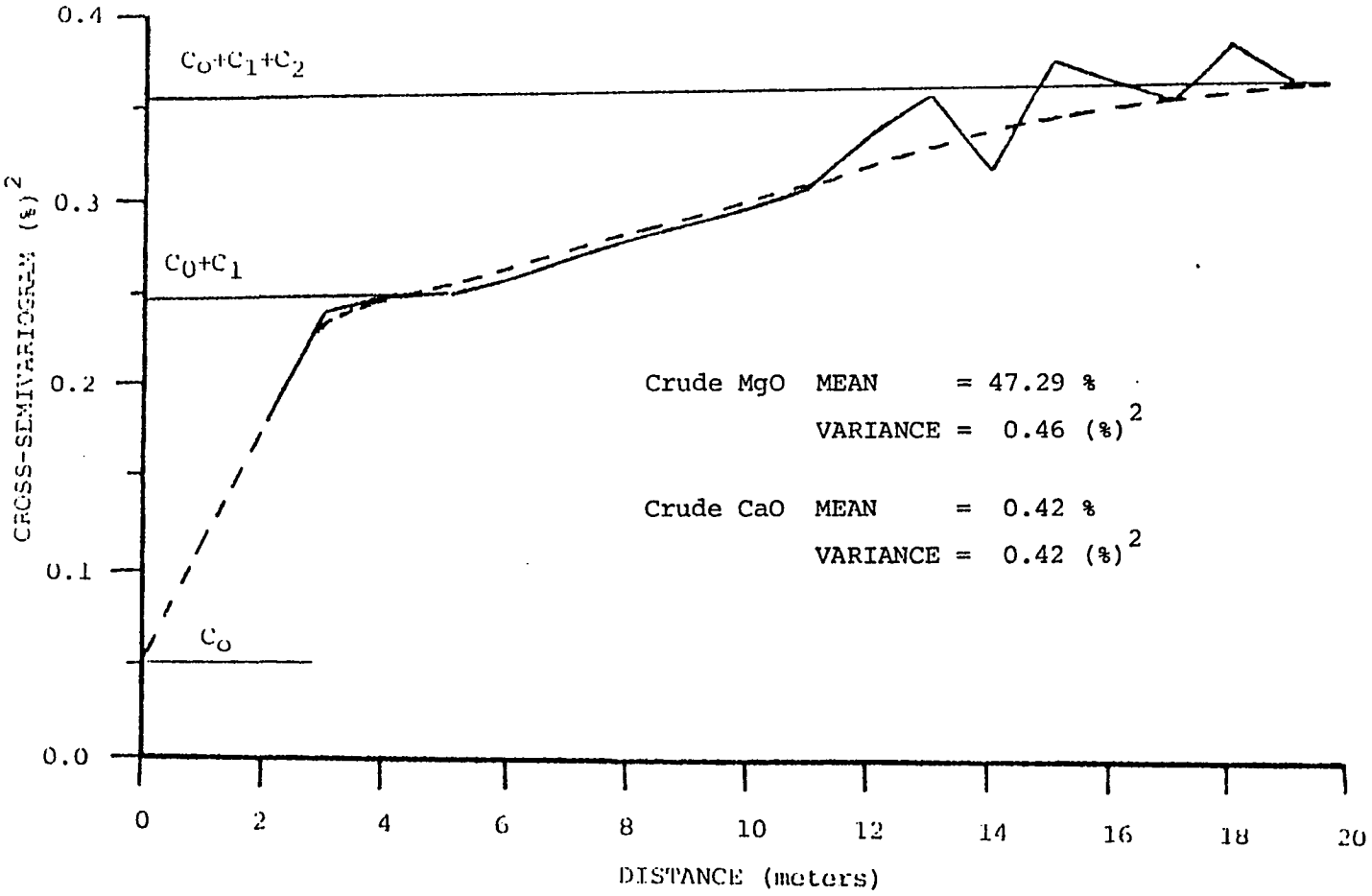

Fig.(6.28): Experimental vertical cross-semivariogram and fitted model for (crude MgO% & CaO%) D.H. 17 Zarghat Magnesite Deposit

3. Drill-hole ZA 18

The vertical cross-semivariograms are given in Figs. 6.29 and 6.30. Fig. 6.30 shows the experimental vertical cross-semivariogram and the fitted model for two variables crude MgO% and crude CaO%. The graph shows the same behaviour shown by semivariograms of crude CaO% and crude MgO% along the same drill-hole (see Fig. 6.24.)

B.3 Horizontal Semivariograms

Horizontal semivariograms for the variables (crude MgO%, crude CaO%, calcined MgO%, and calcined CaO%) were computed using data from 9 drill-holes. Due to the lack of data to give reasonable number of pairs in various directions, isotropy in the horizontal direction was assumed.

The minimum distance between any two samples in the horizontal plane was approximately 55 m, thus it was not possible to identify structures smaller than this distance. Selecting 25 m increments (i.e. 1 lag = 25 m) for the distance, the semivariograms were computed for distances greater than 55 m.

Horizontal semivariograms obtained for the 4 selected variables (see Figs. 6.31 to 6.34) show similar behaviour. They all reach certain sill value at some distances indicating the suitability of spherical models. Fixing the values of nugget variances from the corresponding vertical

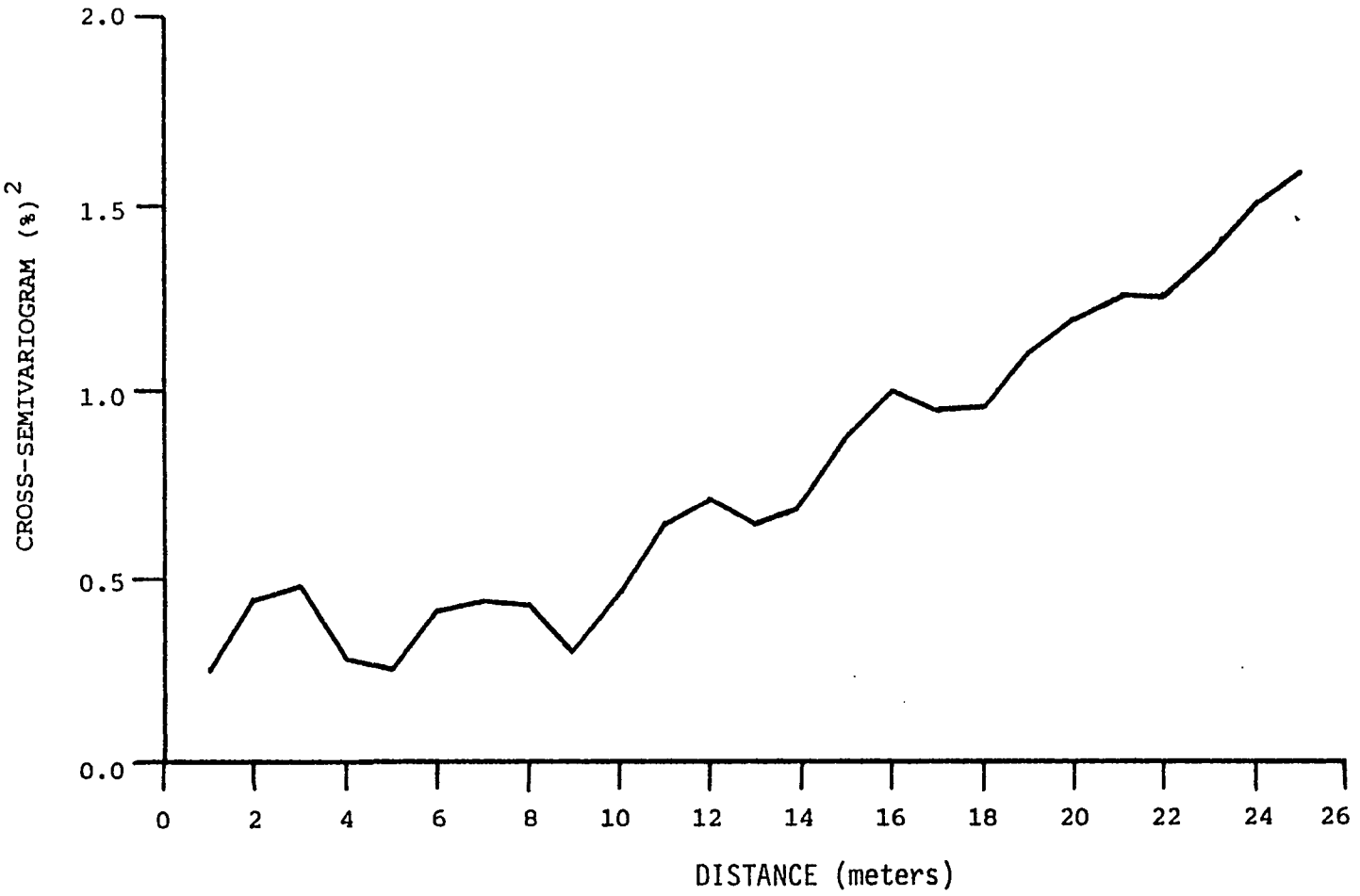

Fig. (6.29) Experimental vertical cross-semivariogram for (calcined MgO% & CaO) D.H. 18 Zarghat Magnesite Deposit.

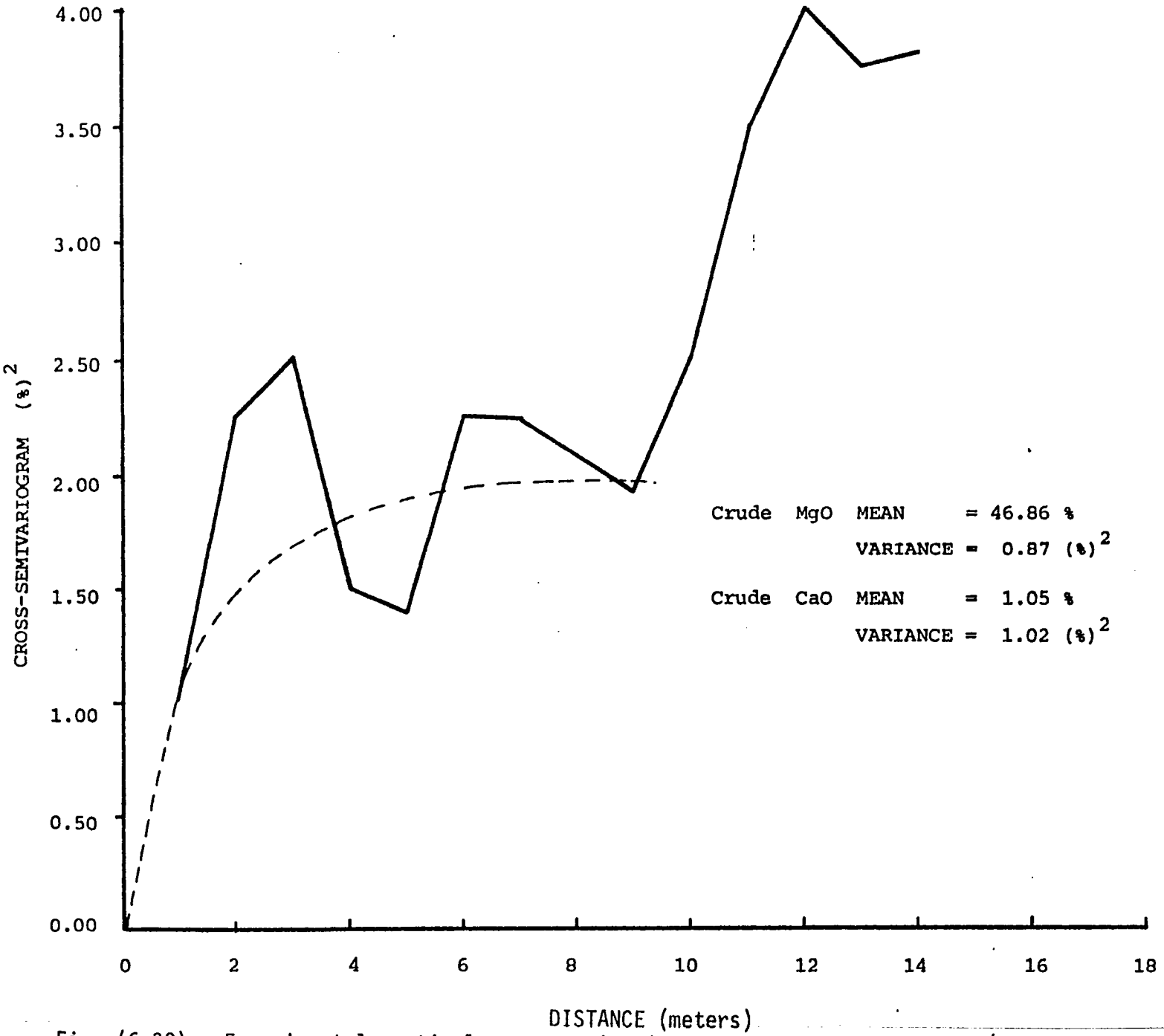

Fig. (6.30): Experimental vertical cross-semivariogram and fitted model for (crude MgO% and CaO%) D.H. 18 Zarghat Magnesite Deposit.

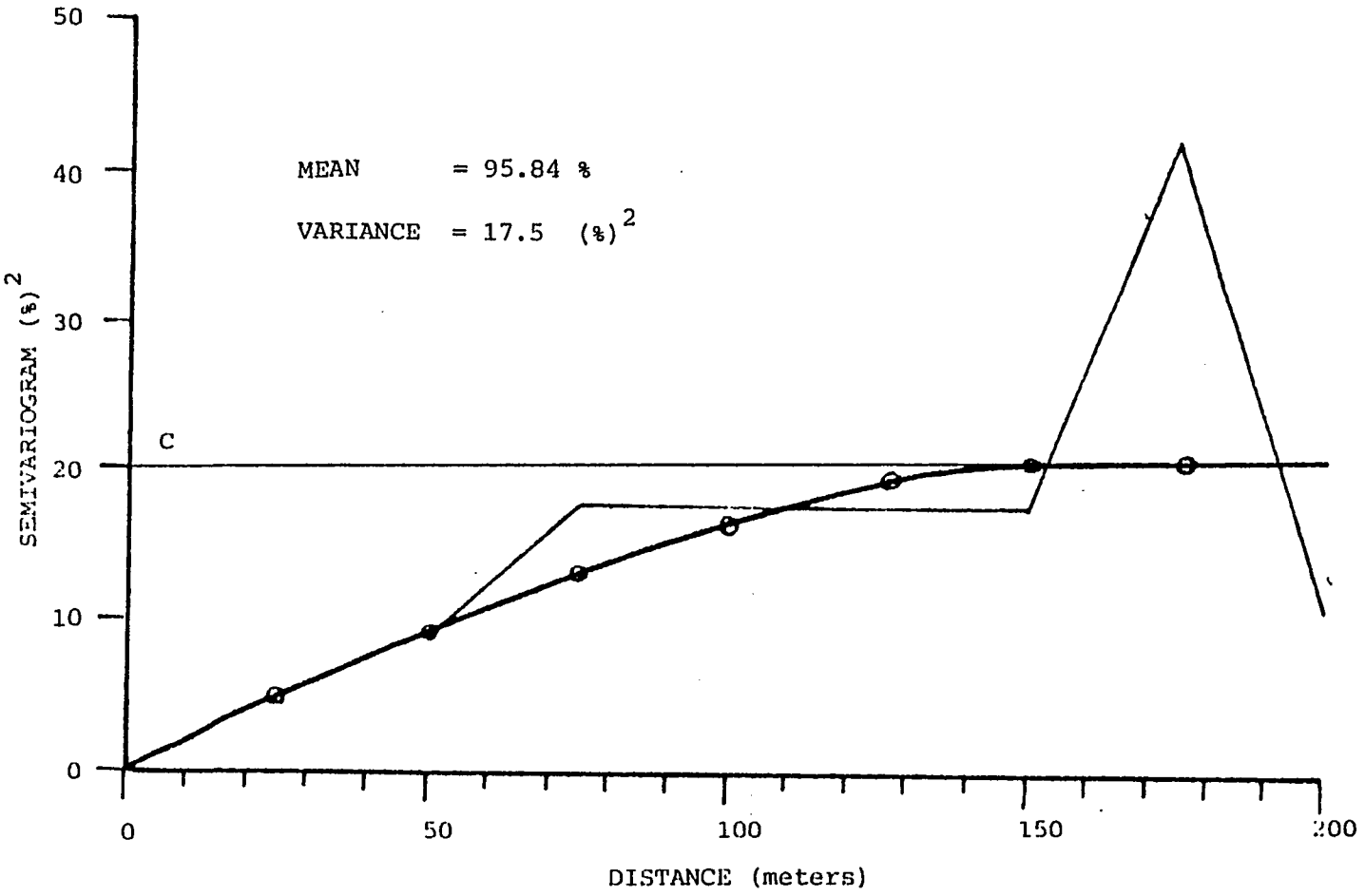

Fig.(6.31) Experimental horizontal semivariogram and fitted model for (calcined MgO%)

Zarghat Magnesite Deposit

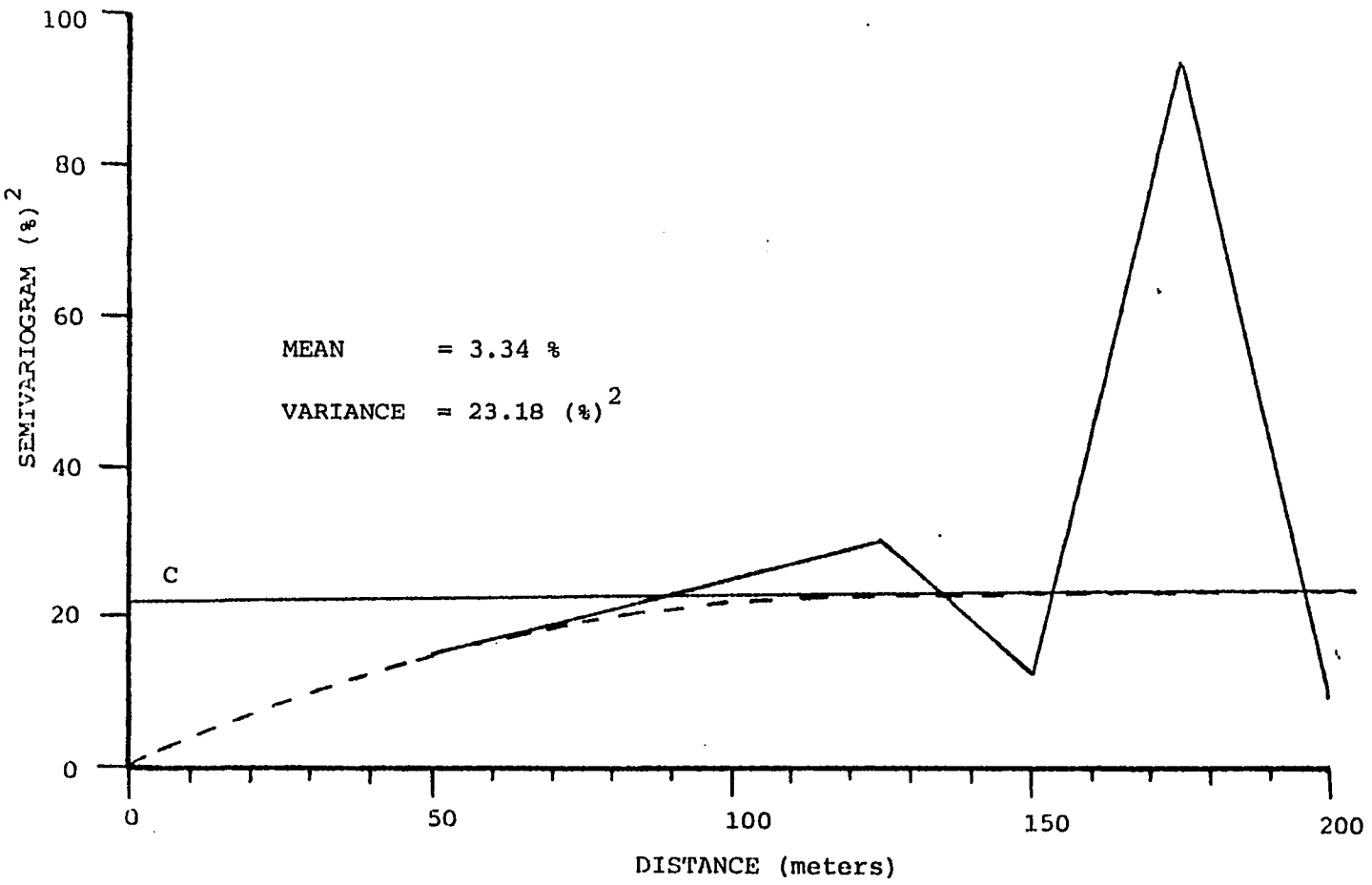

Fig.(6.32): Experimental horizontal semivariogram and fitted model for (calcined CaO%)

Zarghat Magnesite Deposit

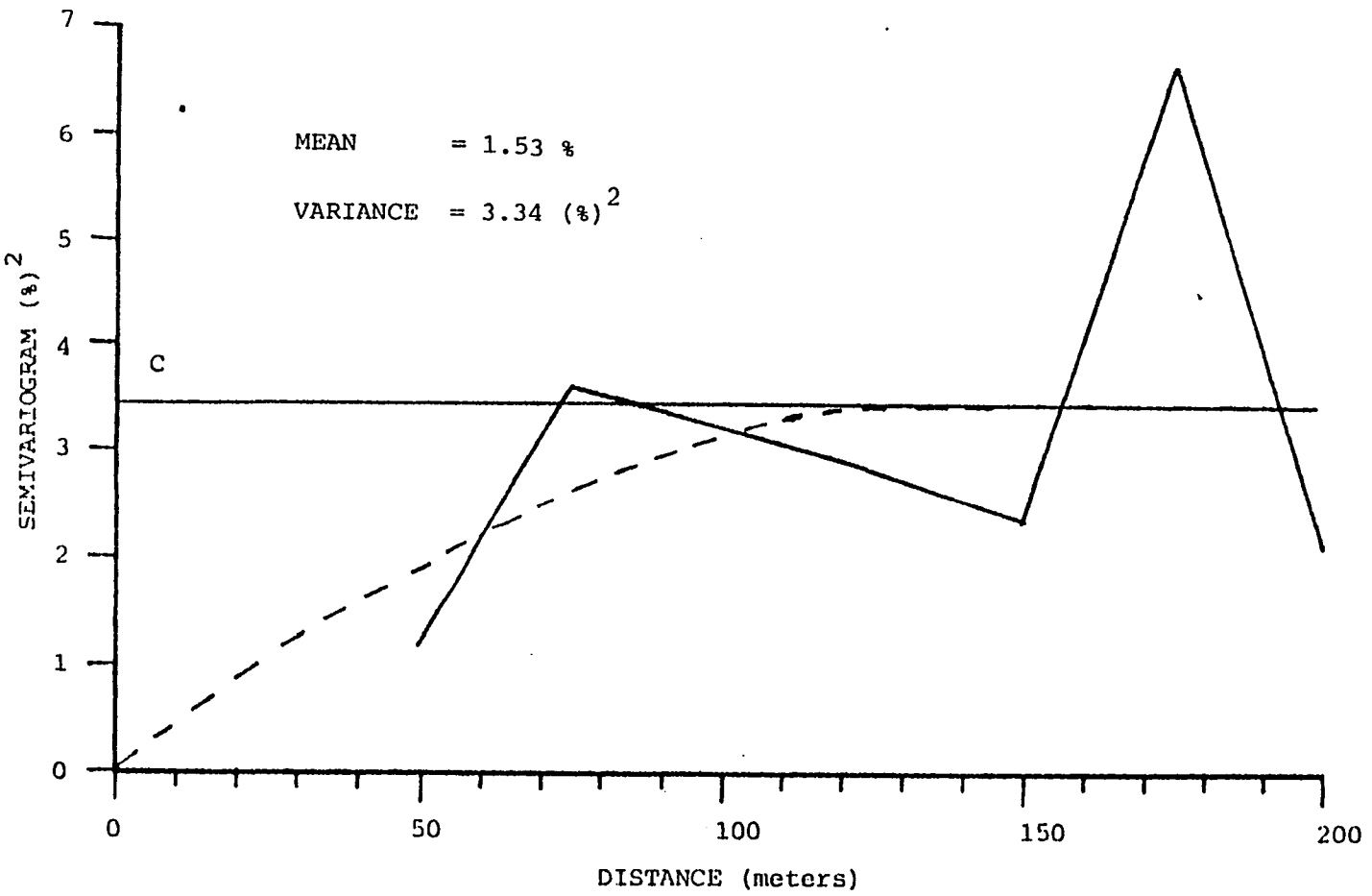

Fig.(6.33) Experimental horizontal semivariogram and fitted model for (crude CaO%)

Zarghat Magnesite Deposit

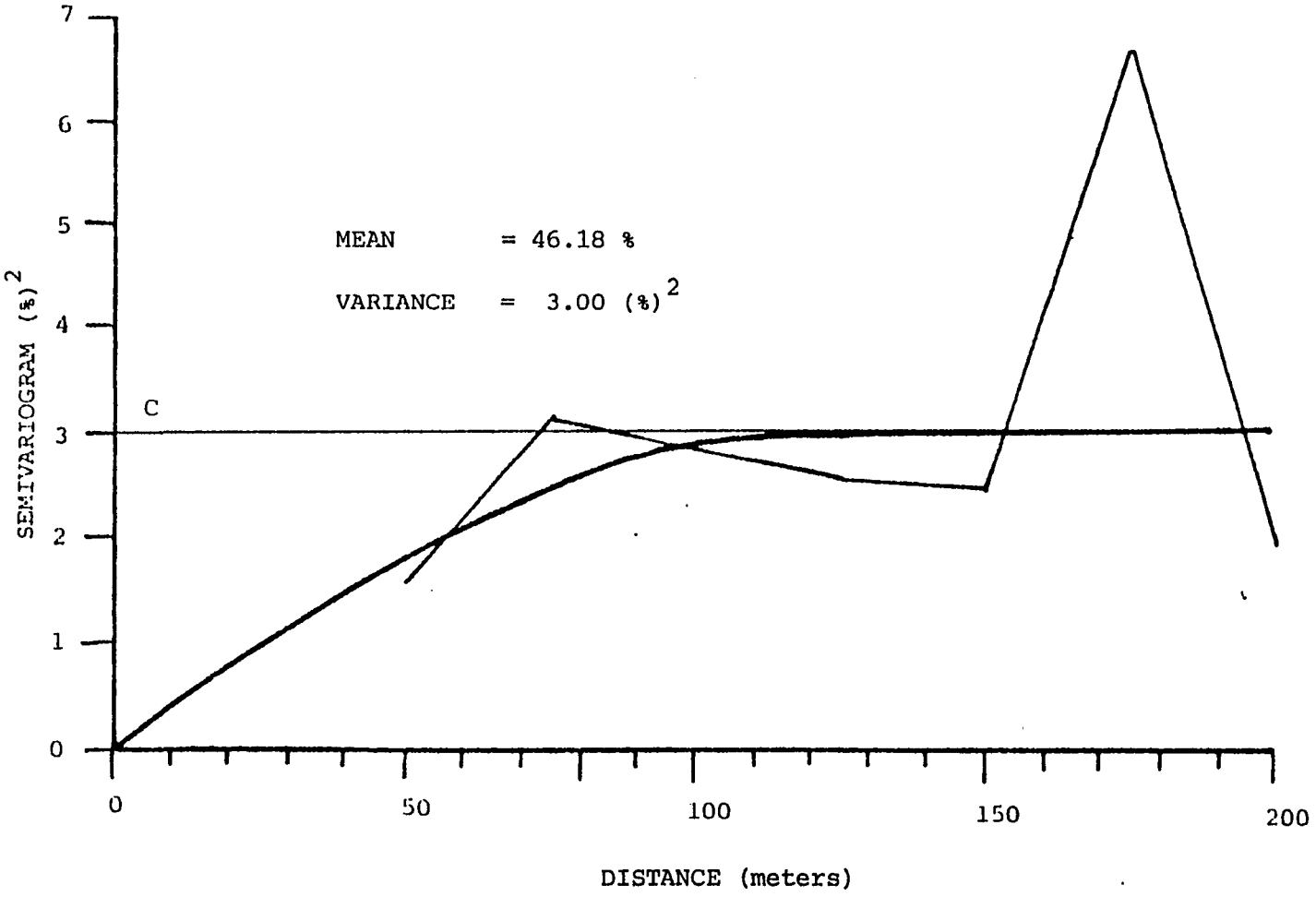

Fig.(6.34): Experimental horizontal semivariogram and fitted model for (crude MgO%)

Zarghat Magnesite Deposit

semivariograms and considering the best fit to the points near the origin, appropriate models were fitted (model parameters listed in Table 6.3)

B.4. Horizontal Cross-semivariogram

Due to the high correlation between MgO% and CaO%, the experimental horizontal cross-semivariograms were computed (see Figs. 6.35 and 6.36). Fig. 6.36 shows the experimental horizontal cross-semivariogram and the fitted model.

When we compare the obtained cross-semivariogram with the individual semivariograms of both variables separately we will find that the general behaviour is similar.

C. Conclusions

Having completed the structural analysis, and defined semivariogram models in both vertical and horizontal directions, we conclude the followings:

1- Semivariogram models are spherical with nugget variances equal to zero.

2- The type of mineralization revealed by the semivariograms is continuous one with gentle growth from the origin in the horizontal direction and rapid growth in the vertical direction suggesting the possibility of the sedimentary origin for the

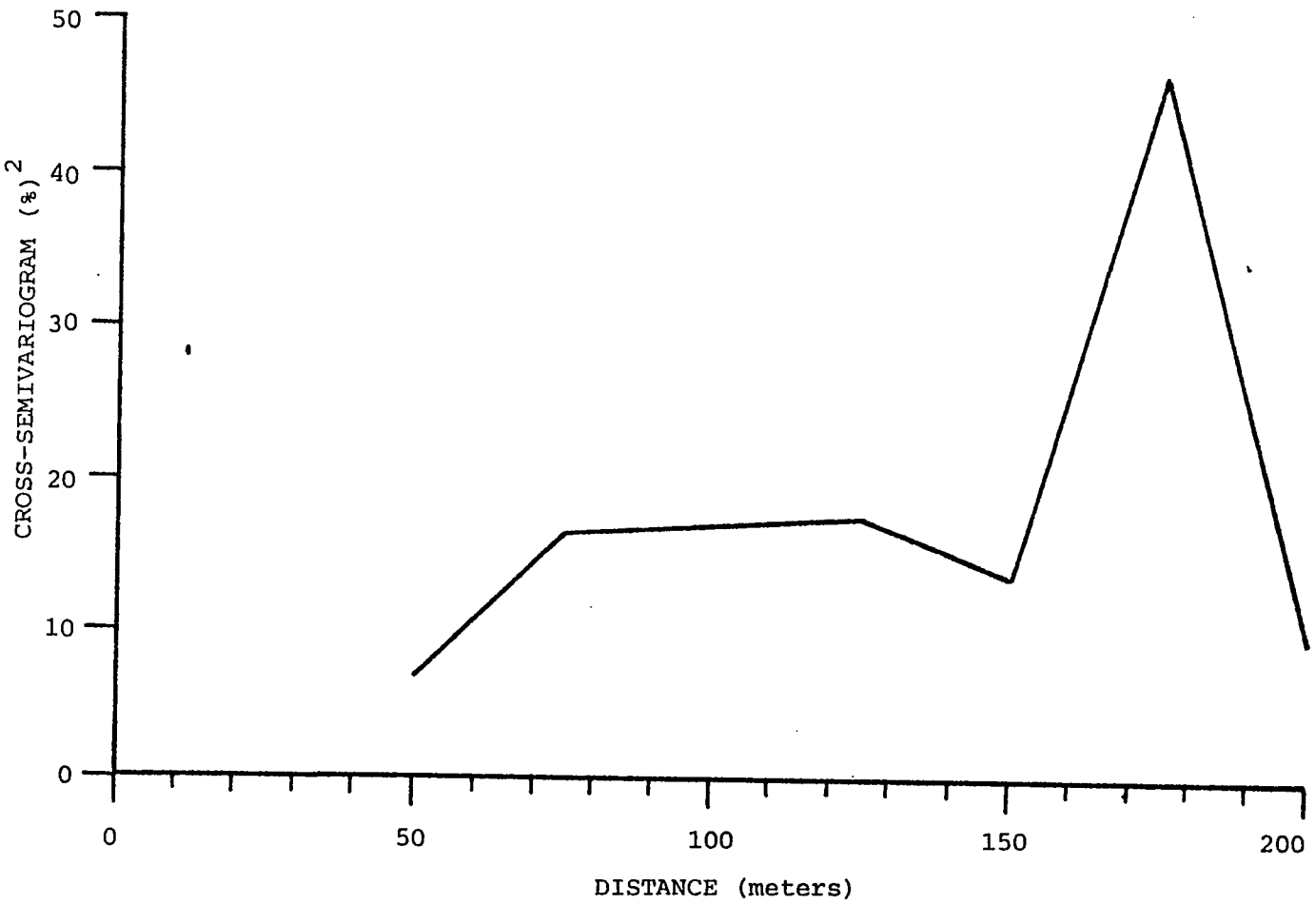

Fig.(6.35): Experimental horizontal cross-semivariogram for (calcined MgO% & CaO%) Zarghat Magnesite Deposit

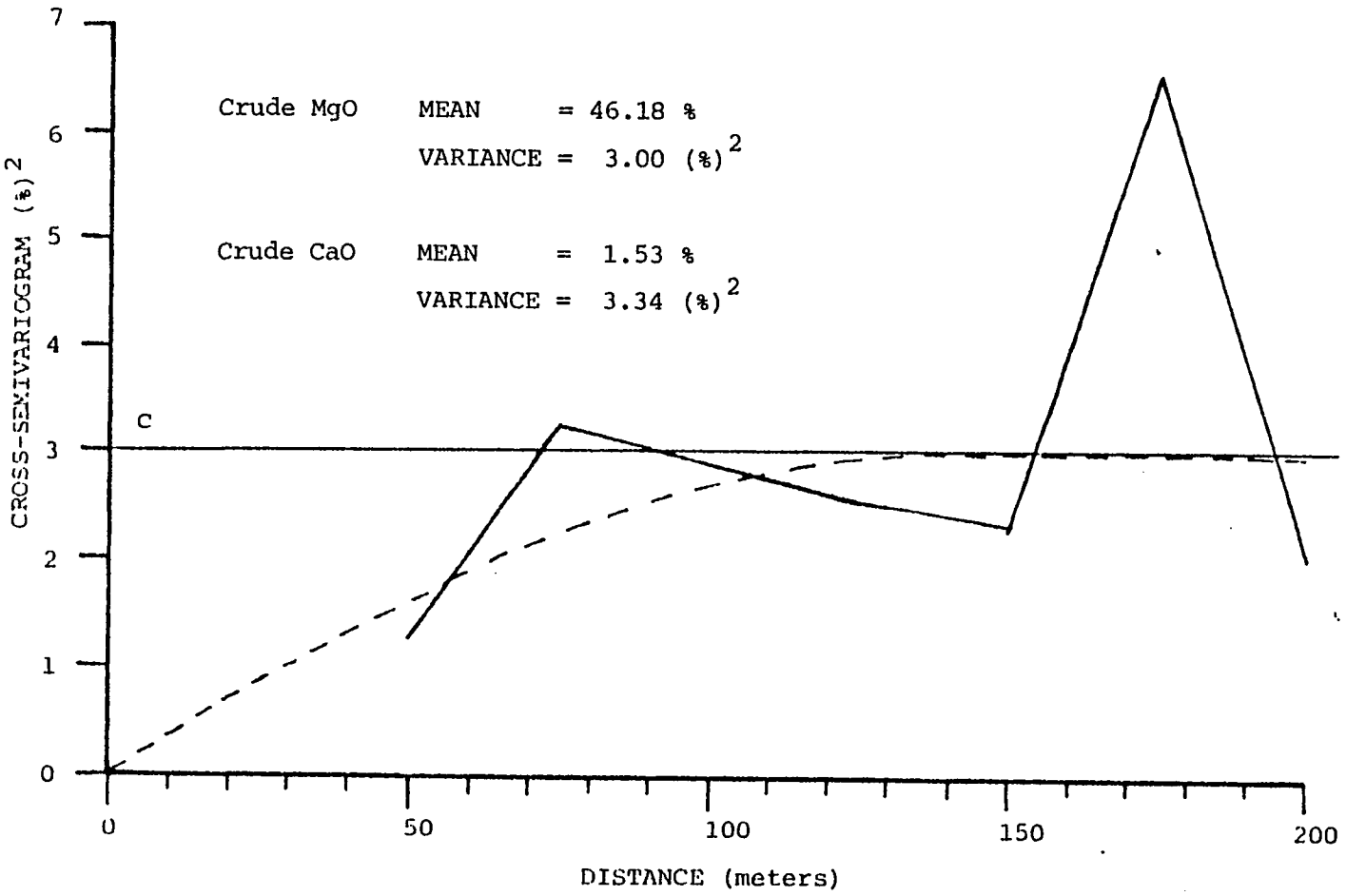

Fig.(6.36): Experimental horizontal cross-semivariogram and fitted model for (crude MgO% & CaO%) Zarghat Magnesite Deposit

Model parameters	Vertical semivariogram (crude MgO%)			Vertical cross-semivariogram (MgO% & CaO%)			Horizontal semivariogram		Horizontal cross-semivariogram (MgO% & CaO%)
	ZA 13	ZA 17	ZA 18	ZA 13	ZA 17	ZA 18	crude MgO%	calcined MgO%	
Nugget variance $(\%)^2$	0.0	0.0	0.0	0.0	0.0	0.0	0.0	0.0	0.0
Spatial variance $(\%)^2$									
C_1	4.0	0.32	0.45	5.0	0.2	1.9	3.0	19.0	3.0
C_2	—	0.40	—	—	0.32	—	—	—	—
Range (m)									
a_1	3.0	5.25	2.0	3.3	4.8	2.0	117	157	135
a_2	—	22.5	—	—	23.4	—	—	—	—

Table (6.3): Summary of semivariogram and cross-semivariogram parameters

deposit.

3- The zone of influence of crude MgO varies vertically from one drill-hole to another (see Table 6.3). In the horizontal direction it was found to be 117 m. Calcined MgO, also shows variable zone of influence vertically while in the horizontal direction it is 157 m.

4- Due to the high correlation between CaO% and MgO% co-kriging method may suitably be adopted in the reserve estimation.

CHAPTER - 7

ORIGIN OF ZARGHAT MAGNESITE DEPOSIT

7.1 Genetic Classification of Magnesite Deposits

One of the early references in literature regarding the classification and origin of magnesite deposits is that of Bain (1924) who classified magnesite deposits into 4 main types:-

Type 1. Magnesite as a Sedimentary Rock: This type includes magnesite deposits formed by a chemical precipitation and subsequent dehydration. Example: Altin, British Colombia.

Type 2. Magnesite as an Alteration of Serpentinite: This type includes magnesite deposits produced from serpentinite rocks by the decomposition in the presence of carbonated water. Example: Eubea, Greece.

Type 3. Magnesite as a Vein Filling: This type includes magnesite that represents an over-concentration of a single mineral (in this case magnesite) in the ordinary type of fissure vein formed by precipitation from rising juvenile water. Example: New West Beach, New Brunswick, Canada.

Type 4. Magnesite as a Replacement of Limestone: the magnesite deposits of this type are produced by the replacement of limestone through the agency of magnesia-bearing solutions.

Example: Argenteuil Co., Quebec, Canada.

Schroll (1961, p. 706) proposed three different models for the origin of magnesite. They include: 1- Evaporitic paragenesis, 2- Serpentine paragenesis, and 3- metamorphic hydrothermal paragenesis.

Borch (1964, p. 781) noted that in the Cooring Lagoon, Australia, a variety of fine-grained carbonate minerals are observed in associations on lake and lagoon floors. The following six carbonate assemblages are found in the Cooring Lagoon:

- Magnesian calcite- aragonite
- Magnesian calcite
- Well crystallized- disordered dolomite
- Hydromagnesite- aragonite
- Magnesite- dolomite

Surface sediments consist of equal proportions of magnesite and dolomite while, at a depth of 6 inches the composition is 20% magnesite and 80% dolomite. Grain size of the magnesite- dolomite sediment is 1 ξm on average. At a depth of 10 inches, magnesite is no longer detectable, and the sediment is entirely dolomitic.

Borch (1964, p. 797) suggested two alternative modes of origin for the magnesite- dolomite assemblage.

1) "Direct precipitation from the saline lake waters, magnesite either co-precipitated with dolomite, or mixed with local dolomite eroded from the old lake floor or from banks adjacent to the lake."

2) "Post-depositional alteration of a hydromagnesite-aragonite assemblage, causing partial dehydration of the hydromagnesite to give the observed expanded cell magnesite, and accompanied by a dolomitization of associated aragonite". He also mentioned that the lake water had a high pH due to the presence of significant aquatic plant life.

Blatt et al. (1972, p. 489) report that " dolomitization by evaporative reflux is currently believed to be the major mechanism by which dolomite is formed in carbonate rocks". The evaporation of sea water will reach a point to precipitate aragonite or gypsum as a first stage of carbonate sedimentation. The pH and Mg/Ca ratio, will increase in the sea-water and dolomite can be formed at this stage. This island of Bonaire is a good example of modern dolomitization in association with gypsum precipitation. They noted also that " dolomitization by evaporative reflux may operate without leaving evaporitic beds, and it is certainly true that the geologic record contains many extensive dolomite units from which no evaporites have

been reported".

Bush (1973, p. 403) noticed that in the sabkha environment at Abu Dhabi, magnesite " occurs exclusively in the sediments which occur above the algal mat, between 2 and 4 kilometers from the lagoon margin".

Petracheck et al. (1977), recently reconstructed the original sedimentary basin of carbonate sedimentation of Eugui-Asturreta in the Spanish Pyrenees, they noticed the enrichment of magnesite where the carbonate section is thickest. This observation indicates deposition of magnesite at the center of a restricted basin.

7.2 Characteristic Features of Some Important Magnesite Deposits.

Numerous magnesite deposits have been investigated throughout the world, and their characteristic features have been well documented. Table (7.1) shows the important geological characteristics of several magnesite deposits in the world with the possible modes of genesis as suggested by the authors. This table and thorough survey of the literature indicate that in the absence of clear relationships with igneous bodies, most workers tend to favour a sedimentary origin, whereas others (i.e. Bodenlos, 1954) even invoke a relationship with a concealed magmatic intrusions of granitic or granodioritic composition.

Table (7.1): Geological characteristics of some magnesite deposits in the world.

Deposit and references	Lithological association and age	Structural setting	Related Igneous Activity	A e
Central Ceara, Brazil (Bodenlos, 1958)	Limestone, Phyllite, Quartzite, Schist, Gneiss and some have Dolomite, Massive and lenticular Magnesite in limestone (Precambrian)	Lens-shaped; in contact with schist and limestone. All strongly folded.	Amphibolite dikes and sills. Small acidic and quartz veins	Tal Sem
Serra Das Eguas, Brazil (Bodenlos, 1954)	Dolomite, Quartzite (Late Precambrian)	The area is a large synclinal structure characterized by close and complex folding.	Pegmatites and simple quartz veins are found in magnesite	Ser Top Qua
Manchuria deposits (Nishihara, 1956)	Magnesite interbedded with dolomite, underlain by phyllite and limestone. (Precambrian)	The sedimentary sequence is folded and faulted.	Cretaceous dikes of various types intrude sedimentary sequence	Tal
State of Washington, U.S.A. (Fox and Rinehart, 1968)	Lenses and beds of magnesite outcrop within narrow stratigraphic zone. Dolomite, Phyllite, Schist, Chert. (Triassic)	The sedimentary sequence is folded, faulted and metamorphosed	———	Chl net Dol Ant
Gabbs, Nevada, U.S.A. (Schilling, 1968)	Laminated dolomite, silt, black limestone. (Triassic)	Sedimentary sequence is intensely folded and faulted.	Intermediate and acidic dikes. Cretaceous granodiorite stock.	Qua rit ant
Kumaun Himalya, India (Vadiya, 1968)	Laminated dolomite and dolomitic limestone includes lentiform magnesite. Olivine-green slate underlaying the dolomite. (Late Precambrian-Ordovician)	Magnesite is folded and faulted with country rocks.	Magnesite intruded by dolerite dikes and sills. No relation between intrusion and magnesitization.	Dol Che
Deloro Twp., Ontario Canada (Griffis, 1972)	The lenses of magnesite in a vicinity of ultramafic rocks. (Precambrian)	———	———	Magn Quar
Jammu, India (Raha, 1975)	Crystalline magnesite in thick sequence of carbonate rocks- Great Limestone. (Precambrian)	The area is folded with approximately N-S axis.	———	D
Calc Zone of Chamoli India (Girish, and others 1977)	Alternating sequence of dolostone and slate. Coarse crystalline magnesite occur as lenticular bodies in the dolostone units. (L. Carb.- E. Permian)	The rocks occur as thrusted doubly plunging anticline.	Basic intrusions	D T Si
Euqui-Asturreta, Spain (Petrascheck, et al. 1977)	Graywacke, Dolomite and Slate. (Carboniferous)	Magnesite interbedded with dolomite. The sedimentary sequence is folded and faulted.	———	Gy Do
Jabal Rokham, Saudi Arabia (Bokhari, 1979)	White massive magnesite, Bluish-gray massive dolostone with algal lamination, and green-siltstone (laminated) (Late Precambrian)	The area is folded and faulted	Dolerite dikes	Ta Al Do
Vavdose Magnesite, Chalkidiki Peninsula Northern Greece (Dabitzias, 1980)	Massive cryptocrystalline magnesite veins up to 2 m thick, in fresh dunite and brown serpentinite. (Cretaceous)	Ultramafic complex	Emplacement of Cretaceous ophiolites	Ma Ch Ca Ta Se
Main Creek, Savage River, Tasmania Australia (Frost, 1982)	Associated with dolomite and talc-chlorite schist. Thickness of magnesite lens is 213 m. (Precambrian)	Geology of the area is very uncertain	———	Ma Qu

l setting	Related Igneous Activity	Accompaning mineralogy	Chemical composition	GENESIS
ed; in contact with d limestone. gly folded.	Amphibolite dikes and sills. Shelf acidic and quartz veins	Talc, Quarts, Chert, Hematite, Pyrite.	About 48% MgO	HYPOGENE replacement of calcium in limestone by Mg probably carried by hypogene solutions.
is a large syncli- ure characterized and complex folding.	Pegmatites and simple quartz veins are found in magnesite	Beryl, Talc, Kyanite, Topaz, Tourmaline, Quartz, Hematite.	Average CaO 2%	HYPOGENE-MESOTHERMAL from concealed magma of granitic or granodioritic composition.
ntary sequence is l faulted.	Cretaceous dikes of various types intrude sedimentary sequence	Talc, Silica.	47% MgO	SEDIMENTARY direct precipitation of magnesite in partially enclosed lagoon in warm, arid or semi-arid climate. Modern analog: Logoons Uralcaspian region.
ntary sequence is ulted and meta-	———	Chlorite, Mica, Magnetite, Calcite, Dolomite, Quartz, Antigorite.	MgO 22-34% Cr and Ni 0.1-0.2%	SEDIMENTARY precipitation of hydromagnesite and huntite in shallow ponded seas. Later converted to magnesite and dolomite. Local hydrothermal redistribution of magnesite.
y sequence is folded and faulted.	Intermediate and acidic dikes. Cretaceous granodiorite stock.	Quartz, talc, Chlorite, Tremolite, antigorite, pyrite	CaO H.G. < 5% L.G. > 5%	EPIGENETIC-HYPOGENE magnesite and recrystallized dolomite formed by hydrothermal replacement at regionally metamorphosed sedimentary dolomite.
is folded and th country rocks.	Magnesite intruded by dolerite dikes and sills. No relation between intrusion and magnesitization.	Dolomite, Sederite Chert, Talc	MgO 42.2%	SEDIMENTARY in lagoons and embayments (back reef). Progressive enrichment in Mg in high PH environment caused by algal activity. Modern analog: Cooring Lagoon, S. Australia.
———	———	Magnesite, Dolomite, Quartz	Magnesite 57%	ALTERATION of a serpentinite parent rock.
folded with ly N-S axis.	———	Dolomite	MgO 40%	REPLACEMENT of limestone either by hydrothermal solutions from some igneous intrusion, or by circulating meteoric waters which remobilized Mg in the dolomite
ccur as thrusted ging anticline.	Basic intrusions	Dolomite, Calcite, Talc, Quartz, Siderite	MgO 38-45% CaO 2% Hematite 2-4%	REPLACEMENT of dolomite volume by volume, by the Mg-rich mineralizing solutions generated along the 'Main Central Thrust' as the result of dedolomitization of the dolostones.
erbedded with sedimentary olded and faulted.	———	Gypsum, Chert, Dolomite		SYN-GENETIC SEDIMENTARY origin
olded and faulted	Dolerite dikes	Talc, Chlorite, Albite, Quartz, Dolomite, Pyrite	Cr 0-50 ppm Ni 0-35 ppm	SEDIMENTARY with probable recrystallization and possibly some remobilization during diagenesis and metamorphism.
plex	Emplacement of Cretaceous ophiolites	Magnesite, Dolomite Chalcedony, Quartz, Calcite, Chlorite, Talc, Tremolite, Serpentine	Magnesite 97-99 mole%	HYPOGENE ascending carbonated solutions leached magnesia from the ultramafic rocks below the zone of deposition. Magnesite was deposited in progressively opening fractures.
area is very	———	Magnesite, Dolomite Quartz	Magnesite 80-90%	Mg-METASOMATISM of dolomite by dilute Mg chloride solution generated at depth.

Nishihara (1956) stated that "the crystallization of igneous rocks appear to use up the magnesium of the magma, so that little, if any, magnesium remains in the final residue. Chemical analyses have shown that magnesium does not occur in detectable amounts in the gases of the volcanoes or fumaroles or in gases occuluded from igneous rocks. Further, analysis of waters believed to be juvenile reveal very minor amounts of magnesium, part or all of which could have been derived from the walls of channelways. For these reasons the magmatic origin of any very large magnesite deposit in sediments is seriously questioned".

7.3 Origin of Zarghat magnesite deposit

The Zarghat magnesite body occurs in a normal stratigraphic sequence, underlain by bedded dolomite and limestone with a clear and sharp contact with the dolomite, and displays sedimentary bedding and crypto- to microcrystalline texture, as well as very simple mineralogy. No related igneous body or geological feature suggestive of hydrothermal activity was found. Typical hydrothermal minerals and replacement texture features such as relicts are totally absent in the magnesite body. All these evidences strongly suggest that the Zarghat magnesite body was deposited by a chemical sedimentary process after the formation of the bedded dolomite during a normal sequence of carbonate deposition.

Extensive experimental work by various investigators on the natural precipitation of magnesium from sea water suggests that conditions governing the formation of anhydrous $MgCO_3$ are highly restricted. According to Tewari (1973) "preparation of magnesium carbonate in the laboratory under anywhere near-sea surface conditions did not result in the formation of anhydrous carbonate so that direct precipitation of anhydrous magnesium carbonate under nature is a remote possibility". Instead Tewari (1973) was able to produce in the laboratory a trihydrate magnesium mineral identified to be nesquehonite ($MgCO_3.3H_2O$) under a variety of conditions generally under elevated pH and higher CO_3 ion concentration. Kazakov et al. (1957) repeatedly produced nesquehonite or hydromagnesite in laboratory at room temperature (15-24°C) and atmospheric pressure, but failed to synthesize magnesite under these pressure-temperature conditions. Experimental work by Schloemer (1952) also suggested that nesquehonite is the stable phase at temperature below 80°C. It appears that no experiment has yet resulted in the precipitation of anhydrous $MgCO_3$ (magnesite), but hydrous carbonate and magnesium hydroxide have been produced.

In nature, the aragonite-hydromagnesite assemblage has been reported from the Recent or Pleistocene sediments (Alderman and Von Der Borch, 1960; Graf et al., 1961). Borch (1965) reported various assemblages of carbonate minerals in modern carbonate sediments in

Cooring Lagoon in South Australia, including hydromagnesite-aragonite, as well as magnesite-dolomite assemblages. X-ray powder diffractometer studies indicated that Cooring magnesite has an expanded unit cell, which according to Borch may be due to partial dehydration of the hydromagnesite to give the expanded cell magnesite.

In spite of all the research, a clear evidence for the natural precipitation of magnesite as anhydrous $MgCO_3$ could not be found. On the contrary most of the experimental as well as modern and recent sediment research indicates a precursor hydrous phase (hydromagnesite or nesquehonite) for the formation of magnesite in natural geological environments. The Zarghat magnesite also presents a convincing evidence to support the precursor hydrous phase. The dolomite veins which range in thickness from microscopic veinlets to about one meter, are found throughout the magnesite body. The occurrence of the dolomite veins at every level and every scale, their absence in the underlying bedded dolomite, and total absence in them of hydrothermal minerals (except traces of microcline , quartz, and iron oxides), all suggest that the solutions responsible for their formation has a source nowhere deeper than the magnesite body itself. Tewari (1973) is quoted here for his explanation of the coarse crystalline nature of the Himalayan magnesite "Nesquehonite, which contains three water molecules, must have been 'stewed in its own juice'..... under a higher than normal temperature and pressure conditions". In Zarghat, pieces

and blocks of magnesite are so surrounded by the dolomite veins that the magnesite appears to have been "squirted and slushed in its own juice".

Many experiments were done by Link (1937), Krumbein and Garrels (1952), Klyachko and Kondratyuk (1947), and Lucas (1949) to study the possible conditions favouring the precipitation of magnesium in the sea water. The experiments suggest that the features favouring that precipitation are: (1) an incease in the concentration of magnesium sulphate, (2) saturation with sodium chloride, (3) the presence of ammonium, or organic, salts, (4) a pressure of CO_2, (5) a pH greater than 7, and some rise of temperature. Expecting the relatively small amount of dissolved CO_2, the restricted arid environment meets these conditions. It is therfore, suggested that the Zarghat magnesite was originally precipitated as hydromagnesite or nesquehonite under high pH restricted marine environments producing increase in the concentration of magnesium sulphate. After deposition, the hydromagnesite/nesquehonite was transformed according to the reaction, $MgCO_3.3H_2O$ ----- $MgCO_3 + 3H_2O$ during diagenesis by relatively higher temperature and pressure resulting from burial. The water thus expelled constituted weak hydrothermal solution which dissolved $CaCO_3$ and $MgCO_3$ (now magnesite) and redeposited them as vein dolomite with minor calcite on cooling. The solution thus produced can be referred as "in situ hydrothermal solution". The vein dolomite occupies

fractures of all sizes, crevices, and brecciated zones etc. which were produced due to shrinkage resulting from the dehydrative transformation of hydromagnesite/nesquehonite phase to magnesite. The partly digested relicts of magnesite within and around vein dolomite testify to the corrosive activity of the in situ hydrothermal solution.

The crypto- and microcrystalline nature of magnesite suggests that the temperature during the diagenesis, and that of the in situ hydrothermal solution was not high enough to" age and stewe in its own juice" the Zarghat magnesite into coarser grained as suggested by Tewari (1973) for the Himalayan coarsely crystalline magnesite deposits. This also explains the total absence of hydrothermal mineralization near Zarghat magnesite, and inside the vein dolomite.

CHAPTER - 8

CONCLUSIONS

1. The microscopic, SEM and X-ray studies revealed that the Zarghat magnesite is cryptocrystalline, massive but highly sheared and fragmented and composes mainly from magnesite with minor dolomite and calcite.
2. The magnesite body is intensively intersected by dolomite veinlets ranging in size from microscopic to one meter in width.
3. Geostatistical study revealed continuous behaviour which characterizes most of the sedimentary deposits.
4. The Zarghat magnesite was originally precipitated as an assemblage of hydromagnesite or nesquehonite under high pH in restricted marine environment. Dehydration of hydromagnesite led to formation of magnesite and vein dolomite.
5. The water expelled by the dehydration deposited the dolomite veinlets along the fractures formed due to shrinkage.
6. The DTA study for thermal behaviour of magnesite showed that the average decomposition temperature of Zarghat magnesite is about 622°C.

REFERENCES

Aksenov, Ye.M.; Igneet'yev, S.V.; Negrusta, V.Z., and Solontsov, L.F., "Magnesite in Jatulian Carbonate Rocks of Southern Karelia", Doklady Akademii Nauk SSSR, vol. 227, no. 3, pp. 672-675, 1976.

Alderman, A.R., "Dolomite sediments and their environments in the southeast South Australia", Geochim. et Cosmochim. Acta, vol. 29, pp. 1355-1365, 1965.

Bain, G.W., "Types of Magnesite Deposits and Their Origin", Econ. Geol., vol. 19, pp. 412-433, 1924.

Berton, Y., "Unpublished field notes on Zarghat magnesite deposit", 1968.

Blatt, H., Middleton, G.V., and R.C. Murray, "Origin of Sedimentary Rocks", Prentice-Hall. Inc., Englewood cliffs, New Jersy, 1972.

Bodenlos, A.J., "Magnesite deposits of Central Ceara, Brazil", U.S. Geol. Survey Bull., 962-C, pp. 121-140, 1950.

Bodenlos, A.J, "Magnesite deposits in the Serra Das Eguas, Brumado, Bahia, Brazil", U.S. Geol. Survey Bull., 975-C, pp. 87-138, 1954.

Bokhari, M.M.A., "Geology and Origin of the Magnesite Deposit in the Jabal Rokham Area", MS Thesis, King Abiulaziz University (KAU), Jeddah, Saudi Arabia, 1979.

Brosset, R., "Zarghat magnesite deposit", BRGM, 70 JED 2, 20 p, 1970.

Brosset,R., "Zarghat magnesite deposit-Completion report on drilling (ZA1-ZA26)", BRGM, 76 JED 20, 19 p, 1976.

Brown, G.F., and others, "USGS Map I-205A, Scale 1:500000", 1963.

Brown, G.F., and Jackson, R.O., "An overview of the geology of Western Arabia", In A.M.S. Al-Shanti (Ed.) Evolution and Mineralization of the Arabian-Nubian Shield: Pergamon Press, vol. 1, pp. 3-10, 1979.

Bush, P., "Some aspects of the diagenetic history of the Sabkha in Abu Dhabi, Persian Gulf", In B.H. Purser (Ed)., The Persian Gulf, Springer-Verlag, New York, pp. 395-407, 1973.

Cahen, L., and others, "The geochronology and evolution of Africa", Clarendon Press, Oxford, pp. 269-285, 1984.

Clark, I., "The semivariogram", In Geostatistics, McGraw-Hill Inc., pp. 17-40, 1980.

Dabitzias, S.G., "Petrology and Genesis of the Vavdos Cryptocrystalline Magnesite Deposits, Chalkidiki Peninsula, Northern Greece", Econ. Geology, vol. 75, pp. 1138-1151, 1980.

David, M., "Geostatistical ore reserve estimation", Netherlands, Elsevier Sci. Pub. Co., 364 p, 1977.

Delfour, J., "Preliminary Data on the Zarghat Magnesite prospect", BRGM, Second Annual Report: Chapters 1-3, 70 JED 1, 8 p, 1970.

Feugueur, L., "Problems concerning the search for nonmetallic minerals in Saudi Arabia", BRGM open-file rept. SG JED 66 A1, 76 p., 26 fig, 1966

Fleck, R.J., Greenwood, W.R., Hadley, D.G., Anderson, R.E., and Schmidt, D.L., "Age and evolution of the Southern part of the Arabian Shield", In A.M.S. Al-Shanti (Ed.) Evolution and Mineralization of the Arabian-Nubian Shield: Pergamon Press, vol. 3, pp. 1-17, 1980.

Fox, K.F., and C.D. Rinehart, "Geology of magnesite deposit in northern Okanogan County, Washington, U.S.A.", U.S. Geol. Survey Bull, 1968.

Frost, M. T., "The magnesite deposit at Main Creek, Savage River, Tasmania", Econ. Geology, vol. 77, no. 8, pp. 1901-1911, 1982.

Frost, M.T.; and H.W. Matzat, "A further large magnesite deposit along the Savage River in Northwestern Tasmania", Econ. Geol., vol. 79, pp. 404-408, 1984.

Girish, Gaur, C.S., Dave, V.K.S., and Mithal, "Magnesite deposits of the Calc Zone of Chamoli, Garhwal Himalaya, Uttar, Pradesh, India", Himalaya Geol. (Delhi), vol. 7, pp. 256-292, 1977.

Griffis, R., "Genesis of a Magnesite Deposit, Deloro Twp., Ontario", Econ. Geology, vol 67, pp. 63-71, 1972.

Gundogdu, N., and Ataman, G., "Sedimentary magnesite occurrence in Tavsanli", Pub. of Inst. of Earth Sciences of Hacettepe University, vol. 2, no. 2, pp. 134-139, 1976.

Hadley, D.G., and Schmidt, D.L., "Sedimentary rocks and basins of the Arabian Shield and their evolution", In A.M.S. Al-Shanti (Ed.) Evolution and Mineralization of the Arabian-Nubian Shield: Pergamon Press, vol. 4, pp. 26-50, 1980.

Journel, A.G., and Ch.J. Huijbregts, "Mining Geostatistics", Academic Press, 600 p., 1978.

Kahr, V. P., "Zarghat magnesite occurrence,DGMR open-file rept", 2 p, 1962.

Mackenzie, R. C., "Differential thermal analysis (2 vol.)", New York, Academic Press, 1970.

Matern, B., "Spatial Variation", Almaenna Foerlaget, Stockholm, 144 p, 1960.

Matheron, G., "The theory of Regionalized Variables and its applications", Les Cahiers du Centre de Morphologie Mathematique De Fontainbleau. Fasc. No. 5, 211 p., Ed. ENSMP, Paris, 1971.

Matheron, G., "Principles of geostatistics", Econ. Geol., vol. 58, pp. 1246-1266, 1963.

Nishihara, H., "Origin of the bedded magnesite of Manchuria", Econ. Geol., vol. 51, pp. 698-711, 1956.

Petrascheck, W.E., Kralik, M., and A. Ranzenbacher, "The strata-bound magnesite deposit of Eugui-Asturreta in the Spanish Pyrenees", In D.D. Klemm and H.J. Schneider (Eds.) Time-and Strata-Bound Ore Deposits, Springer-Verlag, Berlin, pp. 254-259, 1977.

Powers, R.W., Raminez, L.F. Redmond, C.D., and Elberg, Jr., E.L.," Geology of the Arabian Peninsula - Sedimentary Geology of Saudi Arabia", Geol. Surv. Professional Paper 560-D, U.S. Government Printing Office, Washington, 147 p, 1966.

Raha, P.K., "Crystalline Magnesite Deposit in Jammu Limestone, Near Katra, Jammu- its nature and origin", Indian Miner (Calcutta), vol. 29. no. 3, pp. 18-24, 1975.

Reed, A., "Structural geology and geostatistical parameters of the Afton copper-gold mine, Kamloops, B.C.", CIM Bulletin, vol. 76, no. 856, pp. 45-55, 1983.

Rendu, J.M., "An introduction to geostatistical method of mineral evaluation", South African Institute of Mining and Metallurgy, Johannesburg, 84 p. 1978.

Sahin, A, "Spatial Distributions in the Bonthe Rutile Deposits of Sierra

Leone", Unpublished Ph.D., 1977.

Safaya, H.L., "On the Gol Magnesite Deposit near Thal, Pithoragraph District, Uttar Pradesh", Indian Miner (Calcutta), vol. 29, no. 2, pp. 98-102, 1975.

Schilling, J.H., "The Gabbs magnesite deposit, Nye County, Nevada, U.S.A.", In J.D. Ridge (Ed.) Ore deposits of the United States, Am.I.M.M.P.E. Inc., New York, pp. 1607-1627, 1968.

Schroll, V.E., "Uber das Vorkommen von Magnesite in alpinen Salzlagerstatten", Sonderdruck "Radex Rundschau," pp. 704-707, 1961.

Sengupta, D.K.; Sastari, S.R.S.; and Sahoo, R.K., "Salem Magnesite Ore Characteristics and response to Flotation", Indian Min. Eng. J. (Bombay), vol. 19, no. 8, p. 19-24, 1980.

Takasawa, K., and Kuroda, Y., "A Quartz-Magnesite Rock in the Setogawa Zone, Central Japan", Jour. of the Geol. Soc. of Japan, vol. 80, no. 9, pp. 425-427, 1974.

Tewari, D.N., "Nesquehonite- a possible precursor in the origin of Himalayan magnesite deposits", Himalayan Geology (Delhi), vol. 3, p. 94-102, 1973.

Valcha, Z., "Czechoslovak analytical standards of rocks and mineral raw materials. Reference standard material of magnesite (Kosice) ", Sb Geol Ved Rada TG Technol Geochem (Prague), vol. 16, pp. 85-100, 1979.

Valdiya, K.S., "Origin of the Magnesite Deposits of Southern Pithoragarh, Kumaun Himalaya, India", Econ. Geology, vol 63, pp. 924- 934, 1968.

Von der Borch, C.C., "The distribution and preliminary geochemistry of modern carbonate sediments of the Cooring area, South

Australia", Geochim. Cosmochim. Acta., vol. 29, pp. 781-799, 1965.

Weinschenk, E., "Grundzuge der Gesteinkunde-Frieburg", Band II., p. 315. 1905.

Wendlandt, W. VM., "Thermal methods of analysis (2nd ed.)", Canada, John Wiley, 505 p, 1974.

Appendix (1): Pure magnesite - X-ray results.

Sample number	d-spacing (Å)			Detected minerals
E-1	2.74	2.11	1.70	magnesite
E-2	2.74	2.11	1.70	magnesite
E-12	2.74	2.11	1.70	magnesite
E-13	2.74	2.11	1.70	magnesite
E-14	2.74	2.11	1.70	magnesite
E-15	2.74	2.11	1.70	magnesite
E-17	2.74	2.11	1.70	magnesite
	2.88	----	----	dolomite tr.
E-18	2.74	2.11	1.70	magnesite
E-19	2.74	2.11	1.70	magnesite
	2.88	----	----	dolomite tr.
C-7	2.74	2.11	1.70	magnesite
C-8	2.74	2.11	1.70	magnesite
C-10	2.74	2.11	1.70	magnesite
	2.88	----	----	dolomite tr.
C-11	2.74	2.11	1.70	magnesite
C-12	2.74	2.11	1.70	magnesite
C-13	2.74	2.11	1.70	magnesite
C-14	2.74	2.11	1.70	magnesite
C-15	2.74	2.11	1.70	magnesite
C-16	2.74	2.11	1.70	magnesite
C-17	2.74	2.11	1.70	magnesite
	2.88	----	----	dolomite tr.
C-18	2.74	2.11	1.70	magnesite
	2.88	----	----	dolomite tr.
C-19	2.74	2.11	1.70	magnesite
C-20	2.74	2.11	1.70	magnesite
	2.88	----	----	dolomite tr.
C-21	2.74	2.11	1.70	magnesite

Appendix (1): Cont.

Sample number	d-spacing (Å)			Detected minerals
C-22	2.74	2.11	1.70	magnesite
C-23	2.74	2.11	1.70	magnesite
C-24	2.74	2.11	1.70	magnesite
C-25	2.74	2.11	1.70	magnesite
C-26	2.74	2.11	1.70	magnesite
W-1	2.74	2.11	1.70	magnesite
	2.88	----	----	dolomite tr.
W-2	2.74	2.11	1.70	magnesite
W-3	2.74	2.11	1.70	magnesite
	2.88	----	----	dolomite tr.
W-5	2.74	2.11	1.70	magnesite
W-6	2.74	2.11	1.70	magnesite
W-7	2.74	2.11	1.70	magnesite
W-8	2.74	2.11	1.70	magnesite
W-9	2.74	2.11	1.70	magnesite
	3.34	----	----	quartz tr.
W-10	2.74	2.11	1.70	magnesite
	2.88	----	----	dolomite tr.
	3.34	----	----	quartz tr.

Appendix (2): Impure magnesite - X-ray results.

Sample number	d-spacing (Å)			Detected minerals
E-3	2.74	2.11	1.70	magnesite
	2.89	2.19	1.79	dolomite
E-4	2.74	2.10	1.70	magnesite
	2.88	2.19	----	dolomite
E-5	2.74	2.10	1.70	magnesite
	2.88	2.19	----	dolomite
E-6	2.74	2.11	1.70	magnesite
	2.88	----	----	dolomite
E-7	2.74	2.11	1.70	magnesite
	2.88	----	----	dolomite
E-8	2.74	2.10	1.70	magnesite
	2.88	----	----	dolomite
E-9	2.74	2.10	1.70	magnesite
	2.88	----	----	dolomite
E-10	2.74	2.10	1.70	magnesite
	2.88	----	----	dolomite
E-11	2.74	2.10	1.70	magnesite
	2.88	2.19	----	dolomite
E-16	2.74	2.10	1.70	magnesite
	2.88	----	----	dolomite
C-3	2.74	2.10	1.70	magnesite
	2.88	----	----	dolomite
C-5	2.74	2.10	1.70	magnesite
	2.88	----	----	dolomite
C-6	2.74	2.10	1.70	magnesite
	2.88	2.19	----	dolomite
C-9	2.74	2.10	1.70	magnesite
	2.88	----	----	dolomite
W-4	2.74	2.11	1.70	magnesite
	2.88	----	----	dolomite

Appendix (3)

DTA results for samples collected from ESE-hills

Sample number	Peak temperature C^{o}		Range C^{o}
	First peak	Second peak	
E-1	640	815	549 - 685
E-2	640	818	549 - 691
E-3	630	831	545 - 671
E-4	630	821	549 - 678
E-5	639	825	549 - 685
E-6	640	831	549 - 695
E-7	632	820	541 - 681
E-8	632	812	534 - 664
E-9	629	813	541 - 674
E-10	632	813	541 - 678
E-11	637	830	549 - 685
E-12	633	813	541 - 678
E-13	640	812	541 - 685
E-14	640	---	541 - 681
E-15	637	821	545 - 691
E-16	637	817	545 - 685
E-17	637	---	541 - 681
E-18	634	812	541 - 678
E-19	641	827	541 - 688

Appendix (4)

DTA results for samples collected from Central-hill

Sample number	Peak temperature C^{o}		Range C^{o}
	First peak	Second peak	
C-1	626	771	541 - 659
C-3	623	843	540 - 661
C-4	567	835	538 - 605
C-5	625	805	546 - 667
C-6	624	800	523 - 654
C-7	600	817	486 - 650
C-8	639	825	545 - 691
C-9	619	821	537 - 671
C-10	629	817	537 - 664
C-11	630	812	566 - 666
C-12	637	820	566 - 685
C-13	579	795	453 - 605
C-14	609	---	530 - 646
C-15	628	---	543 - 671
C-16	628	---	543 - 674
C-17	633	820	545 - 681
C-18	630	812	545 - 674
C-19	621	802	537 - 662
C-20	630	812	545 - 678
C-21	630	---	541 - 679
C-22	630	811	545 - 674
C-23	630	811	543 - 671
C-24	630	---	541 - 666
C-25	632	812	545 - 674
C-26	632	---	544 - 681

Appendix (5)

DTA results for samples collected from WNW-hill

Sample number	Peak temperature C^{o}	Range C^{o}
W-1	628	537 - 671
W-2	607	537 - 657
W-3	631	537 - 671
W-4	628	537 - 656
W-5	626	537 - 671
W-6	637	541 - 681
W-7	630	543 - 671
W-8	632	543 - 673
W-9	635	541 - 683
W-10	635	541 - 683

Appendix (6): Pure bedded dolomite - X-ray results.

Sample number	d- spacing (Å)			Detected minerals
C-37	2.88	2.19	1.79	dolomite
C-43	2.88	2.19	1.79	dolomite
C-44	2.88	2.19	1.79	dolomite
C-45	2.88	2.19	1.79	dolomite
E-26	2.88	2.19	1.79	dolomite
W-13	2.88	2.19	1.79	dolomite

Appendix (7): Impure bedded dolomite - X-ray results.

Sample number	d-spacing (Å)			Detected minerals
E-30	2.88	2.19	1.81	dolomite
	3.34	----	----	quartz
C-1	2.88	2.19	1.81	dolomite
	2.75	2.11	1.70	magnesite
C-4	2.88	2.19	1.70	dolomite
	2.74	2.10	1.70	magnesite
C-35	2.89	2.18	1.79	dolomite
	4.21	3.34	1.82	quartz
C-40	2.89	2.18	1.79	dolomite
	3.34	----	----	quartz
C-46	2.85	2.18	1.78	dolomite
	4.21	3.30	----	quartz
W-12	2.88	2.18	1.80	dolomite
	4.22	3.30	----	quartz
W-14	2.91	2.20	1.79	dolomite
	3.37	1.82	----	quartz
	3.06	2.29	----	calcite
W-15A	2.88	2.19	1.78	dolomite
	3.00	----	----	calcite
W-21	2.88	2.19	1.78	dolomite
	2.73	2.10	1.70	magnesite
W-23	2.88	2.19	1.81	dolomite
	4.24	3.33	----	quartz
W-24	2.88	2.19	1.78	dolomite
	4.24	3.33	----	quartz

Appendix (8): Vein dolomite - X-ray results.

Sample number	d-spacing (Å)			Detected minerals
E-29	2.88	2.19	1.79	dolomite
E-31	2.88	2.19	1.79	dolomite
C-2	2.88	2.18	----	dolomite
	3.37	----	----	quartz
C-27	2.86	2.01	----	dolomite
	3.34	----	----	quartz
C-29	2.89	2.19	1.78	dolomite
	3.34	----	----	quartz
C-30	2.86	----	----	dolomite
	2.78	----	----	magnesite
	3.30	----	----	quartz
C-31	2.89	2.18	1.78	dolomite
	2.71	2.10	1.70	magnesite
	3.34	----	----	quartz
C-38	2.86	2.18	----	dolomite
	3.01	----	----	calcite
	4.22	3.30	----	quartz
W-11	2.86	2.18	1.78	dolomite
	3.30	----	----	quartz
	3.01	----	----	calcite
W-15	2.88	2.19	1.78	dolomite
	3.33	1.81	----	quartz
	3.01	----	----	calcite

بسم الله الرحمن الرحيم

دراسات جيولوجية ومعدنية وجيوإحصائية على خام الماغنيزيت بمنطقة زرغط بالمملكة العربية السعودية

رسالة مقدمة من

أمين رمضان غالب

(بكالوريوس علوم - مرتبة شرف)

إلى

جامعة البترول والمعادن - الظهران

للحصول على درجة ماجستير العلوم في الجيولوجيا

ربيع ثاني سنه ١٤٠٥هـ الموافق يناير سنه ١٩٨٥م